Characterization of Relatively Large Track Geometry Variations

A. Hamid
R. Owings
M. Kenworthy

ENSCO, Inc.
Transportation Technology,
Engineering Division
5400 Port Royal Road
Springfield VA 22151

March 1982
Final Report

This document is available to the public
through the National Technical Information
Service, Springfield, Virginia 22161.

U.S. Department of Transportation

Federal Railroad Administration

Office of Research and Development
Office of Rail Safety Research
Washington DC 20590

1. Report No.	2. Government Accession No.	3. Recipient's Catalog No.
FRA/ORD-82/13		•

4. Title and Subtitle		5. Report Date
CHARACTERIZATION OF RELATIVELY LARGE TRACK GEOMETRY VARIATIONS		March 1982
		6. Performing Organization Code
		DTS-731

7. Author's)	8. Performing Organization Report No.
A. Hamid, R. Owings, and M. Kenworthy	DOT-TSC-FRA-81-18

9. Performing Organization Name and Address	10. Work Unit No. (TRAIS)
ENSCO, Inc. *	RR219/R2309
Transportation Technology Engineering Division	11. Contract or Grant No.
5400 Port Royal Road	DOT-TSC-1631
Springfield VA 22151	13. Type of Report and Period Covered

12. Sponsoring Agency Name and Address	13. Type of Report and Period Covered
U.S. Department of Transportation	Final Report
Federal Railroad Administration	Dec 78–Oct 79
Office of Research and Development	14. Sponsoring Agency Code
Washington DC 20590	RRD-10

16. Abstract

An analysis of existing track geometry data is described from which the signatures of key track geometry variations related to severe track-train dynamic interaction are identified and quantified. Mathematical representations of these signatures are defined and presented. Track geometry descriptors used to monitor these key signatures are determined. Applications of these descriptors in terms of present track geometry measurement techniques are described. Statistical analysis of these descriptors is performed and the results are presented. Based on limited data preliminary results to quantify changes in these descriptors with time are presented.

17. Key Words	18. Distribution Statement
- Derailment, track geometry, track safety standards, constrained track, RMS processor, track,degradation, cusp, bump, jog, mid-chord offset, space curve	DOCUMENT IS AVAILABLE TO THE PUBLIC THROUGH THE NATIONAL TECHNICAL INFORMATION SERVICE, SPRINGFIELD, VIRGINIA 22161

19. Security Classif. (of this report)	20. Security Classif. (of this page)	21. No. of Pages	22. Price
Unclassified	Unclassified	148	

Form DOT F 1700.7 (8–72)   Reproduction of completed page authorized

In support of the Improved Track Structures Research Program of the Office of Rail Safety Research of the Federal Railroad Administration (FRA), the Transportation Systems Center (TSC) has been conducting studies on the relationship among track geometry variations, wheel/rail forces, and derailment tendencies. To perform these analyses, it was necessary to have realistic analytical representations of existing track geometry. The approach was to establish sound statistical representations of the universe of track geometry in the United States from numerous measurements made by the FRA Test Cars over thousands of miles of track.

In a previous study (1), mathematical representations of randomly varying track geometry variations were obtained based on time series analyses of track measurements. However, it was found that large midchord offset variations occurred with a statistically higher frequency of occurrence than would be predicted. Thus, the statistical characterizations in actual track ... statistical characterization also omitted ... and large amplitude irregularities which would produce ... produce large amplitude vehicle responses. These special situations are characterized by the averaging process associated with PSD's and other statistical processing but represent cases that do occur regularly and should be included in realistic analysis. This report deals with the analytical description of several severe track geometry variations which can cause severe dynamic interaction.

The authors ... track ... Wenstack, the TSC ...

PREFACE

In support of the Improved Track Structures Research Program
of the Office of Rail Safety Research of the Federal Railroad
Administration (FRA), the Transportation Systems Center
(TSC) has been conducting studies on the relationship among
track geometry variations, wheel/rail forces and derailment
tendencies. To perform these analyses, it was necessary to
have reliable analytical representations of existing track
geometry. The approach was to establish sound statistical
representations of the universe of track geometry in the
United States from numerous measurements made by the FRA Test
Cars over thousands of miles of track.

In a previous study (1), mathematical representations of
randomly varying track geometry variations were obtained
based on time series analyses of track measurements. How-
ever, it was found that large midchord offset variations
occurred with a significantly higher frequency of occurrence
than would be predicted from the statistical characteriza-
tions in actual track geometry data. Statistical character-
ization also omitted infrequent large amplitude irregulari-
ties which would produce occasional large amplitude vehicle
responses. These special situations are obscured by the
averaging process associated with PSD's and other statistical
processing but represent cases that do occur regularly and
should be included in vehicle analysis. This report deals
with the analytical description of severe track geometry
variations which can cause severe dynamic interaction.

The authors wish to thank Herbert Weinstock, the TSC Technical
Monitor, for a thorough review and his comments which improved
the quality of this report. Appreciation is also expressed to
all the ENSCO staff members who assisted during this study.

METRIC CONVERSION FACTORS

Approximate Conversions to Metric Measures

Symbol	When You Know	Multiply by	To Find	Symbol
		LENGTH		
in	inches	*2.5	centimeters	cm
ft	feet	30	centimeters	cm
yd	yards	0.9	meters	m
mi	miles	1.6	kilometers	km
		AREA		
in²	square inches	6.5	square centimeters	cm²
ft²	square feet	0.09	square meters	m²
yd²	square yards	0.8	square meters	m²
mi²	square miles	2.6	square kilometers	km²
	acres	0.4	hectares	ha
		MASS (weight)		
oz	ounces	28	grams	g
lb	pounds	0.45	kilograms	kg
	short tons (2000 lb)	0.9	tonnes	t
		VOLUME		
tsp	teaspoons	5	milliliters	ml
Tbsp	tablespoons	15	milliliters	ml
fl oz	fluid ounces	30	milliliters	ml
c	cups	0.24	liters	l
pt	pints	0.47	liters	l
qt	quarts	0.95	liters	l
gal	gallons	3.8	liters	l
ft³	cubic feet	0.03	cubic meters	m³
yd³	cubic yards	0.76	cubic meters	m³
		TEMPERATURE (exact)		
°F	Fahrenheit temperature	5/9 (after subtracting 32)	Celsius temperature	°C

*1 in = 2.54 (exactly). For other exact conversions and more detailed tables, see NBS Misc. Publ. 286, Units of Weights and Measures. Price $2.25, SD Catalog No. C13.10:286.

Approximate Conversions from Metric Measures

Symbol	When You Know	Multiply by	To Find	Symbol
		LENGTH		
mm	millimeters	0.04	inches	in
cm	centimeters	0.4	inches	in
m	meters	3.3	feet	ft
m	meters	1.1	yards	yd
km	kilometers	0.6	miles	mi
		AREA		
cm²	square centimeters	0.16	square inches	in²
m²	square meters	1.2	square yards	yd²
km²	square kilometers	0.4	square miles	mi²
ha	hectares (10,000 m²)	2.5	acres	
		MASS (weight)		
g	grams	0.035	ounces	oz
kg	kilograms	2.2	pounds	lb
t	tonnes (1000 kg)	1.1	short tons	
		VOLUME		
ml	milliliters	0.03	fluid ounces	fl oz
l	liters	2.1	pints	pt
l	liters	1.06	quarts	qt
l	liters	0.26	gallons	gal
m³	cubic meters	35	cubic feet	ft³
m³	cubic meters	1.3	cubic yards	yd³
		TEMPERATURE (exact)		
°C	Celsius temperature	9/5 (then add 32)	Fahrenheit temperature	°F

TABLE FOR METRIC CONVERSION OF PSD LEVELS

	To find:	
	$in^2/cy/ft$	$cm^2/cy/m$
Given:	Multiply by:	
$ft^2/cy/ft$	144.	2.83×10^3
$in^2/cy/ft$	1.00	1.97
$in^2/cy/in$	8.33×10^{-2}	0.164
$ft^2/rad/ft$	9.05×10^2	1.78×10^4
$in^2/rad/ft$	6.28	12.4
$in^2/rad/in$	0.524	1.03
$m^2/cy/m$	5.09×10^3	1.00×10^4
$cm^2/cy/m$	0.509	1.00
$cm^2/cy/cm$	5.09×10^{-3}	1.00×10^{-2}
$m^2/rad/m$	3.20×10^4	6.28×10^4
$cm^2/rad/m$	3.20	6.28
$cm^2/rad/cm$	3.20×10^{-2}	6.28×10^{-2}

TABLE FOR METRIC CONVERSION OF SPATIAL FREQUENCY

	To find:	
	cy/ft	cy/m
Given:	Multiply by:	
cy/ft	1.00	3.28
cy/in	12.0	39.4
rad/ft	0.159	4.85×10^{-2}
rad/in	1.91	4.04×10^{-3}
cy/m	0.305	1.00
cy/cm	30.5	1.00×10^2
rad/m	4.85×10^{-2}	0.159
rad/cm	4.85	15.9

TABLE FOR METRIC CONVERSION OF
ROUGHNESS PARAMETER UNITS

Given:	To find: in² cy/ft	cm²-cy/m
	Multiply by:	
ft²-cy/ft	144.	3.05×10^{-3}
in²-cy/ft	1.00	21.2
in²-cy/in	12.0	254.
ft²-rad/ft	22.9	485.
in²-rad/ft	0.159	3.37
in²-rad/in	1.91	40.4
m²-cy/m	472.	1.00×10^4
cm²-cy/m	4.72×10^{-2}	1.00
cm²-cy/cm	4.72	100.
m²-rad/m	75.2	1.59×10^3
cm²-rad/m	7.52×10^{-3}	0.159
cm²- rad/cm	0.752	15.9

TABLE OF CONTENTS

TABLE OF CONTENTS (Cont)

LIST OF ILLUSTRATIONS

LIST OF ILLUSTRATIONS (Cont)

LIST OF TABLES

SUMMARY

In support of the Improved Track Structures Research Program
of the Office of Rail Safety Research of the Federal Rail-
road Administration (FRA), the Transportation Systems Center
(TSC) has been conducting studies on the relationship among
track geometry variations, wheel/rail forces and derailment
tendencies. To perform these analyses, it was necessary to
have reliable analytical representations of existing track
geometry. The approach was to establish sound statistical
representations of the universe of track geometry in the
United States from numerous measurements made by the FRA
Test Cars over thousands of miles of track.

In a previous study (1), mathematical representations of
randomly varying track geometry variations were obtained
based on time series analyses of track measurements. How-
ever, it was found that large midchord offset variations
occurred with a significantly higher frequency of occur-
rence than would be predicted from the statistical charac-
terizations in actual track geometry data. Statistical
characterization also omitted infrequent large amplitude
irregularities which would produce occasional large ampli-
tude vehicle responses. These special situations are
obscured by the averaging process associated with PSD's
and other statistical processing but represent cases that
do occur regularly and should be included in vehicle analy-
sis. This report attempts to provide an analytic descrip-
tion of these infrequent large amplitude track geometry
irregularities.

The approach has been to analyze track geometry data pre-
viously collected by the FRA Track Geometry measurement
cars to define the key track geometry features which have
been related to recent derailments. Based upon a review of
this data, characteristic track geometry signatures were

defined as cusp, bump and jog. These key signatures, which
are described in the body of the report, may occur either
as localized defects or in succession or in combination
with one another. Analytical representation for the track
signatures were developed as characteristic functions with
two parameters. One parameter defines the amplitude of the
irregularity while the second defines the duration. Sta-
tistics of both parameters were developed based on a review
of track geometry records.

Studies concurrently being conducted by the Transportation
Systems Center indicated that the harmonic roll response of
freight cars, which has been responsible for a significant num-
ber of derailments, could be controlled by limiting the root mean
squared deviation of crosslevel from a 100 foot moving aver-
age taken over 400 feet to a value of 0.3 inch. Based upon
the analytical representations developed in Reference 1, the
statistical distribution of this proposed crosslevel index
was developed. This distribution was verified by processing
segments of track geometry records to calculate the cross-
level index for track representative of the current FRA
Track classes. The results of these analyses indicated that
specification of a limit of 0.3 inches on the crosslevel
index would affect 75% of Class 1 track, between 3 and 37%
of class 2 track and from 2 to 5% of Class 3 track. The
impact on Class 4,5, and 6 track would be negligible.

Data obtained from 10 miles of class 2 and 3 track collected
in 1978 and 1979 were analyzed to estimate track degradation
rates in terms of the crosslevel index. These analyses
indicated that the data base was insufficient to provide a
reliable estimate. It is recommended that an expanded data
base be developed for obtaining more reliable estimates.

Railhead profile is expected to represent an important fac-
tor in rail car dynamic response to lateral track geometry

irregularities. It is recommended that studies be conducted
to provide characterizations of worn railhead profiles for
inclusion in the characterizations of track geometry varia-
tions.

This report presents an analytical description of dynamically
severe track geometry variations. By developing methods of
minitoring and controlling these variations, the severity of
this dynamic interaction can be reduced.

Analytical representations were developed for the cusp, bump
and jog signatures which could be represented by an amplitude
and a parameter related to the duration. Statistics of both
the amplitude and the duration-related parameters were de-
termined from the study of typical track geometry varia-
tions.

1. INTRODUCTION

1.1 BACKGROUND

Based upon time series analyses of track geometry measurements, mathematical representations of the statistics of the continuous randomly varying components of track geometry were obtained in a previous study (1). The random variations in the track free of anomalies were shown to be described by the models based on the power spectral density (PSD). Such models were represented by a roughness parameter and a set of corner frequencies. The roughness parameter was shown to be related with the speed classification of the track. Parameters related to the corner frequency were invariant or only slightly dependent on the speed classification of track.

Because of its averaging property, the PSD does not adequately represent severe track geometry variations corresponding to joints, anamolies, etc. PSD's also destroy the phase information so that the periodic waveshape can not be reconstructed.

Severe track geometry variations at isolated points and periodic geometry signatures play a major role in train dynamics. Accordingly, this report deals with the analytical descriptions of severe track geometry variations which can cause severe dynamic interaction.

1.2 OBJECTIVES

Principal objectives of this study are summarized as follows:

- To define the key track geometry variation signatures which can be related to severe dynamic interaction.

- To develop the analytical representations of the track variations associated with the key signatures.

- To develop the track geometry descriptors which can be used to monitor the essential dynamic inputs of the key signatures.

- To determine the statistical distribution of track descriptors and to find the relationship between descriptor limits and the U.S. track population.

- To develop the automated and non-automated field measurement techniques for evaluating track descriptors.

- To generate a statistical description of the track which is constrained such that a track descriptor does not exceed a specification limit.

1.3 APPROACH

Recent derailments were studied to identify track features which can be related to severe track-train interaction. Existing track geometry data were reviewed to define the key track geometry signatures associated with these track features, and analytical representations of the key signatures were developed.

Simplified vehicle dynamic analyses were performed to determine the wavelength region of the track inputs which has the greatest effect on vehicle dynamics. Based on these analyses, several track descriptors were developed to monitor the dynamic inputs of key signatures.

Statistical representations of selected geometry descriptors were developed using the existing analytical descriptions of track geometry variations. Results were verified

by processing the existing track geometry data. In addition, statistical analyses were performed to determine the portion of the U.S. track affected by applying the new descriptors as track specifications. A representative sample of the track geometry data were processed to determine the statistical representation of the constrained track. Automated and non-automated measurement procedures were developed to evaluate the selected track descriptors. Conclusions and recommendations that were made based on this study are included in Section 4. of this report.

2. TECHNICAL APPROACH

Severe dynamic interaction can be caused by poor train make-up, poor train handling, equipment failures, human errors, severe track geometry variations, or a combination of these. Severe track geometry variations have been found to play a major role in many derailments because of their interaction with the dynamic characteristics of a vehicle. Vehicle dynamics were analyzed to determine the frequency region of track inputs to which carbody is most responsive.

2.1 TRACK FEATURES RELATED TO DERAILMENTS

National Transportation Safety Board bulletins (2) on derailments were reviewed for the years 1976-1978. These bulletins showed that although poor train make up, poor train handling, and wheel fractures were significant contributors to derailments, track related features may have been major contributors to derailments. Most of the derailments were found to occur on curved track. Of the derailment scenarios studied, 31 percent of the derailments could be attributed, in part, to track related features.

Seventeen trains derailed between 14 January 1974 and 16 December 1976 because of the lateral movement of the outside rail. Two major derailments were, in part, caused by curve-rail (3). In the case of two other major derailments, cross-ties had been replaced and the track regaged just before the derailments. Examinations of track in the vicinity of some derailments indicated variations in gage and irregularities in alignment and crosslevel.

In general, track features related to derailments can be summarized as follows (4):

- Defects in track geometry--These may occur as single severe events, in combination with each other or periodically. All may lead to a derailment. Examples of single events are defects in crosslevel, superelevation, alignment, profile and gage. Combined track geometry defects such as outward alignment in curves along with profile dips may create severe situations. Periodic phenomena may be caused by staggered low joints and/or 90-foot oscillations of alignment. The periodic phenomenon caused by staggered low joints is widely recognized as rock and roll.

- Metallurgical defects--Metallurgical defects include broken rail ends, split head, split web, curve-worn rail, broken switch points, etc.

- Lack of maintenance of track appliances--These include missing guard rails, broken or worn frog points, defects or failures of interlocks and block signal systems, joint failures, etc.

- Vehicle/track interactions--These include dynamic wide gage, rail roll over, dynamic curving, etc.

Track geometry defects related to derailments can be characterized by track geometry parameters such as gage, crosslevel, alignment and profile.

2.2 WAVELENGTHS OF INTEREST

The vehicle, its components and the lading can be considered to be a system of coupled masses, springs and dampers. Track inputs at the wheel/rail interface are first modified by the geometry of the vehicle and then either attenuated or amplified through the vehicle suspension system. The level of attenuation or amplification to the inputs depends on the frequency of the

input excitations. For example, when the excitation frequency coincides with the natural or resonant frequency of the system, the amplification of the input is at a maximum. The dhyamic response of a vehicle can be analyzed to determine the frequency region of track inputs to which the carbody is most responsive.

The vehicle dynamic response can be analyzed by the simple vehicle model shown in Figure 2-2. This model is sufficient to illustrate some of the important points concerning vehicle dynamic response to track geometry variations.

Referring to Figure 2-2, m is the body mass, k is the spring constant, b is the damping coefficient, and m_0 is the unsprung mass. In response to track geometry inputs, x, a displacement, y, is induced in the body mass and a relative displacement, u, is induced between m and m_0. Displacements x, y and u are all functions of time. The equation of motion can be written as

$$m\ddot{y} + b(\dot{y}-\dot{x}) + k(y-x) = 0, \qquad (2.1)$$

where the dots indicate time derivatives.

The transmissibility equation for the motion of m due to motion m_0 is given by (6):

$$|F_1(\omega)| = \sqrt{\frac{1 + 4\beta^2 \dfrac{\omega^2}{\omega_0^2}}{\left(1 - \dfrac{\omega^2}{\omega_0^2}\right)^2 + 4\beta^2 \dfrac{\omega^2}{\omega_0^2}}}$$

$$\text{and} \quad \omega_0 = \sqrt{\frac{k}{m}} \qquad (2.2)$$

$$\beta = \frac{b}{2\sqrt{mk}},$$
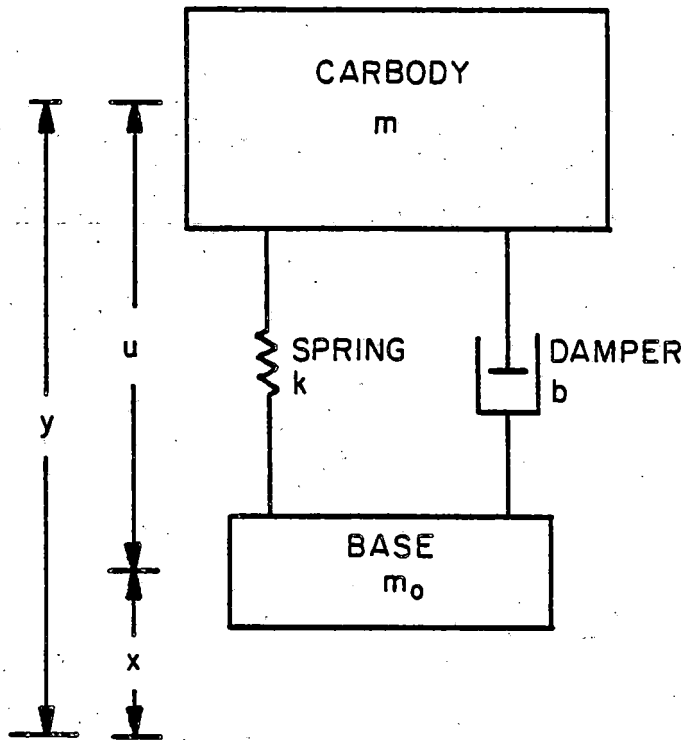
Figure 2-1. Simple Model Illustrating Vehicle
Response to Track Geometry Input

where ω is the frequency of the track geometry input, ω_0 is the natural frequency of the system and β is the damping ratio.

From Equation 2.2, the response function is equal to unity for low frequencies. The sensitivity is at its maximum when the frequency of the track geometry input coincides with the natural frequency of the system where

$$|F_1(\omega)| = \sqrt{1 + \frac{1}{4\beta^2}} .$$

The track inputs with frequencies higher than 1.4 times the natural frequency of the system are attenuated and the response function tends to zero as ω approaches infinity.

As shown in Appendix B, by using the model developed in Reference 1, the standard deviation of the acceleration induced in the carbody due to track profile or alignment with frequencies below the natural frequency of the system, is given by

$$\sigma_a = 4\pi^2 \sqrt{V^3 A \phi_c^2 f'} , \qquad (2.3)$$

where V is the speed of the train in ft/sec, A is the roughness coefficient in in^2-cy/ft, ϕ_c is the break frequency in cycle/ft, and f' is some frequency below the natural frequency of the system in Hz.

Values of σ_a were calculated for f' equal to 0.5 Hz for different track classes and tabulated in Table 2-1. The induced accelerations for frequencies up to 0.5 Hz are less than 0.007 g.

From Reference 6, the response function for the relative displacement between the carbody and the wheelset/side frame is given by:

$$F_2(\omega) = \frac{(\frac{\omega}{\omega_0})^2}{1 - (\frac{\omega}{\omega_0})^2 + 2\beta i (\frac{\omega}{\omega_0})} . \qquad (2.4)$$

2-5

Table 2-1. Acceleration Levels due to Track Profile Inputs
below 0.5 Hz

TRACK CLASS	SPEED		$A^* \times 10^{-4}$ $(in^2 - cy/ft)$	$\phi_c \times 10^{-3}$ (cy/ft)	σ_a $(g's)$	RMS** Acceleration from 0-54 Hz $(g's)$
	mph	fps				
1	15	22	7.9	7.1	0.001	0.025
2	30	44	4.5	7.1	0.003	0.029
3	60	88	2.5	7.1	0.006	0.048
4	80	117	1.4	7.1	0.007	0.050
5	90	132	0.79	7.1	0.007	0.042
6	110	161	0.45	7.1	0.007	0.040

*From Statistical Representations of Track Geometry (1).
**For resonant frequency of 1.0 Hz and damping ratio of 0.7.

For very low frequencies, the relative displacement sensitivity
varies as ω^2/ω_0^2. In the high frequency limits, the response
function approaches unity.

From Appendix B, the relative displacement, σ_d, due to profile or align-
ment inputs of frequencies below the resonant frequency, f_0, is
given by

$$\sigma_d = \sqrt{\frac{V^3 A \phi_c^2 f'}{f_0^4}}.$$

(2.5)

Values of σ_d due to track profile are listed in Table 2-2. These
values were calculated for $f' = 0.5$ and $f_0 = 1$ Hz. It can be seen
that the relative displacement induced is less than 0.07 inch.

Table 2-2. Relative Displacements due to the Track Profile Inputs below 0.5 Hz

TRACK CLASS	SPEED (fps)	$A^* \times 10^{-4}$ $(in^2 - cy/ft)$	$\phi_c \times 10^{-3}$ (cy/ft)	σ_d (inches)	RMS** Displacement from 0-54 Hz (in.)
1	22	7.9	7.1	0.014	0.07
2	44	4.5	7.1	0.028	0.12
3	88	2.5	7.1	0.064	0.17
4	117	1.4	7.1	0.071	0.17
5	132	0.79	7.1	0.071	0.15
6	161	0.45	7.1	0.071	0.14

*From Statistical Representations of Track Geometry (1)
**For resonant frequency of 1 Hz and damping ratio of 0.7.

The response function (see Appendix B) for the forces induced at the wheel/rail interface due to track inputs is given by

$$F_3(\omega) = -m_0\omega^2 \left(\frac{-m\omega^2 + \left(1 + \frac{m}{m_0}\right)\left(bi\omega + k\right)}{-m\omega^2 + bi\omega + k} \right). \qquad (2.6)$$

For low frequencies, $F_3(\omega)$ varies as $-(m_0 + m)\omega^2$. In high frequency limits, $F_3(\omega)$ varies as $- m_0\omega^2$ and the suspended mass is effectively isolated. The forces acting across the wheel/rail interface due to track inputs of very small frequencies below the resonant frequency are less than one percent of the vertical static.

The track inputs of frequencies below the resonant frequency of the system have been shown to induce insignificant amounts of acceleration in the carbody, the relative displacement, or the forces across the wheel/rail interface. Also, at very high

frequencies, all the displacement is taken by the suspension
system and the suspended mass is effectively isolated. Thus
the track inputs at frequencies well removed from the resonant
frequencies of the system are not expected to be significant for
vehicle dynamic response analyses.

Rail cars and locomotives are sprung by one or more stages of sus-
pension such that the natural frequencies of the rail vehicle
motion, such as bounce, yaw, roll and pitch, are between 0.7 and
3 Hz. These frequencies correspond to different wavelengths
depending on the speed of the train.

Wavelength is related to the temporal frequency by

$$\lambda = \frac{v}{f},$$
(2.7)

where f is the temporal frequency in cycles/second, v is the speed
in feet/second and λ is the wavelength in feet.

A top speed of 110 mph corresponds to a wavelength of 230 feet at
a resonant frequency of 0.7 Hz. On the other hand, a low speed of
10 mph corresponds to a wavelength of 4 feet at a resonant fre-
quency of 3.5 Hz. Thus the wavelength region of interest lies
between wavelengths of 3 and 300 feet. Track inputs of wave-
lengths outside this region are not as important to the vehicle
dynamics. However, such inputs may be important for other
reasons.

In the broad spectrum of 3 to 300 feet, certain wavelengths are of
particular interest. It was shown in the study of statistical
characterization of track (1), that track with jointed rails
has a strong periodic component induced by wavelengths equal
to the rail length. This periodic phenomenon causes the well
known rock and roll behavior which can lead to derailments.

The geometrical construction of a truck makes it more sensitive to
a certain range of inputs and less sensitive to others. Vehicle
sensitivity in lateral and yaw modes of motion is analyzed in

Appendix B. Figures 2-3 and 2-4 show the ratio of vehicle motion
amplitude to track input amplitude in the lateral and yaw modes due
to truck spacing. The most significant input wavelength is equal
to the truck spacing for translation and twice the truck spacing
for yaw. These figures can also be used to indicate the sensitivity
to track input in carbody bounce and pitch modes for a two axle
truck if ℓ is set equal to the axle spacing. The profile per-
turbations of wavelengths close to the axle spacing would strongly
affect truck bounce; whereas wavelengths close to twice the axle
spacing would have a more pronounced effect on truck pitch.

In summary, track inputs can be divided into three wavelength
regions. The wavelengths much larger than the resonant wavelengths
are important primarily for train handling and need not be con-
sidered for single vehicle dynamic response analysis. Wavelengths
shorter than 3 feet could cause component fatigue, but as such are
not related to dynamic response motion which could cause a car to
leave the track. The wavelength region between 3 and 300 feet is
important from the vehicle dynamic point of view. Track inputs
in this region may lead to response motions which could result in
derailments. Thus, track geometry descriptors and measurement
techniques should emphasize these wavelengths.

2.3 CURRENT TRACK GEOMETRY MEASUREMENTS

Track maintenance standards based on geometrical measurements have
been used by railroad engineers since the early years of railroad-
ing. The availability of automated measuring equipment has in-
creased the usage of track geometry measurements, and classifica-
tion thresholds have been defined in the Federal Track Safety
Standards (5). These standards are now used by the railroad in-
dustry in addition to their own standards.

During the initial layout and construction of railroad tracks,
station and line references are established through survey tech-
niques. The vertical and lateral alignment of rails is accomplished
by maintaining the proper distance offsets from the survey refer-
ence lines to the lining rail. Gage then determines the position
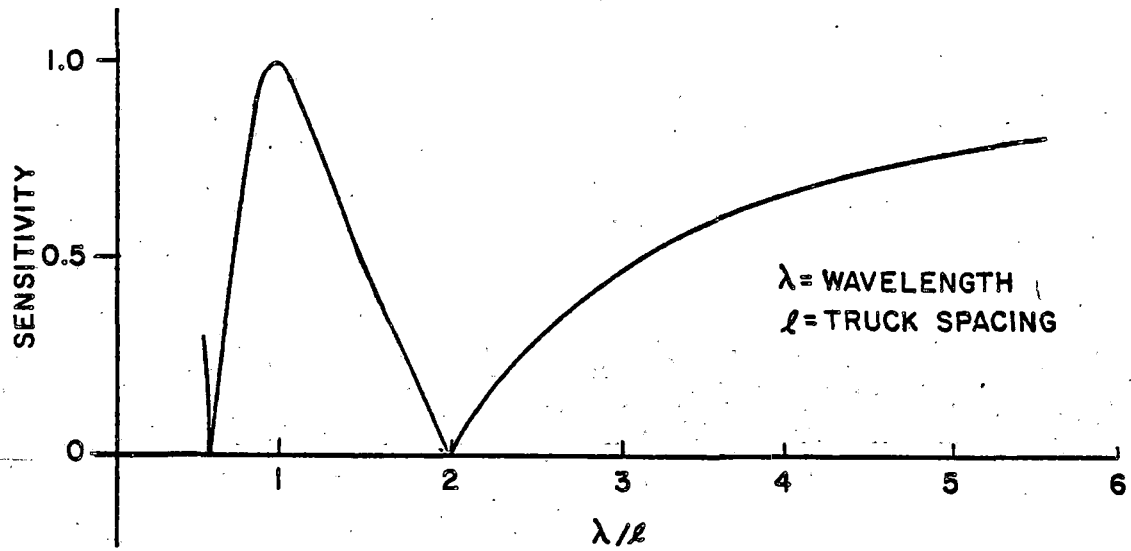
Figure 2-2. Vehicle Lateral Response to Track Alignment
Disturbances
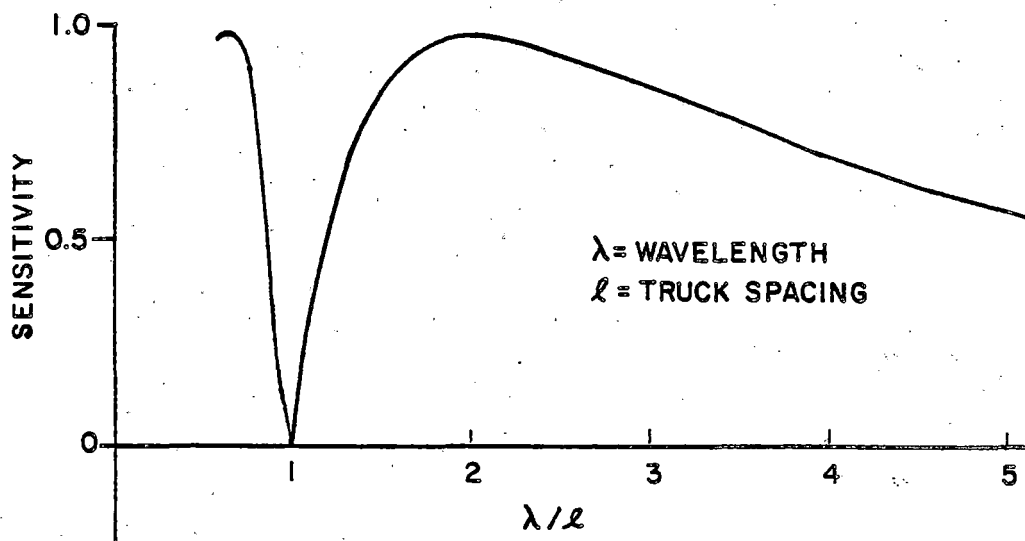
Figure 2-3. Vehicle Yaw Response to Track Alignment
Disturbances

of the second rail, followed by the introduction of proper super-
elevation to the outer rail in curves. The survey-type absolute
references are generally lost after the initial construction.
Evaluation or maintenance of the track in subsequent years are
largely based on relative measurements of track geometry. Param-
eters like gage, profile mid-chord offset (MCO) and alignment MCO
are commonly used. Track geometry standards in the form of maximum
allowable deviations in the relative measurements are used both in
maintenance and for assuring safety. These relative measurements
do not give a direct indication as to whether the rails conform to
their original design which allows any long-term drift of track
position to go undetected.

The simplest method to make a field measurement of rail vertical
or horizontal variations (profile or alignment) is the process of
"string lining" the track. This involves stretching a string
against the rail and measuring the gap between string and rail at
the center of the string. This is known as the mid-chord offset,
and is the traditional method of measuring track variations. The
most commonly used MCO is the 62-foot MCO which is incorporated
in the current Federal Track Safety Standards.

As shown in Appendix C, the frequency/wavelength response of an
MCO is given by

$$F(\phi) = 2 \sin^2 (\pi\phi L), \tag{2.8}$$

and

$$F(\lambda) = 2 \sin^2 \left(\frac{\pi L}{\lambda}\right), \tag{2.9}$$

where ϕ is the spatial frequency in cycles/foot, λ is the wave-
length in feet and L is one-half the length of the MCO in feet.

The wavelength response of a 62-foot MCO is shown in Figure 2-5.
Several features of the wavelength response of an MCO are important.
For example, the sensitivity to wavelengths larger than 200 feet
is less than 0.5. In addition, an infinite number of zero
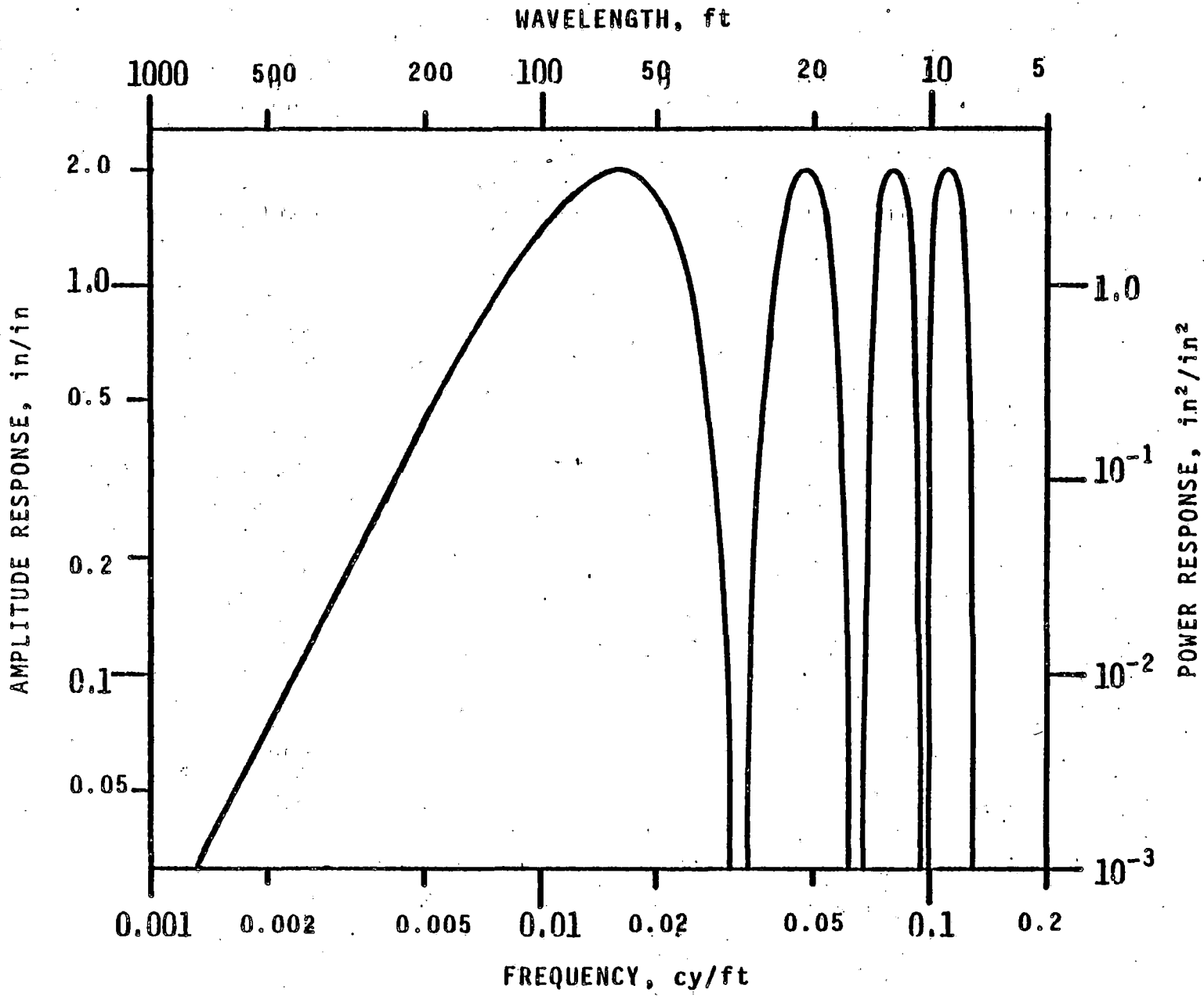
WAVELENGTH, ft

Figure 2-4.   Frequency/Wavelength Response of 62-Foot Mid-chord Offset

sensitivity or "blind" spots exist in the chordal response. As shown in Figure 2-5, a 62-foot MCO will not detect wavelengths of 31 feet, 15.5 feet, 10.33 feet ... (31/n, n = 1, 2, 3 ...). The node at 31 feet is particularly important due to the presence of some track with rail lengths of 33 feet which can show up as a strong periodic variation. Even the wavelength of the 39-foot rail lengths is attenuated to 72 percent of its amplitude. Wavelengths of 62 feet, 20.67 feet, 12.4 feet ... (62/n, n = 1, 3, 5 ...) appear at 200 percent of their amplitude indicating that variations of these wavelengths will be over emphasized. The blind spots and unequal weighting make the use of the 62-foot MCO (and for that matter an MCO of any other chord length) deficient since it does not give sufficient coverage of the important spatial wavelengths.

2.4 NEED FOR ADDITIONAL TRACK GEOMETRY DESCRIPTORS

In the previous section, it was shown that the 62-foot MCO does not adequately cover the wavelength region of interest. Since the wavelengths from 3 to 300 feet are important to vehicle dynamic response, it is necessary to develop additional track geometry descriptors that can be more closely identified with significant track inputs to the vehicle dynamic response. An alternate set of descriptors will be given in Section 3.0 which will be adequate to control severe track geometry variations.

2.5 METHODOLOGY

Track geometry data collected by the automated track inspection vehicles were reviewed to identify key track geometry signatures which might cause severe dynamic response. Track geometry descriptors were developed to monitor the essential dynamic inputs which result from key track geometry signatures. These descriptors are the result of arithmetic operations on the basic track geometry parameters. Alternate descriptors were developed to provide equivalent information for key signatures.

Of these descriptors, a set capable of yielding information on selected key signature inputs was selected. Measurement techniques are described to monitor these track descriptors.

Statistical representations of the selected descriptors were developed analytically based on available track geometry varia- tion models. Track geometry data for each of the current FRA track classes were processed to verify the statistical dis- tribution of selected track geometry descriptors. In each of the FRA track classes, twenty miles of track geometry data from different sections of U.S. track were selected at random. A constraint was applied to the track such that the track descriptors would not exceed the values specified in a candidate performance statement provided by TSC for controlling harmonic roll inducing crosslevel track inputs. The track geometry data were processed to determine the statistical representation of this constrained track.

Regression analysis was performed on track geometry data col- lected in 1978 and 1979 to determine the track degradation rates. Based on the results of this analysis, inspection strategy was developed to ensure track compliance with the track descriptor specifications.

3. RESULTS AND DISCUSSIONS

3.1 KEY SIGNATURES

3.1.1 IDENTIFICATION

Observations of track geometry data reveal that the variations of crosslevel, profile, and alignment are made up of three key signatures, the cusp, bump and jog.* These key signatures occur either as singularities, in succession or in combination with each other. The severity, number and arrangement of these signatures can combine to cause a derailment.

3.1.1.1 Cusp

A cusp is a pointed-end signature formed by two oppositely directed curves. This signature is usually observed at joints in bolted rail in crosslevel and profile. The shape of the cusp signature is shown in Figure 3-1. The disturbance has its peak amplitude at the center and returns to the baseline on either side. A distinguishing feature of the cusp is a distinct discontinuity in the first derivative at the center. The cusp can be described by any of the following analytical forms.

$$
\begin{align}
&\text{(a)} \quad y = Ae^{-k|x|} \\
&\text{(b)} \quad y = A(1-\sin|\pi kx|) \tag{3.1}\\
&\text{(c)} \quad y = A(|2kx|-1)^2,
\end{align}
$$

where A is the peak amplitude and k is the duration related constant.

---

*Track geometry data were analyzed in the space curve representation. The space curve is a pseudo reconstruction of track without the effects of local terrain. The shapes of signatures are distorted due to the high-pass nature of the space curve.
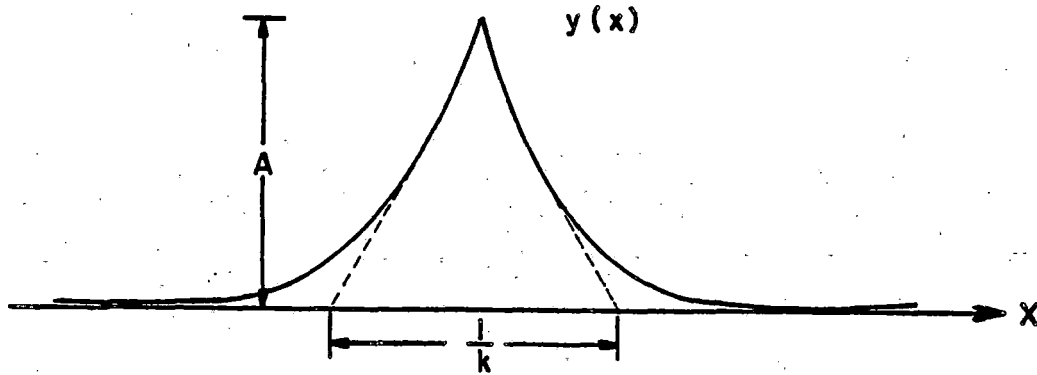
(a)   ABSOLUTE   SURVEY
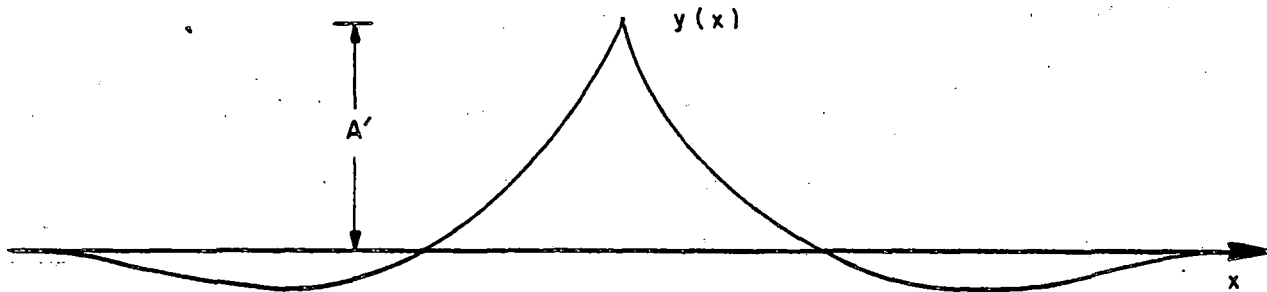
(b)   RESPONSE OF SPACE CURVE

Figure 3-1.   Cusp Signature

The exponential form (a) is suitable for mathematical analysis, however, it cannot be simulated by stable recursive algorithms. The sinusoidal form (b) is more easily simulated than the expontial form. The quadratic form (c) is most readily simulated by a moving strip algorithm.

3.1.1.2 Bump

The bump signature is shown in Figure 3-2. This is a bell shaped curve which usually occurs at a depression in the rail. This signature also attains the peak amplitude at the center and returns to the baseline on either side. The function and at least its first derivative are continuous throughout the disturbance. The descriptive analytical forms for bump are

(a) $\quad y = D \text{ sech } (kx)$

(b) $\quad y = De^{-\frac{1}{2}(kx)^2}$ $\hspace{3cm}$ (3.2)

(c) $\quad y = \dfrac{D}{1+k^2x^2}$,

where D is the amplitude at x=0, and k is the duration related constant.

The bump signature can be simulated by the following finite impulse form:

$$y = D \begin{cases} 0, & \dfrac{\sqrt{6}}{k} \leq |x| \leq \infty \\[3mm] \dfrac{3}{2} + \dfrac{1}{4}(kx)^2 - \sqrt{\dfrac{3}{2}}(\text{sgn } x)kx, & \dfrac{\sqrt{\frac{2}{3}}}{k} \leq |x| \leq \dfrac{\sqrt{6}}{k} \\[3mm] 1 - \dfrac{1}{2}(kx)^2, & |x| \leq \dfrac{\sqrt{\frac{2}{3}}}{k} \end{cases} \quad . \quad (3.3)$$

y(x)

$D[1 - \tfrac{1}{2}(kx)^2]$

$\dfrac{1}{k}$

a) ABSOLUTE SURVEY

y(x)

D' D''

б) RESPONSE OF SPACE CURVE
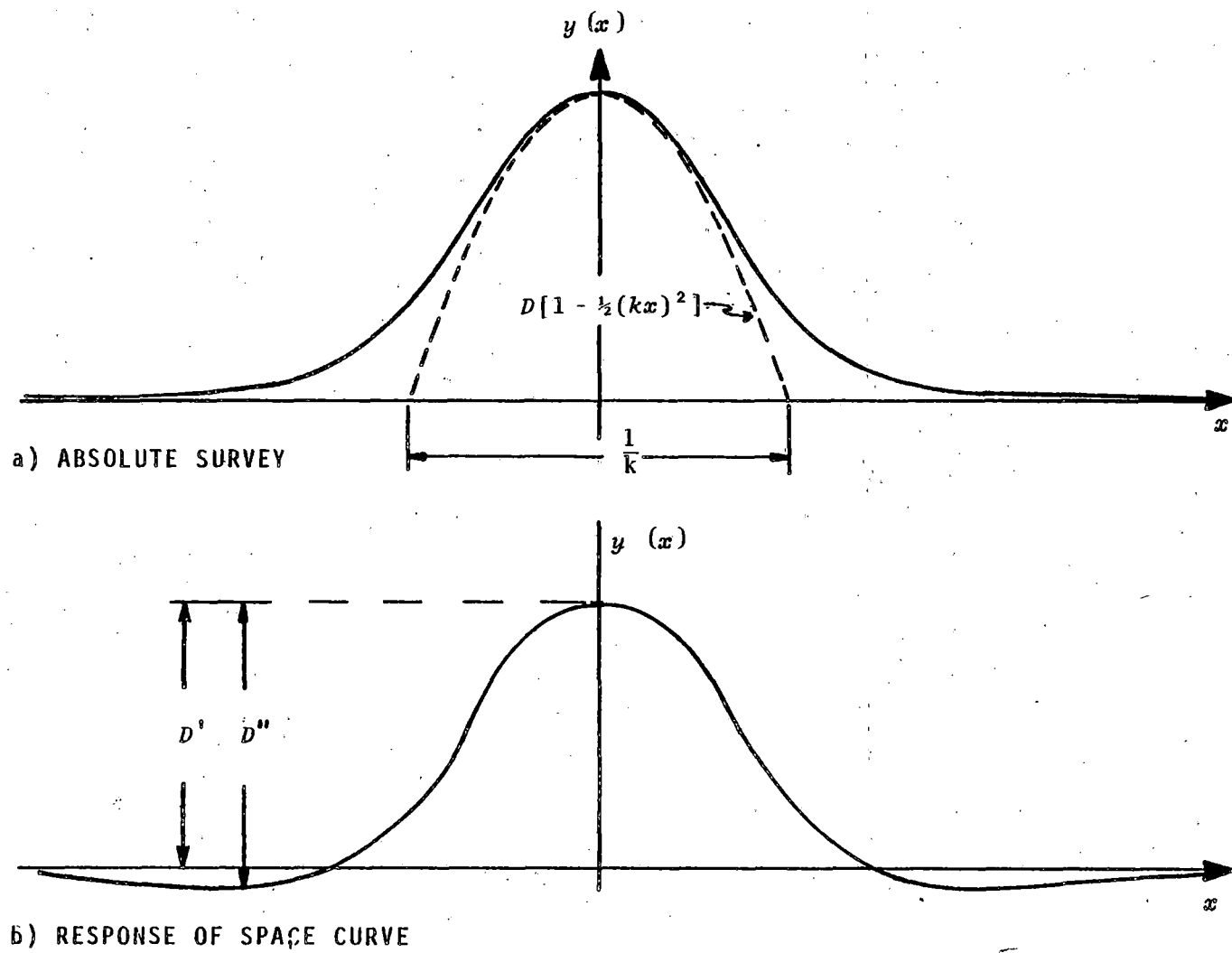
Figure 3-2.   Bump Signature

3.1.1.3 Jog

The jog signature is shown in Figure 3-3. This is a very
critical signature and can occur in both the profile and
alignment. In the case of jog, the signature does not return
to the base line and the disturbance reaches its maximum
amplitude away from the center. The candidate analytical
forms for jog are:

(a) $y = \frac{1}{2} D \tanh (2kx)$

(b) $y = \frac{D}{\pi} \tan^{-1}(\pi kx)$ $\qquad$ (3.4)

(c) $y = \frac{1}{2} D \; \text{erf} \; (\sqrt{\pi} kx)$

(d) $y = \dfrac{Dkx}{\left[1 + 4k^2 x^2\right]^{\frac{1}{2}}}$,

where D is the maximum amplitude and k is the duration related
constant.

The jog signature can be simulated by the following finite
impulse form:

$$y = D \begin{Bmatrix} \frac{1}{2} \, \text{sgn} \, x, \; \frac{9}{8k} \le |x| \le \infty \\[2mm] \frac{32}{81} (kx)^3 + \frac{3}{2} \, kx - \text{sgn} \, x\left[\frac{4}{3} (kx)^2 + \frac{1}{16}\right], \\[2mm] \frac{3}{8k} \le |x| \le \frac{9}{8k} \\[2mm] -\frac{64}{81} (kx)^3 + kx), \; |x| \le \frac{9}{8k} \end{Bmatrix} . \quad (3.5)$$
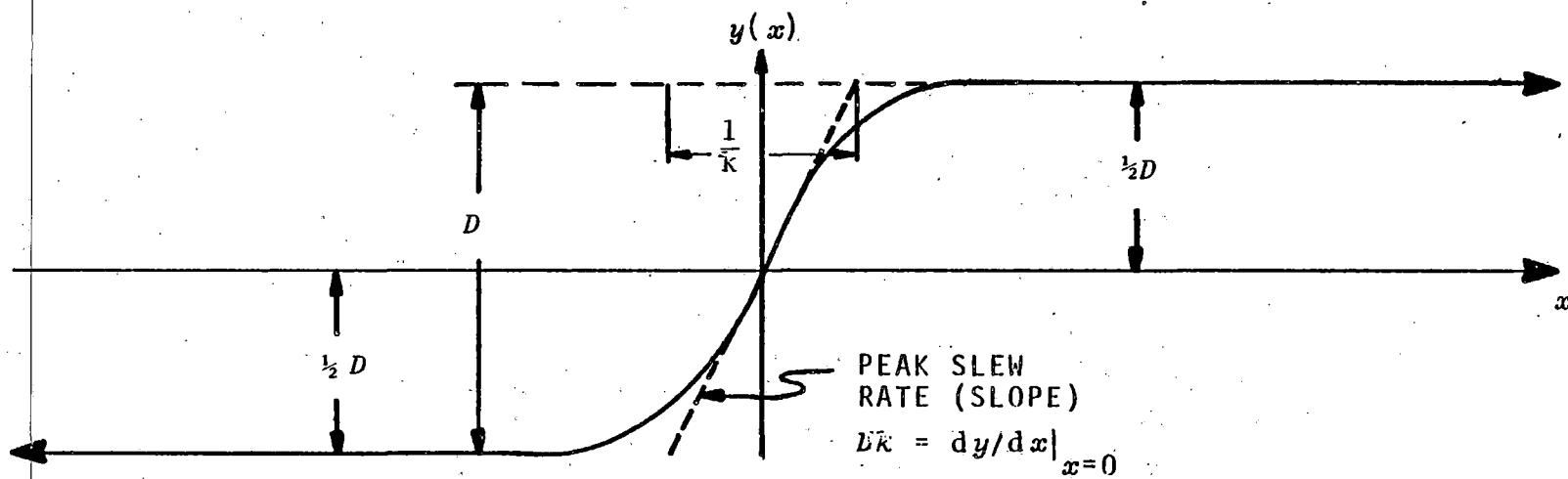
a) ABSOLUTE SURVEY
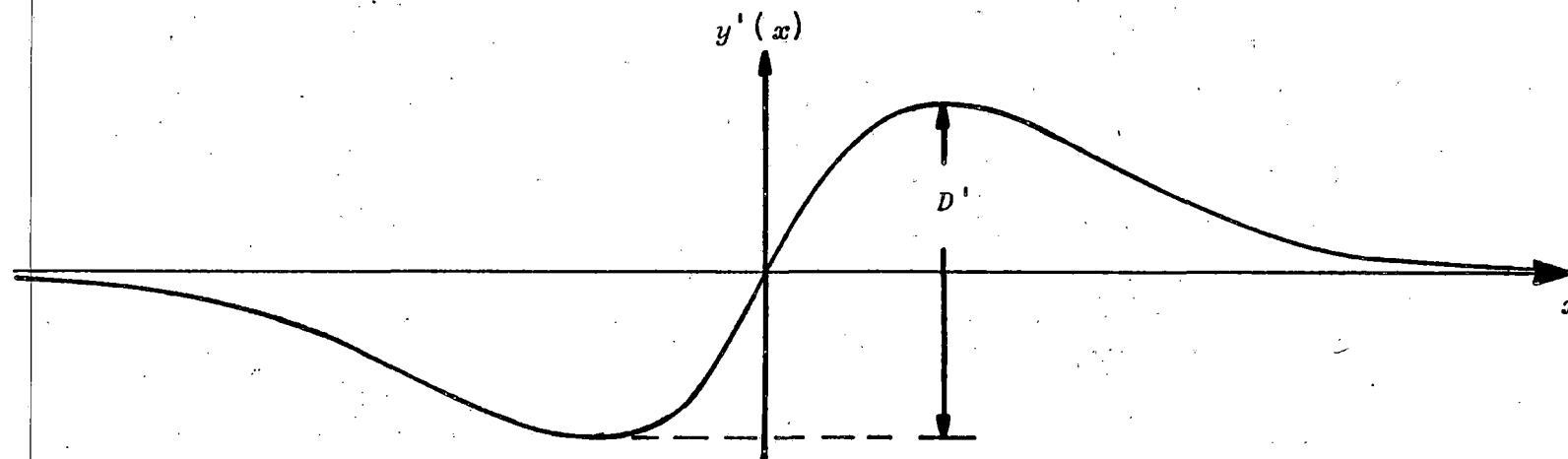
b) RESPONSE OF SPACE CURVE

Figure 3-3. Jog Signature

3.1.1.4 Periodic Structures

When the behavior of the track is considered in the context of its interaction with vehicles, periodic structures are seen to be important factors in producing potential derailment situations. The periodic behavior often observed in crosslevel for lower class track can result in dangerous oscillatory behavior of a consist.

The periodic crosslevel deviations usually arise on lower class track with half-rail-length, staggered, bolted track. Since depressions often develop at joints, the half-stagger results in alternating low spots on each rail. In the track geometry data, this behavior is usually evident in the crosslevel traces.

Other periodic behavior can exist in track. For example, alignment measurements often reveal 90-foot wavelengths which have been impressed on the track due to the dynamic behavior of passing consists. This again creates a situation where a perturbation can cause a derailment.

Data from a region of track exhibiting this periodic behavior are shown in Figure 3-4. This section includes a reverse curve with a short bridge over a river. The geometry traces reveal that at the bridge there are oscillations with 90-foot wavelengths (2½ rail lengths) in alignment. These oscillations are in phase for both rails, build up through five discernible cycles in the spiral west of the bridge, reach a maximum excursion of 1.0 inch peak-to-peak at the middle of the long span, and decay through four discernible cycles in the reverse spiral at the east end of the bridge. These alignment oscillations, which are analogous to the rock and roll behavior observed in crosslevel, have apparently been impressed on the track by the dynamic behavior of the vehicles. Marshy characteristics of this region have probably played a role in the development of this signature.
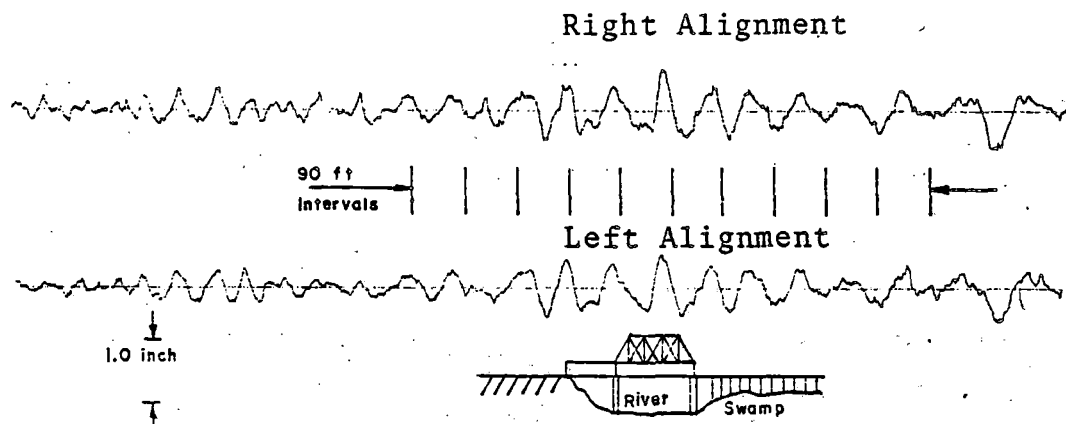
Figure 3-4. Periodic Alignment Behavior

3.1.2 TYPICAL OCCURRENCES OF KEY SIGNATURES

Typical occurrences of key signatures are identified in Table
3-1. These are listed as individual occurrences, occurrences
in combination with each other, and as periodic structures as
observed in track profile, alignment and crosslevel. The
columns left blank are occurrences that could not be found
in the observed track geometry data.

The cusp sometimes appears by itself in either one or both
rail profiles. Isolated cusps occur at a joint in continuous
welded rail (CWR). A single cusp usually occurs at joints
where a cusp on one rail is usually accompanied by a depres-
sion on the opposite rail. This may be due to vehicle dynamic
behavior or track structure. An example of cusps on one
rail and bumps on the opposite rail is shown in Figure 3-5.
A series of cusps can occur in single rail profile or cross-
level near turnouts and interlocks. Alternating cusps in
crosslevel causes rock and roll phenomena. An example of
the typical rock and roll track is shown in Figure 3-6.

3-8

Table 3-1. Indentification of Critical Track Geometry Variation Signatures

		Individual Occurrence	Systems of Occurrences			Periodic Structures
			CUSP	JOG	BUMP	
Mean Profile	CUSP					
Mean Profile	JOG	Change in track structure (Stiffness)		Bridges and Grade Crossings		
Mean Profile	BUMP	Localized soft spot		Bridges and Grade Crossings	• Mud Spots (a succession of bumps)	Quasi-Periodic Succession of Bumps
Single Rail Profile (Crosslevel)	CUSP		• Insulated joints • CWR Buffer Rail • Turnouts	------------->	• Bumps in rail opposite single or double cusps	Rock and Roll
Single Rail Profile (Crosslevel)	JOG					
Single Rail Profile (Crosslevel)	BUMP	Low Spot in one rail				
Mean Alignment	CUSP					
Mean Alignment	JOG					
Mean Alignment	BUMP				Succession of Bumps at 90-foot intervals	Vehicle induces 90-foot bumps (S, C, I)
Single Rail Alignment	CUSP	Bolted Joint is CWR (Curve or Spiral)		Turnout (Points and Frog)		• 39-foot high-rail • 39-foot alternating in/out joints high-rail (S or C)
Single Rail Alignment	JOG					
Single Rail Alignment	BUMP					

S - Spiral, C - curve, I - Hi-speed interlock

Left Profile Space Curve

Right Profile Space Curve
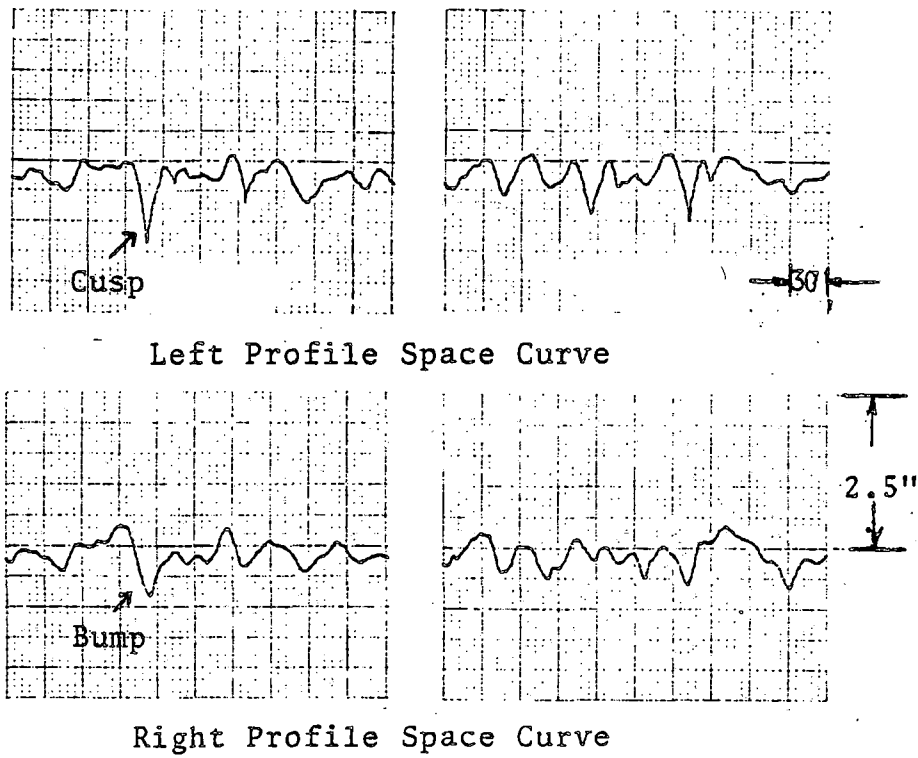
Figure 3-5(a). Bumps and Cusps in Profile in Turnout
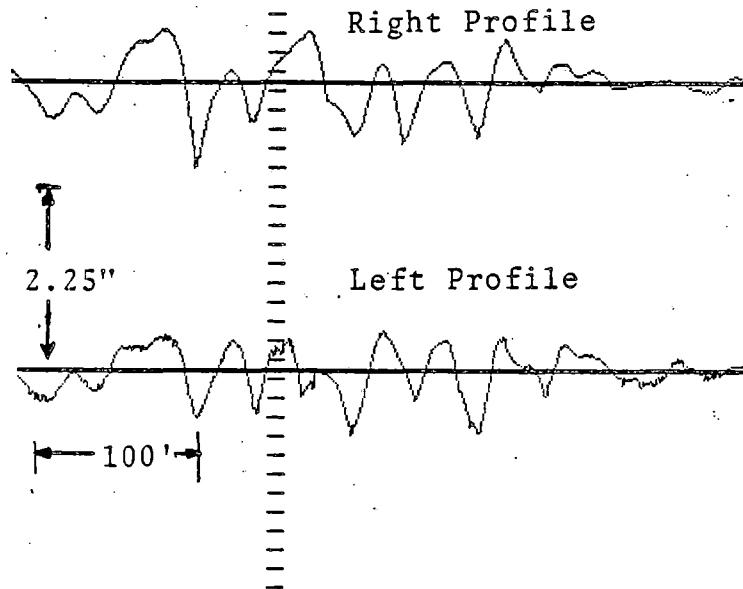
Figure 3-5(b). Series of Bumps in Profile Near
Road Crossing
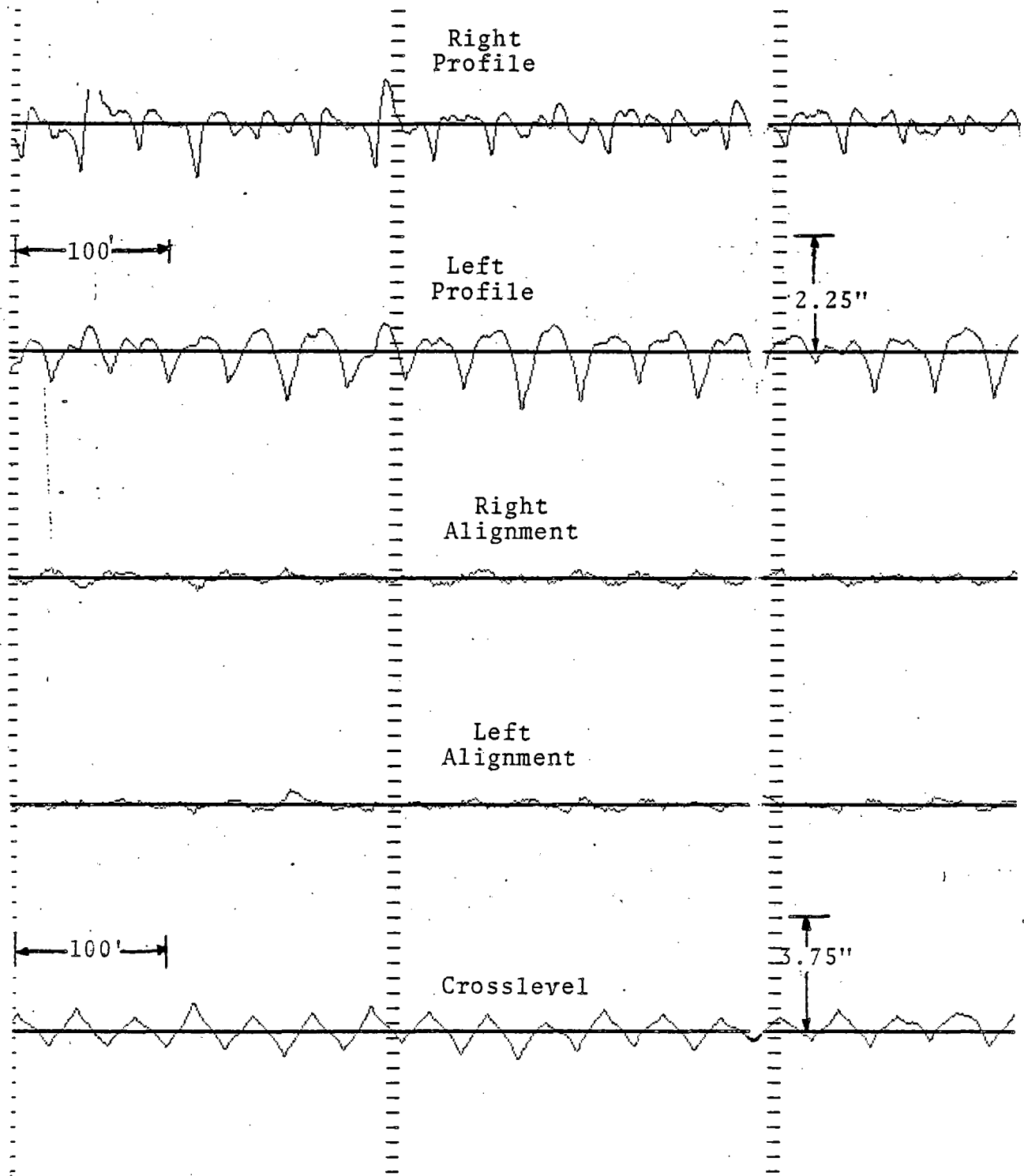
Figure 3-6. Example of Series of Cusps In
Profile and of Rock and Roll Track
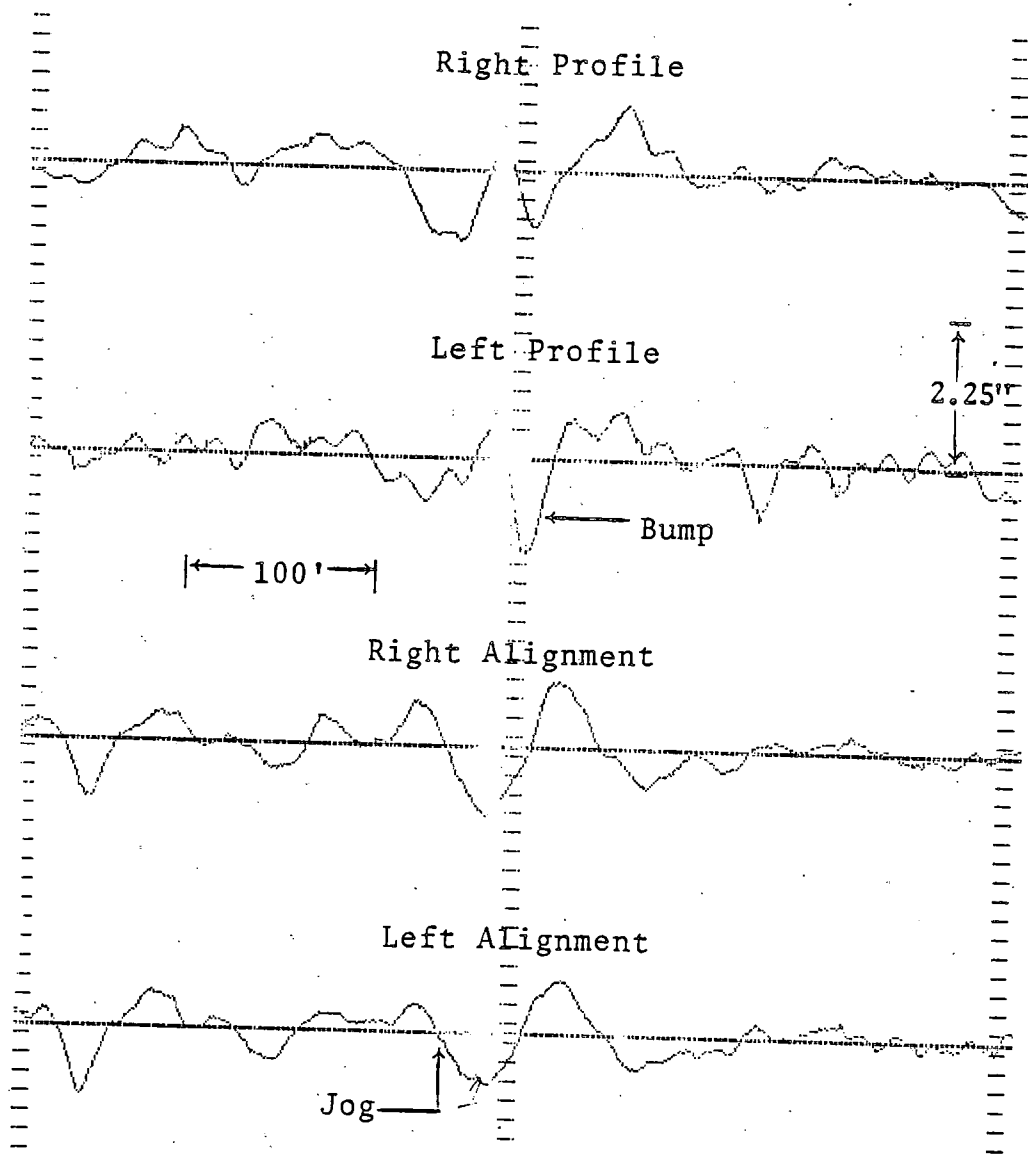
Figure 3-7. Single Bump in Profile and a Jog in Alignment Near River Bridge

A periodic cusp-behavior in single rail alignment is sometimes observable in curves and spirals. This usually occurs every 39 feet (one rail length) in the high rail. The alternating 39-foot joints may create a periodic 78-foot wavelength behavior. A periodic behavior in alignment can interact with crosslevel roll and result in a serious derailment situation.

A bump in one rail is also normally accompanied by a bump in the opposite rail. However, a single bump may occur in profile due to localized soft spots. An example of a single bump is shown in Figure 3-7. A single bump can also occur in mean alignment in curves and grade crossings as shown in Figure 3-8. Periodic bumps are observed in tangents near interlocks. When the train exits high speed interlocks it changes from a curve-type motion to tangent-type motion and as a result bounces back and forth a few times. This produces characteristic 90-foot periodic bumps in mean alignment which are a vehicle induced phenomenon caused by a typical 45-foot distance between truck centers.

A jog in mean alignment can occur by itself (Figure 3-9(a)) due to changes in track structure. This happens when going from one weight rail to another, from a solid track to a bridge or from an area of track which has been maintained to one which has not been maintained. A pair of jogs can occur in alignment near grade crossings and bridges. An example of a pair of jogs found in a curve is shown in Figure 3-9(b). Systems of jogs are found both in profile and alignment near bridges and in curves. A jog typically occurs in a dogleg spiral. Spirals are laid out as a transition region to ease vehicles from tangent sections into curves and vice versa; however, over many years and under megatons of traffic per year, the curve body will work outward. The change that occurs is illustrated in Figure 3-10(a). As track is moved outward from its original curve, a dogleg develops at the
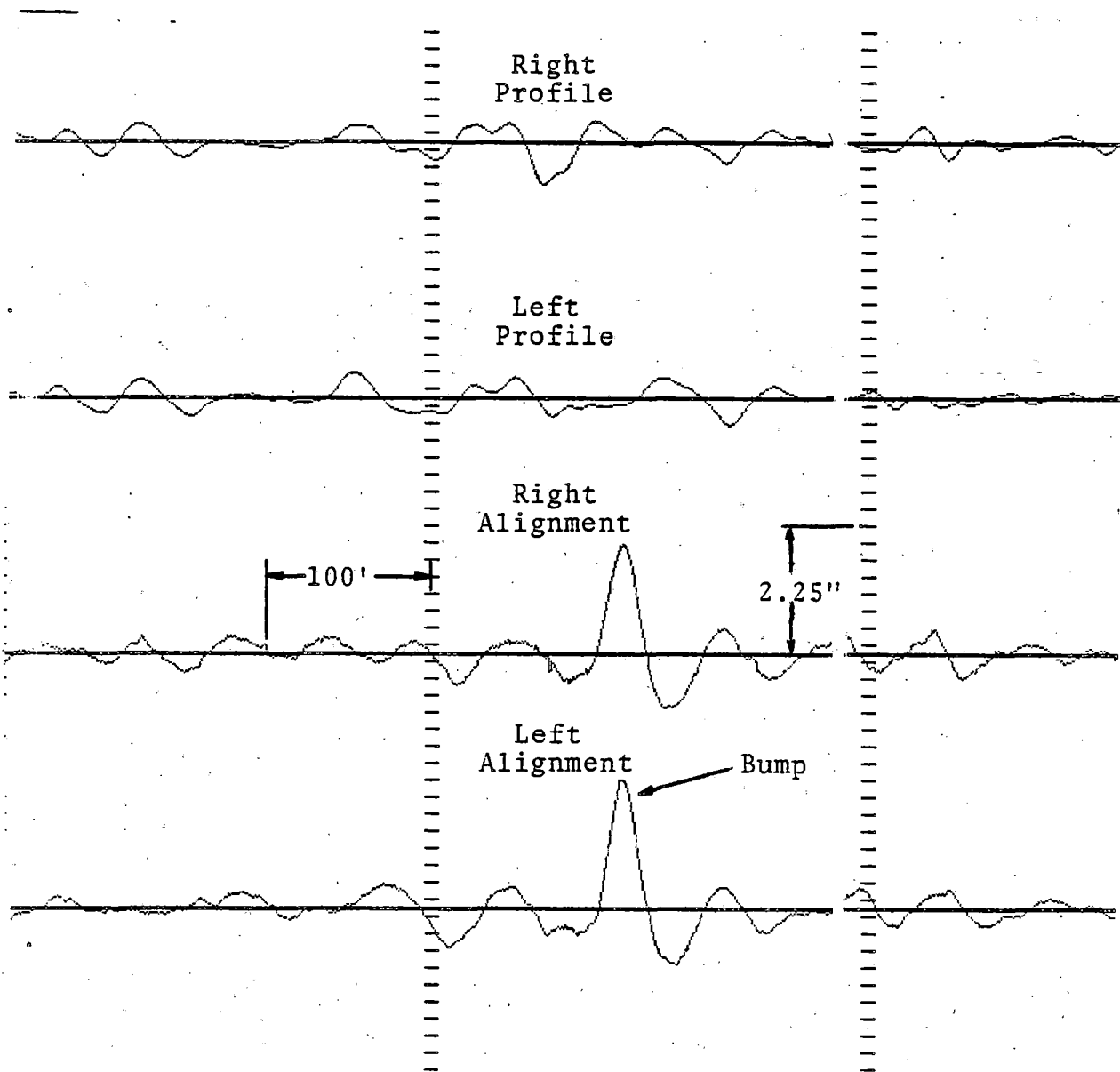
Figure 3-8. Single Bump in Alignment
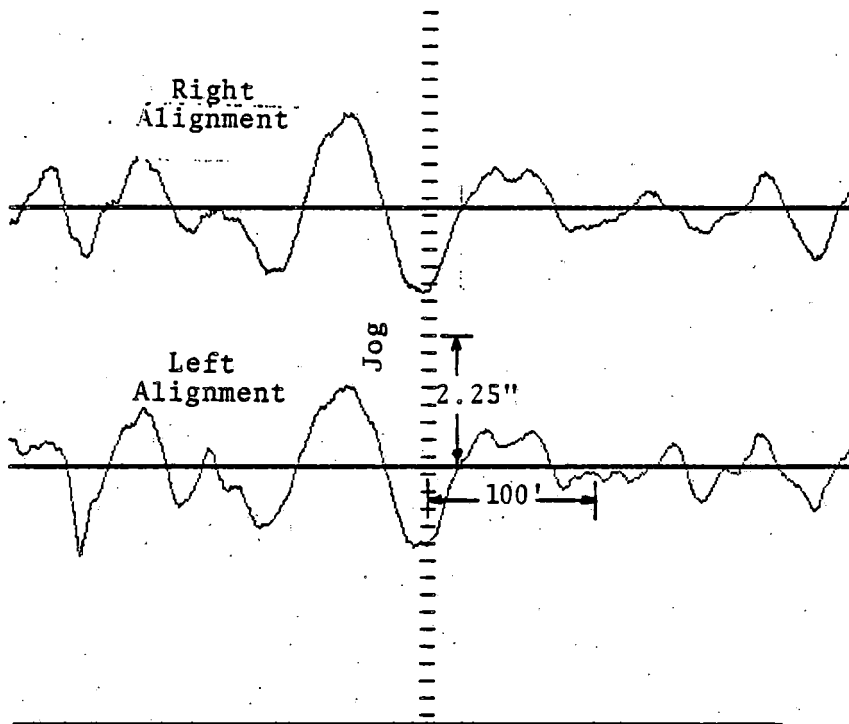
Figure 3-9(a). Single Jog in Alignment Near Bridge
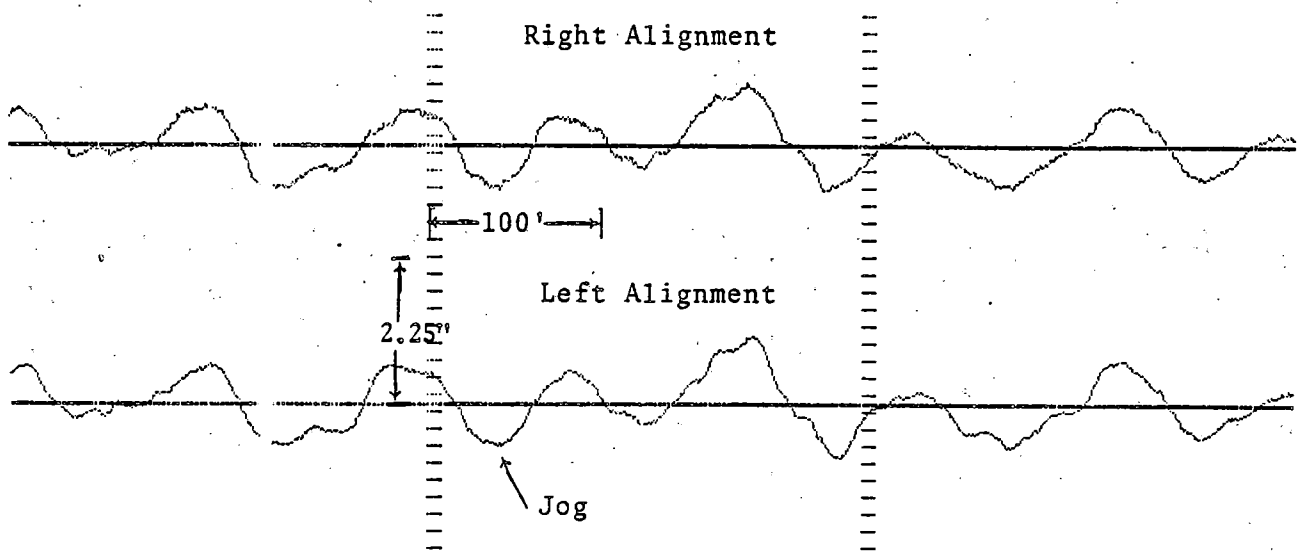
Figure 3-9(b). Series of Jogs in Alignment Near a Curve

Tangent ——►|◄— Transition ►|◄— Curve Body

Current Track Line
(As Refurbished)

Original
Survey Line
(As Laid)

A
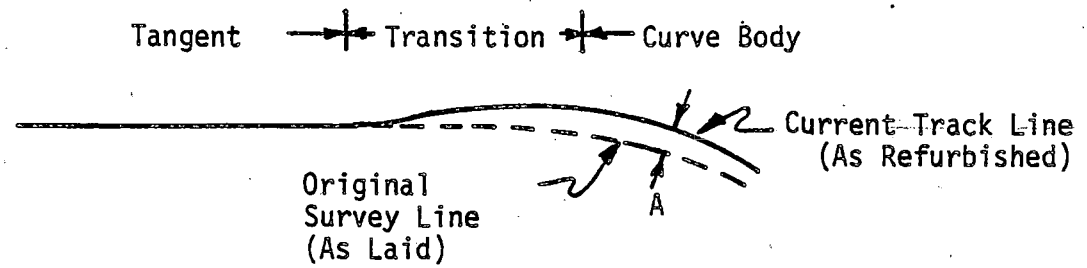
a. Plan View, Absolute Space Curve
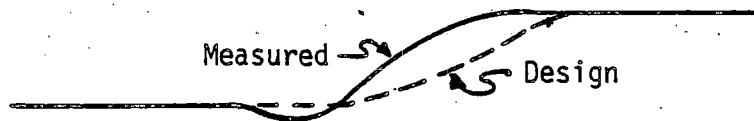
Measured

Design

b. Design vs. Measured Curvature

½A

A
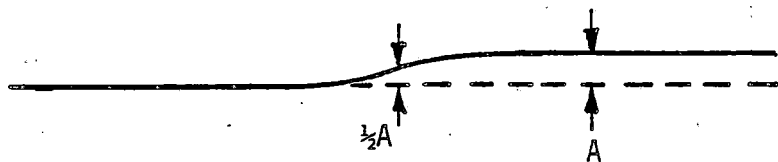
c. Design vs. Measured Alignment Deviations:
   Absolute Deviation Space Curve

90 feet

½ A'   A'
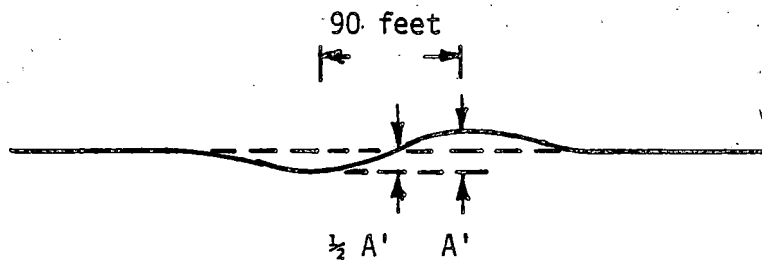
d. Design vs. Measured Alignment Deviation:
   Pseudo Space Curve

Figure 3-10. Dogleg Alignment Anomaly

3-16

entry point. Figure 3-10 also illustrates how this anomaly
appears in the track geometry data. Figure 3-10(b) indicates
the effect on curvature data. Figure 3-10(c and d) illustrates
how alignment traces are affected by this mis-spiral condition.
Doglegs developing in spirals can be a serious maintenance
problem for two reasons: the lining and surfacing machines
could enhance the dogleg characteristics and maintenance crews
may attempt to correct the problem by adjusting crosslevel
rather than alignment, again enhancing the problem.

3.1.3 STATISTICAL PARAMETERS

Table 3-2 lists the parameters associated with critical
signatures as found in various track structures. Duration
related parameters are usually a function of track stiff-
ness and are fixed for a section of track. Free parameters
are related to track degradation.

The key signatures are characterized by amplitude which is
a free parameter and duration which is a fixed parameter.
Values of the fixed parameter as found in track geometry
data are listed in Table 3-3. The duration of a signature
is proportional to $1/k$ where k is the constant used in the
analytical forms of key signatures. Different values of
k are found in different track classes. The value of k
usually decreases with the track class.

A 62-foot MCO was passed through the fundamental signatures.
An analytical description of this process is given in Appendix
C. The ratios of 62-foot MCO's to the maximum amplitude of
key signatures are given in Table 3-4. As the duration of
a signature increases, the sensitivity of the MCO decreases.
The 62-foot MCO does not badly distort the amplitude of a

Table 3-2. Statistical Parameters of Analytic
Representation of Critical Track Signatures

Situation	Analytic Representation	Free Parameters	Restricted Parameter
Normal new welded rail	Periodically modulated random process	1 Mean amplitude	1 Decay rate
Bolted jointed rail	Periodically modulated random process	1 Mean amplitude	1 Decay rate
Bridges	Jog↑, jog↓ + bump↑, bump↓	2 Amplitude, Length	1 Duration
Grade Crossings	Jog↑,↓jog	2 Amplitude, Length	1 Duration
Dogleg Spiral	Jog↓, and Spiral	2 Amplitude, Spiral rate	2 Duration Distance into spiral
90-foot oscillation of mean alignment and spiral	Quasi periodic and spiral	3 Amplitude, spiral rate, Number of cycles	2 Duration, location of instigator
90-foot oscillation of mean alignment preceding and following the interlock	Quasi-periodic	2 Amplitude, Number of cycles	2 Duration, Phase related to interlock points

Table 3-3. Values of Fixed Parameters in Track Geometry Data

Track Geometry	Key Signature	Free Parameter	Fixed Parameter, k $\left(Ft^{-1}\right)$
Profile	Cusp	Amplitude	$\frac{1}{5}$ to $\frac{1}{8}$
	Bump	Amplitude	$\frac{1}{5}$ to $\frac{1}{10}$
	Jog	Amplitude	$\frac{1}{10}$ to $\frac{1}{50}$
Alignment	Cusp	Amplitude	$\frac{1}{2}$ to $\frac{1}{9}$
	Bump	Amplitude	$\frac{1}{8}$ to $\frac{1}{20}$
	Jog	Amplitude	$\frac{1}{30}$ to $\frac{1}{50}$

Table 3-4. Ratio of 62-Foot Mid-chord Offset to the Maximum
Amplitudes of Key Signatures

k (ft^{-1})	CUSP*	BUMP**	JOG$^+$	
			Ratio	Distance, S from origin (ft)
1/2	1.0	1.0	0.495	18
1/5	1.0	1.0	0.485	18
1/6	0.99	1.0	0.48	18
1/8	0.98	1.0	0.475	18
1/10	0.95	0.99	0.47	18
1/15	0.87	0.88	0.45	18
1/20	0.79	0.70	0.435	18
1/30	0.64	0.41	0.39	19
1/40	0.54	0.26	0.355	19
1/50	0.46	0.17	0.315	20

* $y = D\,e^{-k|x|}$, MCO is maximum at x = 0

** $y = D\,e^{-\frac{1}{2}(kx)^2}$, MCO is maximum at x = 0

\+ $y = \frac{D}{\pi}\tan^{-1}(\pi kx)$, MCO is maximum at S feet from origin

Table 3-5. Amplitude of Key Signatures Permitted by Track Safety Standards

Track Geometry	Key Signatures	$\frac{1}{k}$ (ft)	Track Class											
			1		2		3		4		5		6	
			TSS*	A**	TSS	A	TSS	A	TSS	A	TSS	A	TSS	A
Alignment (Tangent Track)	Cusp	6	5	5.1	3	3.03	1.75	1.77	1.5	1.52	0.75	0.76	0.5	0.51
	Bump	8	5	5	3	3	1.75	1.75	1.5	1.5	0.75	0.75	0.5	0.5
	Jog	20	5	11.5	3	6.9	1.75	4.0	1.5	3.45	0.75	1.7	0.5	1.15
Profile	Cusp	6	3	3.03	2.75	2.78	2.25	2.27	2.0	2.02	1.25	1.26	0.5	0.51
	Bump	8	3	3	2.75	2.75	2.25	2.25	2.0	2	1.25	1.25	0.5	0.5
	Jog	20	3	6.9	2.75	6.32	2.25	5.17	2.0	4.6	1.25	2.87	0.5	1.15
Cross-level (Tangent and Curves Between Spirals)	Cusp	6	3	3.02	2	2.02	1.75	1.77	1.25	1.26	1	1.01	0.625	0.63
	Bump	8	3	3	2	2	1.75	1.75	1.25	1.25	1	1	0.625	0.625
	Jog	20	3	6.9	2	4.6	1.75	4	1.25	2.87	1	2.3	0.625	1.44

+   Federal Railroad Administration, Track Safety Standards, P. 6-7, 1973

*   Track Safety Standards (inches)

**   Maximum amplitude of a signature (inches)

single bump or a cusp of common duration. However, its maximum sensitivity to the jog signature is limited to 0.5. Table 3-5 lists the amplitudes of key signatures which would exceed the current federal track safety standards. These values are for single occurrences of key signatures. It should be noted that these signatures may occur individually or in combination as discussed above.

3.2 TRACK GEOMETRY DESCRIPTORS

A track geometry descriptor is derived from the basic track geometry variables through arithmetic operations and is used to describe variations in the track geometry parameters over a prescribed length of track.

It was noted in Section 3.1 that severe track geometry variations can be described by a combination or a series of key signatures of different wavelengths. A descriptor must be able to accurately indicate the severity of these signatures. From an analysis of vehicle dynamics, wavelengths much longer than the longest resonant wavelength of the vehicle do not need to be considered. This allows the track geometry data to be high-pass filtered to preserve the short wavelengths and to eliminate long wavelengths which do not influence the vehicle response of interest. Very short wavelength variations, such as a cusp at a joint, induce very large forces across the wheel/rail interface which can result in component-fatigue related failures. Track inputs can be magnified due to the resonance and periodic behavior of the track. Therefore, a descriptor must be sensitive to broadband, short-wavelength inputs particularly to periodic and resonance type inputs.

A candidate set of descriptors was developed and tested on the available track geometry data. These descriptors can be used to monitor the severe track geometry variations previously mentioned. Section 3.2.1 presents the candidate descriptors.

3.2.1 GAGE NINETY-NINE PERCENTILE

Gage is a very well defined parameter and is the most traditionally used track geometry measurement. The 99 percentile of gage over a prescribed length of track can be used to monitor severe variations of gage.

3.2.2 RMS VALUE OF SECOND FINITE DIFFERENCE

The Second Finite Difference (SFD) is a complete representation of the sampled alignment or profile data. This measurement produces a signal whose amplitude is twice that of a short MCO which is two sample intervals long. The rms value of the SFD over a prescribed length of track can be used as a descriptor for short wavelength variations.

The wavelength response of the SFD is given by:

$$F(\lambda) = 4 \sin^2 \frac{\pi x}{\lambda}, \qquad\qquad (3.6)$$

where λ is the wavelength and x is the sample interval.

The long wavelength response is given by:

$$F(\lambda) = 4 \frac{\pi^2 x^2}{\lambda^2}, \qquad\qquad (3.7)$$

The wavelength response characteristics are shown in Figure 3-11. The SFD is highly responsive to all of the shorter wavelengths including the shortest valid wavelength for sampled data. The insensitivity to longer wavelengths is not a shortcoming, however. In the inertial

WAVELENGTH/SAMPLE INTERVAL, (ft/ft)
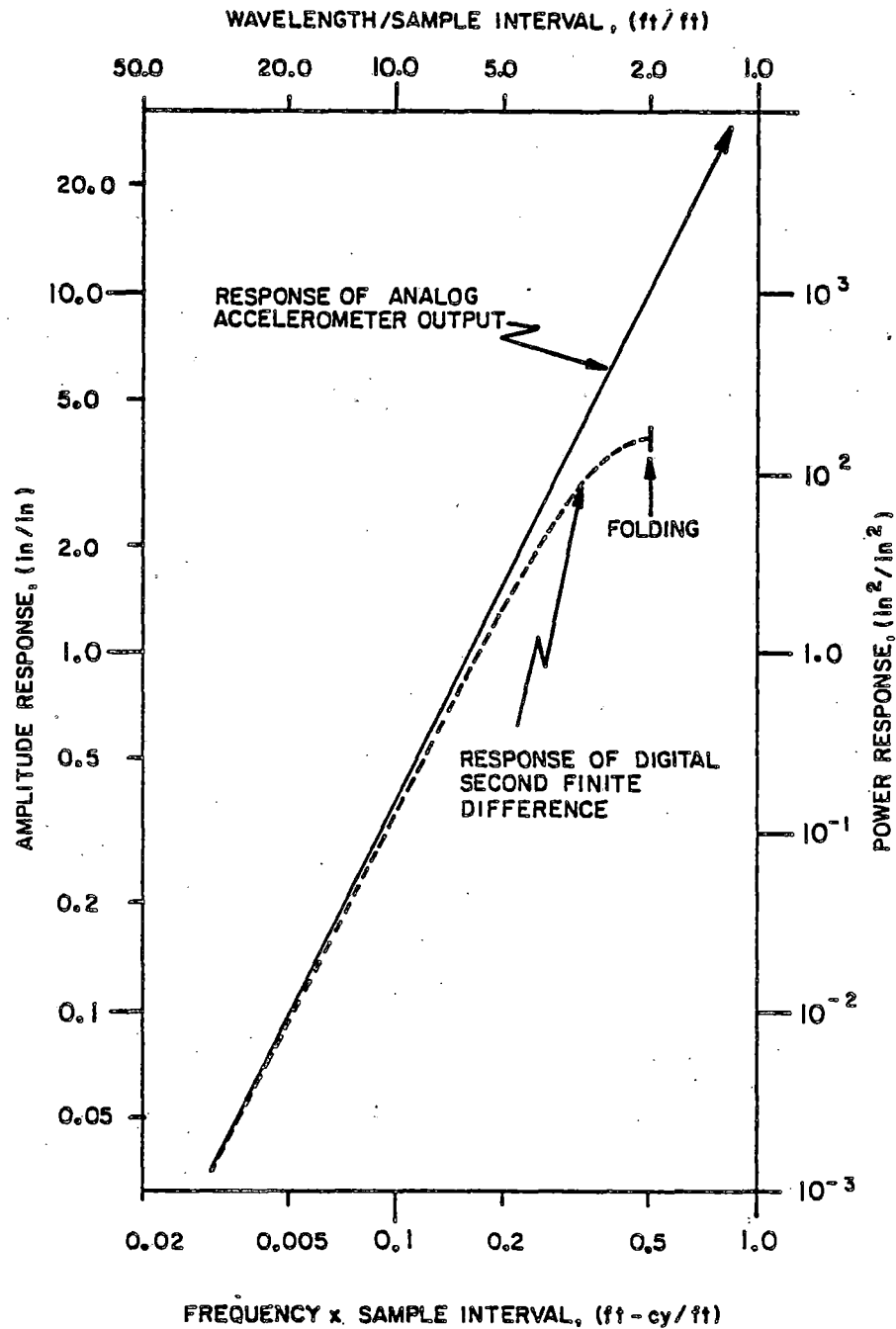
Figure 3-11. Response of Accelerometer and
Second Finite Difference

measurement systems currently used, an accelerometer generates the long wavelength portion of the geometry data. The response of an accelerometer to these wavelengths when corrected for forward speed is shown as the dashed line in Figure 3-11. A comparison of the long wavelength response of the SFD and of the accelerometer reveals that they are identical. Therefore, the SFD has as much long wavelength information bearing capacity as an unprocessed accelerometer signal.

The SFD is generated as an intermediate working step on two track geometry inspection cars: T-6, operated by the FRA, and RDC, operated by the C&NW. It is the first signal in the processing chain which is corrected for phase distortion and speed dependence which usually appear in unprocessed accelerometer data. The alternate representations of track geometry which emphasize longer wavelengths can be obtained by processing the SFD signal with digital filters.

The SFD for typical track geometry data is shown in Figure 3-12. It resembles a completely random signal. However, it has detailed information about short wavelength variations such as corrugations and rail discontinuities.

The rms value of SFD over a prescribed length of track is potentially useful for evaluating the impact of short wavelength roughness or component fatigue. Periodically large pulses indicate the location of joints or welds in the rail. Otherwise, this descriptor gives little indication of the longer wavelength deviations in the rail that are capable of causing a derailment.

RIGHT PROFILE

0.38" LEFT PROFILE

|← 100' →|

RIGHT ALIGNMENT

LEFT ALIGNMENT
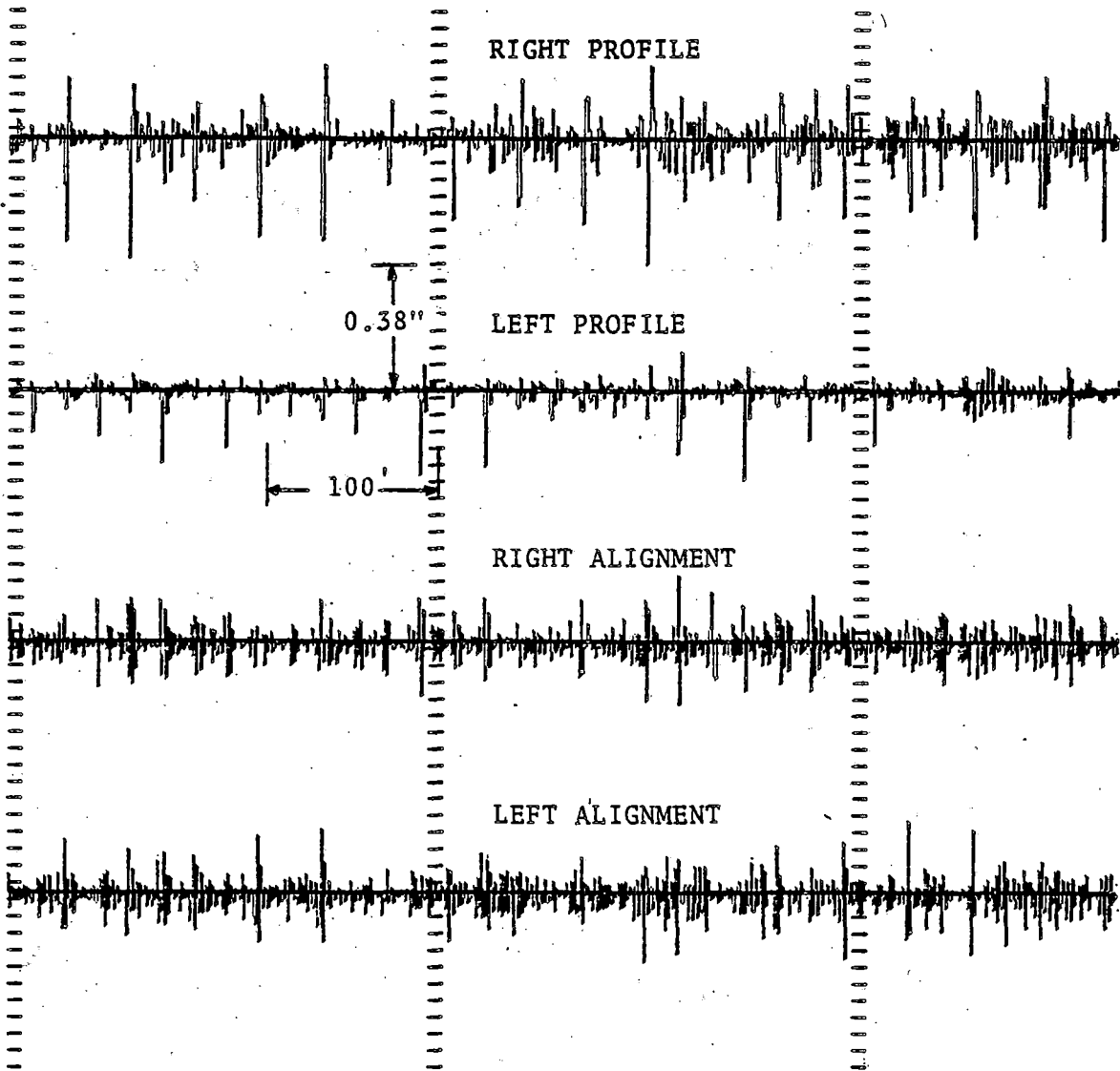
Figure 3-12.   Second Finite Difference for Typical Track
Geometry Data

3-26

3.2.3 PEAK-TO-PEAK VALUE OF SPACE CURVE

Track geometry variations are completely described by the absolute space curve of a given track segment. Peak-to-peak value of space curve over a specified length of track can monitor the severe track geometry variations.

The space curve can be obtained from a survey of both rails in space referenced to a fixed coordinate system. However, an automated track inspection program whose processing is based on an absolute space curve would be needlessly costly. It is possible to construct a pseudo-space curve from a sampled track geometry data using digital signal processing techniques. The SFD is the digital equivalent of analog double differentation. In principle the inverse operation that restores an absolute space curve is a two-fold numerical integration and two initial survey constants. Accelerometer noise and the sensitivity of accelerometers to uncompensated gravitational input prevent integrations over unlimited distance along the track.* However such long term integration is not necessary. An integration filter is adequate if it produces a reasonably constant response for all wavelengths from folding (1-5 feet) to some maximum wavelength (approximately 300 feet).

Algorithms to generate alignment and profile space curves were developed. The space curve used in this study is constructed from the alignment/profile data collected by the T-6 track inspection vehicle. A second finite difference is first computed and is corrected for speed and gravitational effects. A running mean is removed from this data to eliminate long wavelength trends. A double integration

---

*In a rail car, accelerometer axes are continually changing due to variations in crosslevel and grade angle. The accelerometer can not distinguish between gravity, whose direction is constant, and true acceleration.

is then performed on the mean-removed SFD to obtain the space curve. This space curve is high-pass filtered to remove any residual long wavelength offsets.

The frequency/wavelength response of the space curve is shown in Figure 3-13. The gain for all the short wavelengths are filtered out. The cut-off wavelength can be selected by varying the filter window, N, for a fixed sample interval.

The cut-off wavelength (-3db point) is given by

$$\lambda_c \simeq 1.3 \ Nx, \qquad\qquad (3.8)$$

where

   x = the sample interval in feet
   N = the number of samples
   λ_c = the cut off wavelength in feet.

The space curve response to the critical track signatures was shown in Figures 3-1 to 3-3. For signatures of short durations, the space curve indicates the true severity of the signature. However, it will be insensitive to signatures of very long duration.

Space curves for typical track geometry data for class 2 and 4 track are shown in Figure 3-14. The traces shown are the left alignment space curve, right alignment space curve, left profile space curve, and right profile space curve. Note that a larger number of severe variations appear on class 2 track than class 4 track. This is especially true for the alignment traces.
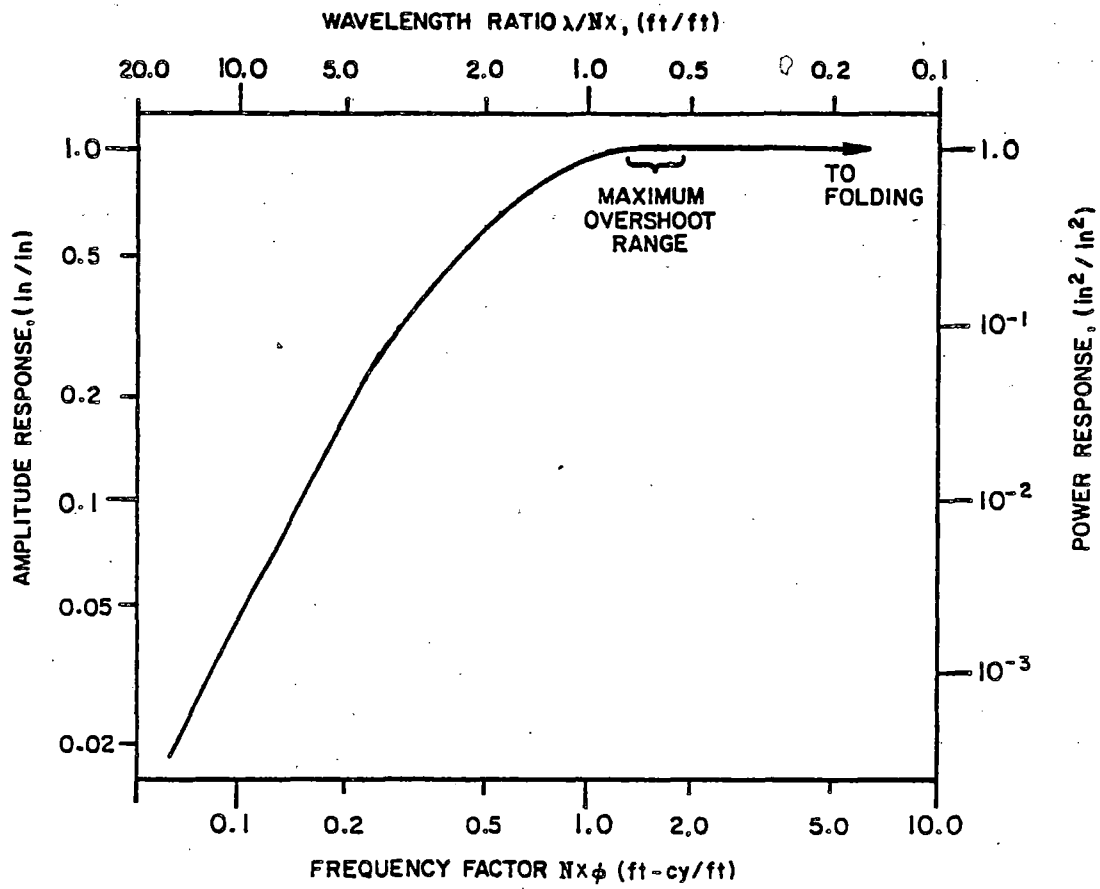
Figure 3-13. Frequency/Wavelength Response of Space Curve
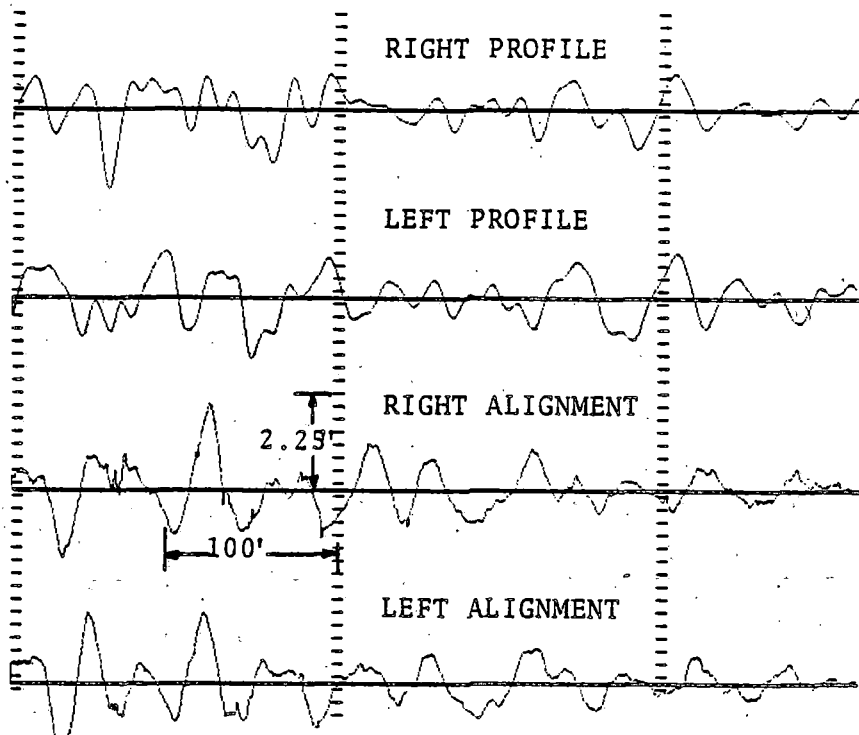
(a) Class 2 Track
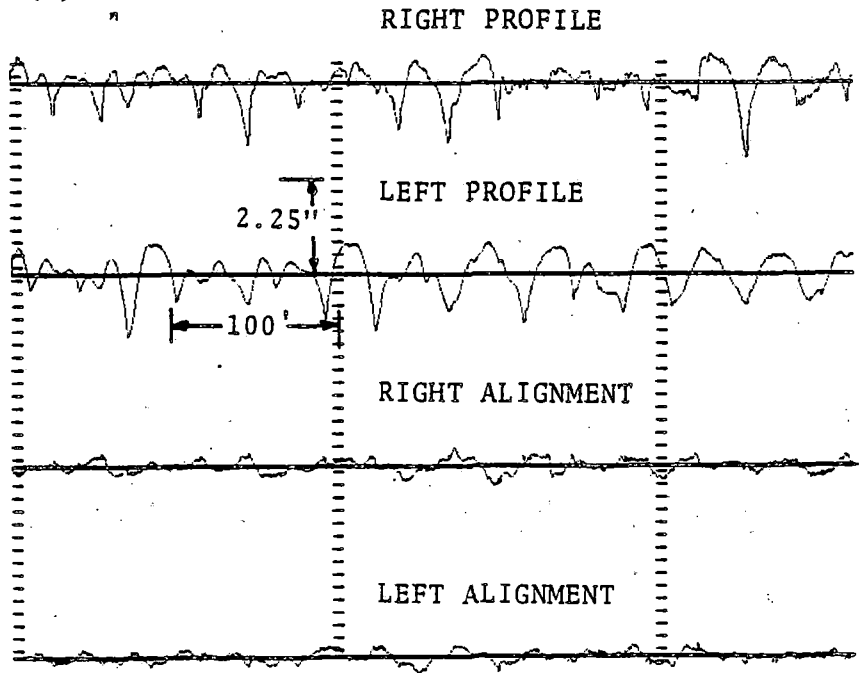
(b) Class 4 Track

Figure 3-14. Space Curves for Class 2 and 4 Track
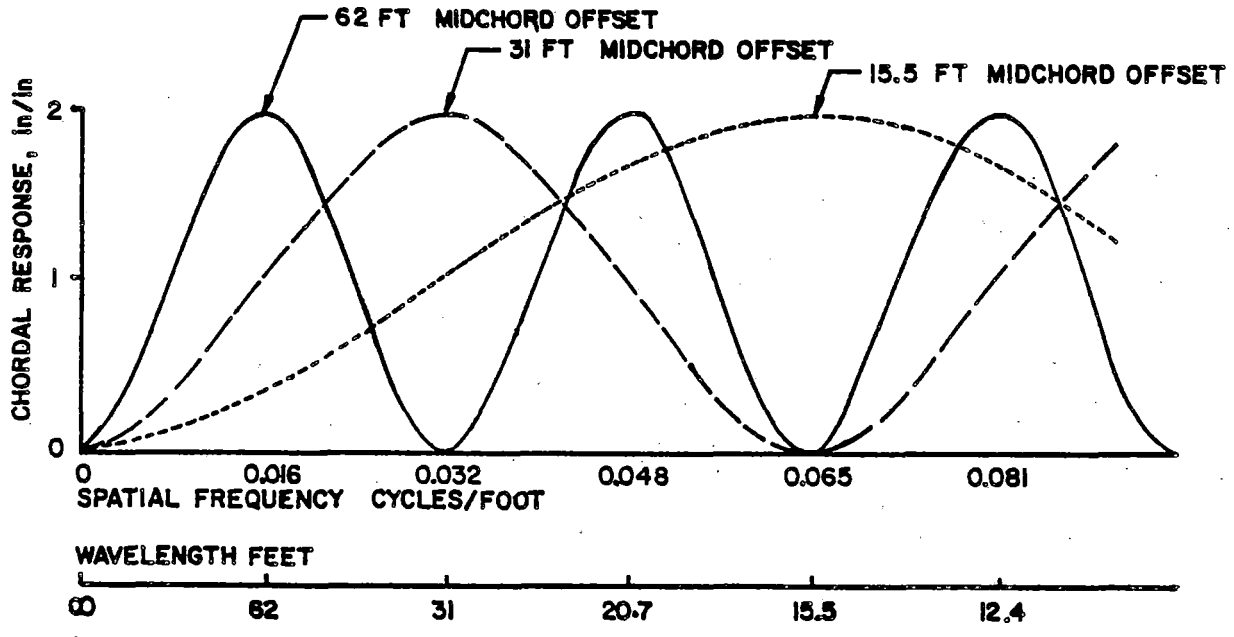
Figure 3-15. Response of Three Complementary Chords
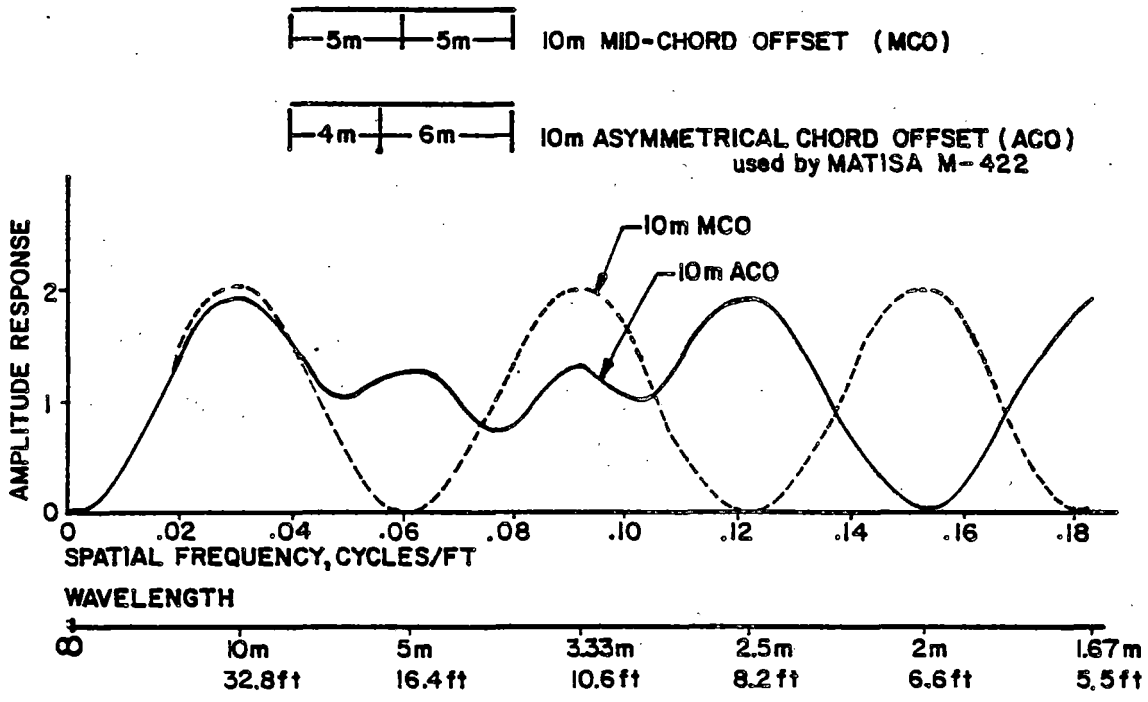
Figure 3-16. Response of Asymmetric Chord

3.2.4 PEAK-TO-PEAK VALUE OF COMPOSITE MCO

One way to correct the deficiencies of the MCO measurements is to use two or more chords that are complementary. For instance, a combination of a 62-foot chord, a 31-foot chord and a 15.5 foot chord can eliminate the blind spots at very short and long wavelengths (see Figure 3-15). In actual practice, this will require that three MCO measurements be made at each location and peak-to-peak value of the composite measurement over a certain distance be used as a track descriptor. The construction specifications (7) of the 250 mph LIMRV track built at the FRA Transportation Test Center (TTC) used 4 chord lengths to define the profile and alignment of each rail. The associated thresholds are shown in Table 3-6. While it is questionable that these tolerances could be met physically, it is a first attempt at defining performance-oriented track specifications.

Although a combination of MCO's of appropriate length can remove the blind spots from the chordal response; the response is not uniform through the wavelength region of interest. Nevertheless, the multi-chord system is suitable for obtaining estimates of track variations using non-automated approaches in field measurements made by track inspectors.

3.2.5 PEAK-TO-PEAK VALUE OF ASYMMETRICAL CHORD

A simpler method to correct for deficiencies of MCO measurements is the use of an asymmetrical chord or a multi-point chord, the effect of which is to merge the response of two or more chord lengths into a single measurement process. The response of the asymmetrical chord system used in the Matisa M422 profile system is shown in Figure 3-16 by the solid line. Also shown (by dotted line) is the response of an MCO measurement.

Table 3-6.   A Multichord System

Chord Length (Feet)	Maximum Allowable MCO Deviation for Profile and Alignment (inches)
10	3/64
31	3/32
100	9/64
700	1/4

The peak-to-peak value of asymetrical chord offset over a
certain distance is a useful descriptor, since by a proper
choice of the ratio of the distance between the three measur-
ing points, the chordal response can be molded to achieve
a desired shape.   Due to the asymmetry of the chords different
values of offset will be obtained for different directions
of measurements.   This is a major disadvantage of the ACO
since a lot of track is bidirectional.

3.2.6   NINETY-FIVE PERCENTILE OF WARP

Ninety-five percentile of warp over a prescribed length of
track can be used as a descriptor for the periodic rock and
roll phenomena.   Warp is the difference in superelevation
between two points.   It is a measure of the variation of the
horizontal plane of the track over the selected chord length.
Since warp is the spatial rate of change of crosslevel, it
can be calculated from crosslevel measurements.   An appropriate
chord length for warp measurements is one-half the rail length
since periodic low joints occur every one-half the rail length
due to staggering of rail lengths.

Figure 3-17 shows the warp measurements along a section of
class 3 track. Since the rail length in this section of
track was 39 feet, computations were made for 20-foot warp.
An examination of Figure 3-17 shows strong alternating pos-
itive and negative peaks every one-half the length of rail.

3.2.7 RMS PROCESSOR

From the previous sections, periodic track behavior was shown
to be more serious than localized defects. Thus in addition
to the peak level information, the characteristics of extended
regions of track from which periodic behavior can be deter-
mined are of interest. An extended region of track can be
described by an rms processor. This processor can be used
to describe the crosslevel and alignment oscillations.

An rms processing technique investigated in this study involves
crosslevel data, with the running mean removed (to eliminate
long wavelength trends), which is squared and averaged over some
desired length of track, e.g., 100 feet. The square root of
this value gives the rms deviation for crosslevel at the mid-
point of the averaging interval. This process is repeated
for each data point measured along the rail, yielding an rms
deviation as a function of distance along the track. (This
is easily calculated by a computer using a recursive algorithm).

Figure 3-18 shows the rms crosslevel for a section of track.
The traces shown from bottom to top are: raw crosslevel,
100-foot mean removed crosslevel, 100-foot rms, and 400-foot
rms. The rms value is larger around an area of large periodic
crosslevel values and also in the vicinity of an isolated
large crosslevel value. In addition, the 400-foot rms is
smoother than the 100-foot rms because the 100-foot rms re-
tains more localized information than the 400-foot rms.
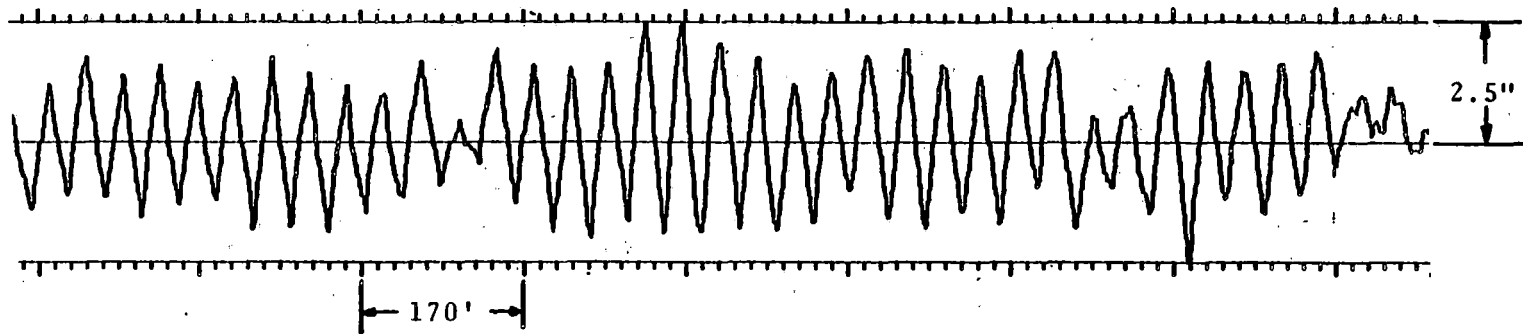
Figure 3-17. Warp Measurement Along a Section of Class 3 Track

400-Foot rms

0.25"

100-Foot rms

0.25"

100-Foot Mean-Removed Crosslevel

1.25"

Raw Crosslevel

1.25"

200'
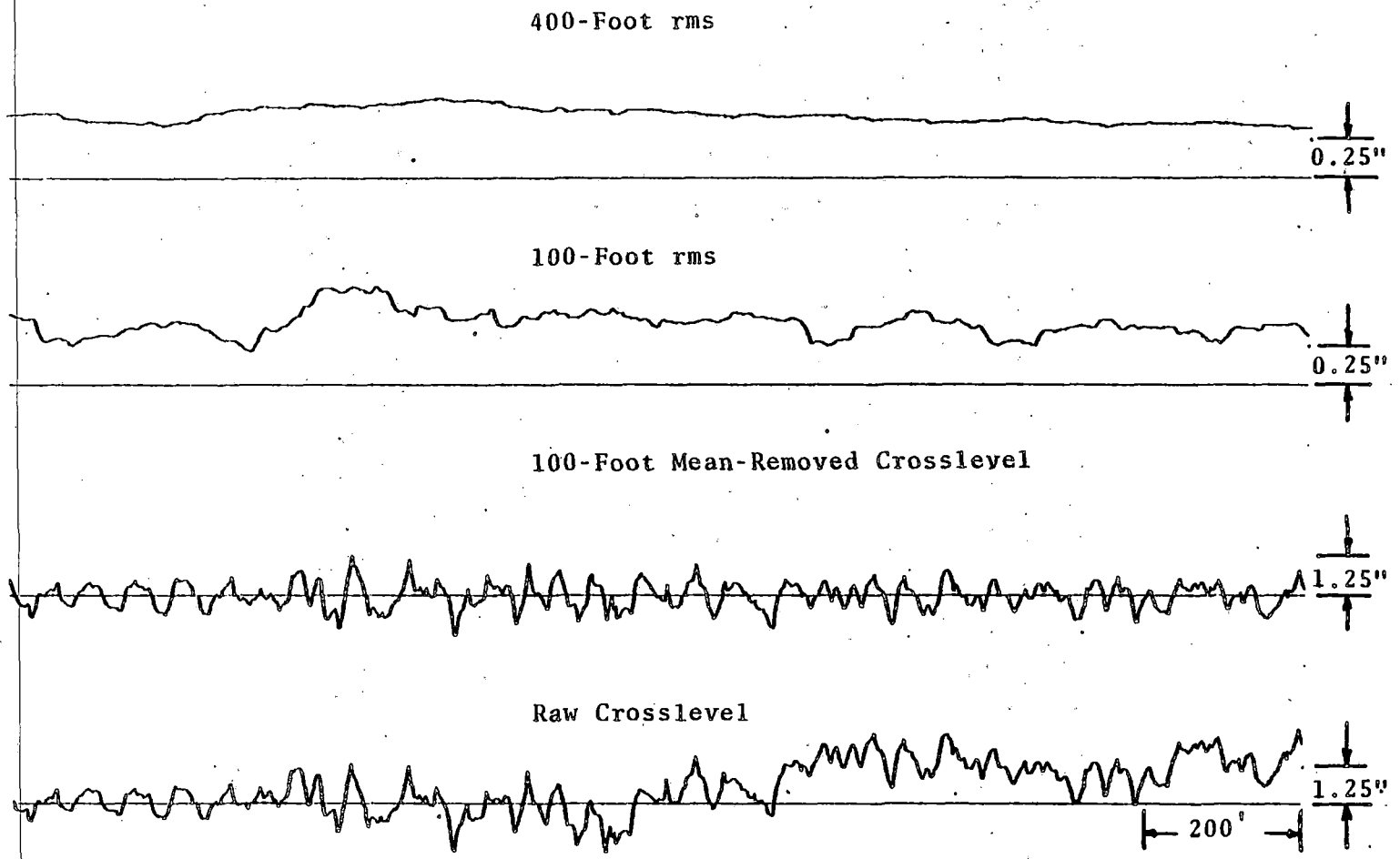
Figure 3-18. RMS Crosslevel

3.2.8   NARROW BAND RMS PROCESSOR

An alternate descriptor for periodic phenomena is a band-
limited rms processor. A band-limited rms processor has a
response which is tuned to a chosen wavelength. To produce
band-limited rms deviations, sine and cosine of the desired
wavelength are generated along with mean-removed crosslevel
data. These two signals are filtered through a running
average of five-wavelength duration. The results are squared,
summed, and the square root of the results is taken.

Results of this processing are shown in Figure 3-19. The
seven traces shown are, from bottom to top: raw crosslevel,
mean-removed crosslevel, full-band 100-foot rms deviation,
full-band 400-foot rms deviation, narrow-band rms at 33-feet,
narrow-band rms at 36-feet, and narrow-band rms at 39-feet.
The x-axis is scaled to 2000 feet of data per inch, and the
y-axes are scaled to 5:1 for the corsslevel traces and 1:1
for the rms traces. The 33-foot rms trace systematically
shows larger rms deviations than the 36-foot or 39-foot rms
traces. In several instances, strong spikes in the crosslevel
signal appear as large, total-band rms variations but do
not appear in the narrow-band rms signals. Additionally,
several instances occur where clearly visible, narrow-band
variations are not emphasixed in the full-band signal.

The band-limited rms processor can be used to single out
periodic phenomena by tuning it to a certain resonant wave-
length. It can also be extended to study the effects of
joint parameters such as alignment and crosslevel.
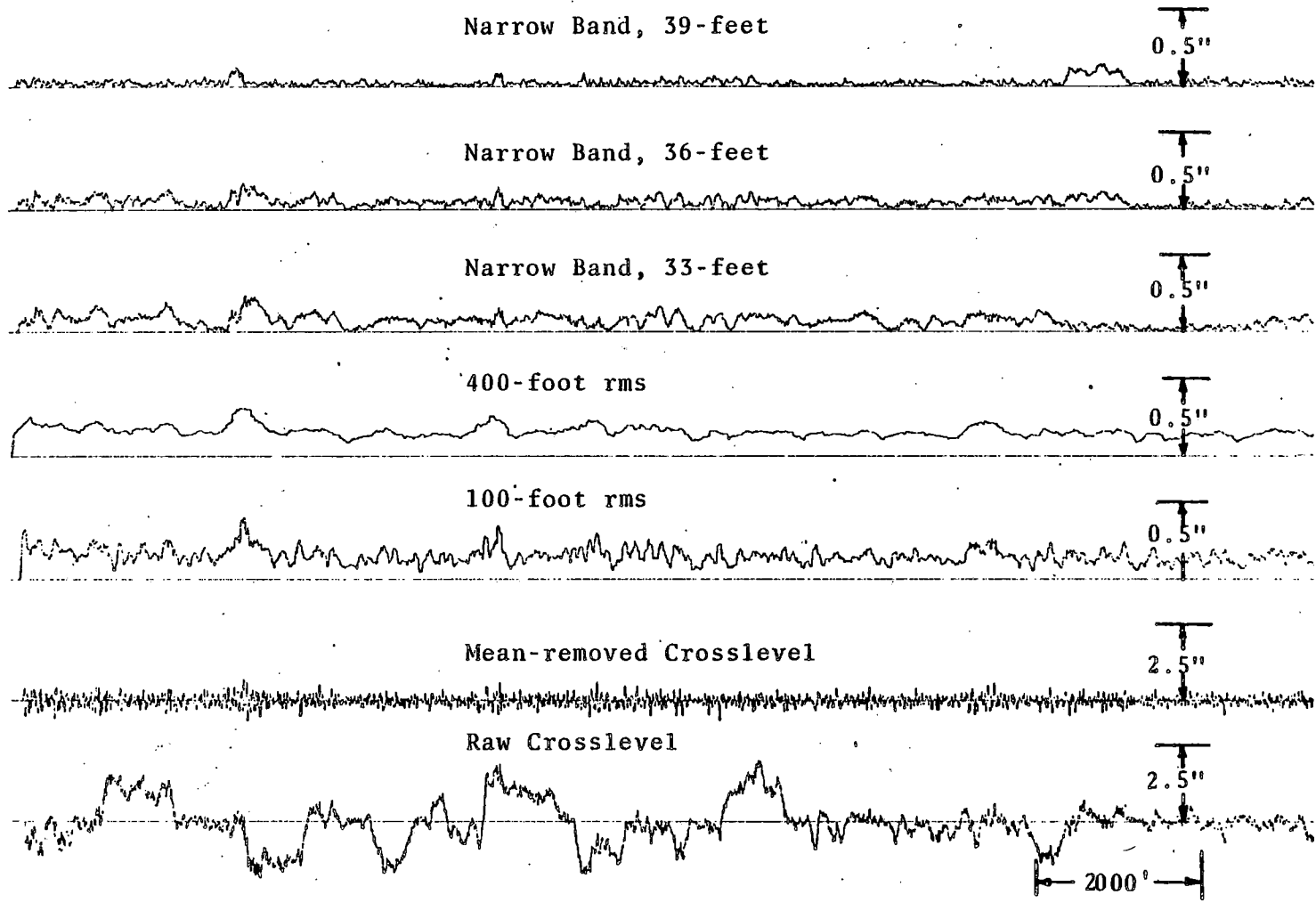
Figure 3-19. RMS Processing of Crosslevel Data

3.3 MEASUREMENT TECHNIQUES

The track geometry descriptors are based on gage, crosslevel, alignment and profile measurements. These measurements must be made accurately for a reliable estimate of track conditions and should also be made under a load to obtain an exact description of the track under normal traffic.

Conventional track measuring tools have two major deficiencies. First, the measurements are made with no load on the track and thus, do not give an accurate description of track under loaded conditions. Second, the measurements are limited to distantly-spaced sampling stations because the process is tedious and time consuming. Aside from the loss of short wavelength information, the distantly-spaced data points preclude the use of mathematical techniques to derive adequate track descriptors as discussed in the previous section. However, a rough estimate of the track condition can be obtained using some of the alternate forms of descriptors which will be discussed later. The automated techniques to obtain track descriptors are discussed in the following paragraphs.

3.3.1 AUTOMATED TECHNIQUES

Automated test cars are currently available which make the continuous measurement of track geometry at fixed sample intervals. The collected data contains detailed information on the track including as broad a range of wavelengths as the sensing system covers. Full size track measuring vehicles with axle loads greater than ten tons can generally take up all the slack in the track structure such that further deflections due to additional static or dynamic loads are relatively small. Thus, the measurements made with these vehicles give a description of track as it actually is.

One of the most sophisticated test cars is the T-6 vehicle operated by FRA. This car measures track geometry using one of the most advanced instrumentation systems available. However, the data processing techniques currently used do not produce the track geometry descriptors as proposed in Section 3.2. Gage and crosslevel are currently available in the form of the space curve. However, alignment and profile measurements are made in terms of the 62-foot MCO. Track descriptors as given in section 3.2 can be derived from the basic track geometry measurements. The measurement technique for the rms processor is given in the following paragraphs. Crosslevel is used as an example here; however, the same technique can be applied to rms alignment measurements.

The first step in processing the rms crosslevel data is to subtract the average crosslevel of a rectangular window, N, from the raw crosslevel measurements. This process removes the effects of long wavelengths. The mean-removed crosslevel is squared and averaged over a window of length, M. The square root of this quantity is the rms value of the crosslevel at the center of the mid-point of the averaging window. This process is repeated by shifting one point at a time to obtain the moving-point rms crosslevel for a section of track.

Assuming $N = 2n + 1$ and $M = 2m + 1$, the rms crosslevel can be computed by the following recursive algorithm:

$$s_i = s_{i-1} + x_{i+n} - x_{i-n-1}$$

$$y_i = x_i - s_i/N$$

$$t_j = t_{j-1} + \left(y_{j+m}\right)^2 - \left(y_{j-m-1}\right)^2 \qquad (3.9)$$

$$u_j = \sqrt{t_j/M} \, ,$$

where x_i is the crosslevel, s_i is the running sum, y_i is the mean-removed crosslevel, t_j is the running sum of squares and u_j is the rms crosslevel. Note that j should be adjusted with respect to i depending on the values of m and n.

A stand alone rms processor can be implemented with either the analog or digital circuitry as shown in Figure 3-20. The hardware for the measurement of crosslevel is given in Appendix D. In the analog rms processor, the crosslevel signal is first passed through a high-pass filter and is then passed through an rms filter. The rms crosslevel can be displayed on a strip chart recorder. The process can be simplified by establishing the thresholds on the mean-square value of the crosslevel, which will allow the use of a mean-square filter instead of the rms filter. RMS crosslevel can also be obtained by making the warp measurements. The analog rms processor is usually much faster than its digital equivalent; however, it lacks the flexibility of a digital processor. Furthermore, the time constants of filters must be adjusted for the test car speed. The analog averaging and squaring operations are only approximate and it is very hard to achieve an accuracy of better than three percent.

In the case of a digital rms processor, the crosslevel signal is digitized and fed to a microprocessor. The microprocessor performs the filtering operations required to generate the rms crosslevel. The digital crosslevel data can be displayed for visual inspection and/or stored on magnetic tape for future analysis. A microprocessor can easily handle the rate of data acquisition and the processing required for normal test car speeds. The digital processor also has the advantages of accuracy, flexibility and real-time feedback. In addition, the test car speed variations can be handled in the software. Furthermore, the permanent data records can be used for future analysis.
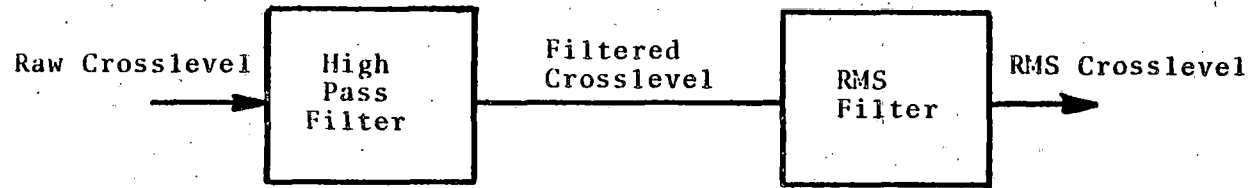
(a) Analog Processor
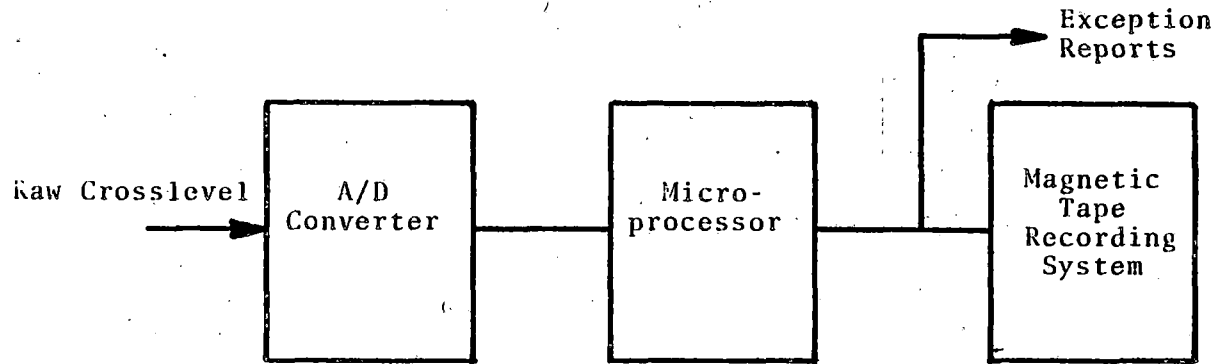
(b) Digital Processor

Figure 3-20. Block Diagram of an RMS Crosslevel Processor

3.3.2 NON-AUTOMATED FIELD MEASUREMENTS

The track geometry descriptors such as peak-to-peak space curves
and rms crosslevel which are suitable for automated techniques
can not be measured as such using non-automated techniques. It
would be very expensive to perform a survey to obtain an absolute
space curve for any extended section of track. Similarly the
processing involved to obtain the rms crosslevel is almost
totally impracticable. The manual measurement of track is
limited to distantly-spaced sampling stations due to the labor-
iousness of the operation. Therefore, alternate measurement
procedures should be used which can give an estimate of track
descriptors without a need for either continuous sampling or
complex processing.

It was noted in the previous section that the deficiencies of
the 62-foot MCO can be corrected by using an asymmetrical chord
or a combination of two or more chords that are complementary.
Both techniques are suitable for non-automated measurements.
In the case of asymmetrical chords, measurements should be
made in both directions for the bi-directional track. A com-
bination of 62-foot, 31-foot and 15.5-foot chords can eliminate
most of the blind spots in the wavelength region of interest.
This will require that three MCO measurements be made at each
location and checked against selected thresholds.

Crosslevel variations of track can be investigated using
a 20-foot warp measurement. This measurement technique is
practical and can be implemented in the field. An alternative
technique involving the "stacking" of crosslevel data was in-
vestigated as an indicator of periodic behavior. In this
process, five points of data at intervals of one rail length
are averaged to produce the trace. Figure 3-21 shows the
results of this process on class 3 track. Trace 1 (lower most)
is the raw crosslevel data, trace 2 is the mean removed cross-

RMS Deviation

— 0.25"

39-Foot Stacking

0.25"

36-Foot Stacking

0.25"

33-Foot Stacking

0.25"

Mean-Removed Crosslevel

1.25"

RAW Crosslevel

1.25"

|←—200'—→|
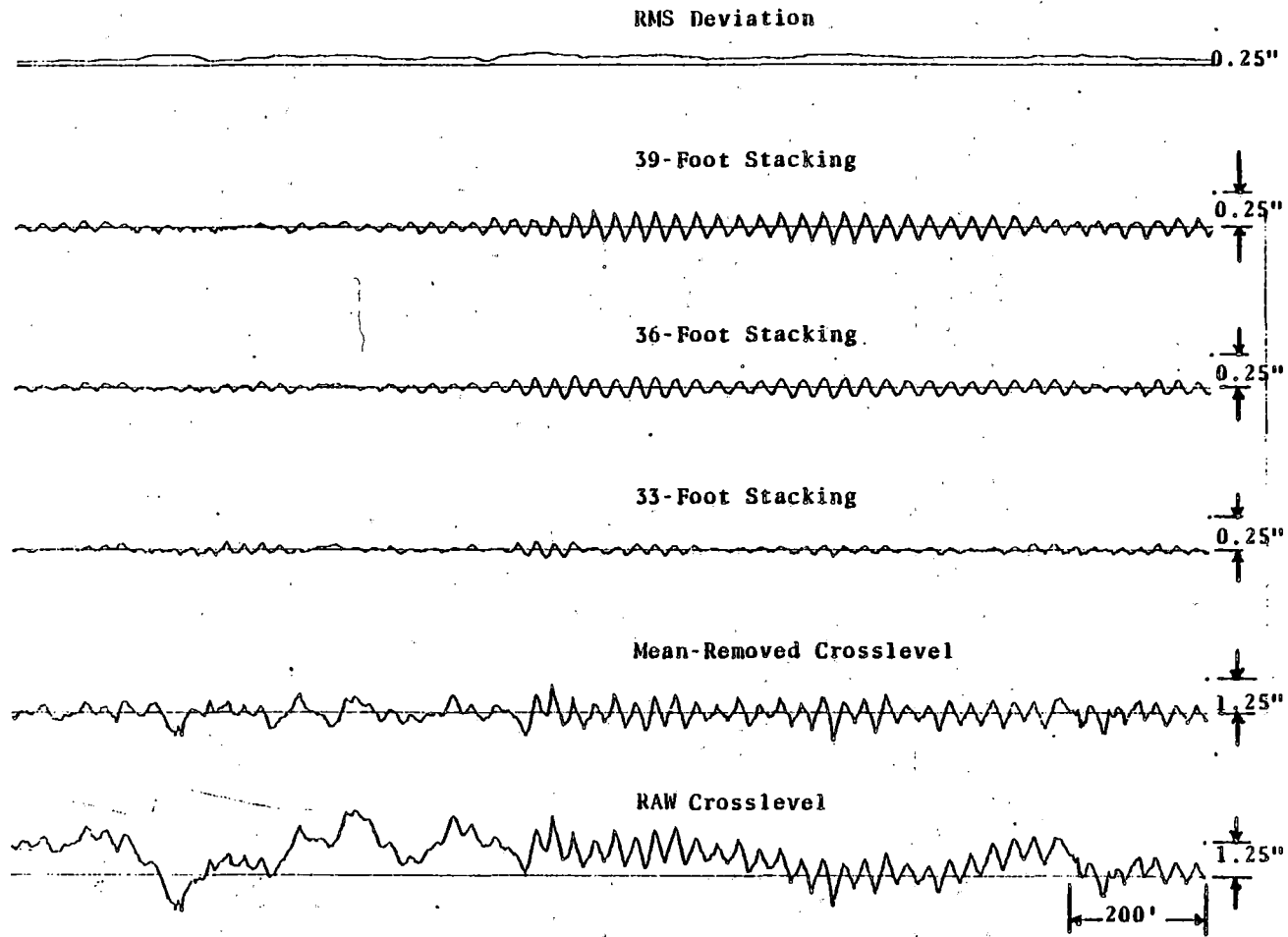
Figure 3-21. Different Techniques of Crosslevel Processing

level data and trace 6 (uppermost) is the rms deviation func-
tion. Traces 3 through 5 are the results of stacking five
points together which are 33 feet, 36 feet, and 39 feet apart,
respectively. Note that the periodic tendency of crosslevel is
emphasized by the stacking operation, particularly for the
39-foot stack. In this case, 39 feet corresponds to the actual
rail length of this section of track. Thus the periodic
behavior of crosslevel can be studied by the stacking operation.
The automated processing technique is a continuous operation
including all of the points of the rail. However, this can be
implemented in the field by measuring and averaging the cross-
level at each of five consecutive joints.

In summary, it is difficult to measure the track geometry des-
criptors that are necessary to monitor the dynamic inputs of
critical track signatures using non-automated techniques. An
estimate of localized defects can be made using an asymmetrical
chord or a combination of more than one chord that are comple-
mentary. The periodic behavior of track, especially for
crosslevel, can be estimated either by 20-foot warp measure-
ments or by stacking operations on consecutive joints.
However, the automated techniques are preferred since the
measurements can be made continuously and under load and since
the actual track descriptors can be computed.

3.4 STATISTICAL DISTRIBUTION OF TRACK DESCRIPTORS

3.4.1 RMS CROSSLEVEL

The distributional properties and expectations of rms crosslevel
are derived in Appendix D. The analytical description is
based on the assumption that the joints of bolted rail are
represented by a random amplitude operating on a joint shape

function. The crosslevel for the half-stagger bolted track can be represented by(1):

$$y_4(x) = \sum_{n = -\infty,}^{\infty} c_n(-1)^n e^{-k|x-\frac{1}{2}nL|} \qquad (3.10)$$

where:

x = distance along the track

$y_4(x)$ = crosslevel as a function of distance along the track

n = counting index

c_n = amplitude of the nth joint

k = joint decay rate

L = rail length.

The amplitudes of each joint are independent of each other and have a probability distribution given by

$$p(c) = \frac{128c^3}{3\bar{c}^4} = e^{-4c/\bar{c}} . \qquad (3.11)$$

It is assumed that randomness in the joints is independent of variations associated with the stationary process, both in the raw geometry, filtered geometry, and filtered geometry squared.

These assumptions yield the expectation value and the standard deviation for the rms deviation as follows:

$$\bar{y} = \left(\frac{e\beta_1}{1 + e}\right)^{\frac{1}{2}} \simeq \sqrt{\beta_1} \qquad (3.12)$$

and

$$\sigma_y = \left(\frac{\beta_1}{1 + e}\right)^{\frac{1}{2}} \simeq \sqrt{\beta_1/e} , \qquad (3.13)$$

where

$$\beta_1 = \frac{5}{2kL} \bar{c}^2 + \sigma^2 ,$$

$$e = 4R + \frac{1}{2}$$

$$R \equiv \beta_1^2/\beta_2$$

$$\beta_2 = \frac{1}{N} \left(\frac{55}{32kL}\right)\bar{c}^4 + 2\sigma^4.$$

Analytical results of the rms crosslevel are summarized in Table 3-7. The results are given for class 2 and class 3 track since these classes are known to exhibit the periodic behavior. RMS crosslevel was calculated for a 100-foot and 400-foot moving window for the above track classes. The expected value for class 2 track for both the 100-foot and 400-foot window is 0.28 inch. The standard deviation is 0.06 inch for the 100-foot window and 0.03 inch for the 400-foot window. For class 3 track, the expected value for both the 100-foot and 400-foot window is 0.22 inch. Values of standard deviation for this class are 0.048 and 0.024 inch for the 100-foot and 400-foot windows respectively.

As shown in Table 3-7, e, which is analogous to degrees of freedom, is of the order of 22 or more. Hence the associated T-distribution is well represented by a normal distribution. Using this assumption, the following additional information is computed and tabulated:

- The probability of exceeding thresholds of 0.35 inch and 0.6 inch.

- The thresholds needed to produce an exceedance one percent and 10 percent of the time.

Table 3-7.   Analytic Results for RMS Processing of Crosslevel
            Data

PARAMETER	CLASS 2 100 FOOT RMS	CLASS 2 400 FOOT RMS	CLASS 3 100 FOOT RMS	CLASS 3 400 FOOT RMS	COMMENTS
$\bar{c}$	0.32 in.	0.32 in.	0.25 in.	0.25 in.	Values from Reference 6
KL	6.25	6.25	6.25	6.25	
σ	0.20 in.	0.20 in.	0.16 in.	0.16 in.	
β_1	$8.0 \times 10^{-2} in^2$	$8.0 \times 10^{-2} in^2$	$5.0 \times 10^{-2} in^2$	$5.0 \times 10^{-2} in^2$	Intermediate Computations
N	5	20	5	20	
β_2	$1.2 \times 10^{-3} in^4$	$3.0 \times 10^{-4} in^4$	$4.8 \times 10^{-4} in^4$	$1.2 \times 10^{-4} in^4$	
β_3	$4.8 \times 10^{-5} in^6$	$3.0 \times 10^{-6} in^6$	$1.2 \times 10^{-5} in^6$	$7.5 \times 10^{-7} in^6$	
R	5.3	21.3	5.3	21.3	
e	22	86	22	86	
$\bar{y}$	0.28 in.	0.28 in.	0.22 in.	0.22 in.	Expected value and fluctuations about expected value
σ_y	0.060 in.	0.030 in.	0.048 in.	0.024 in.	
y_1	0.60 in.	0.60 in.	0.60 in.	0.60 in.	Threshold of 0.60 inch
$P(y>y_1)$	----	----	----	----	
REQ'D	5.3 σ event	10.7 σ event	8.0 σ event	16 σ event	
y_2	0.35 in.	0.35 in.	0.35 in.	0.35 in.	Threshold of 0.35 inch
$P(y>y_2)$	0.12	0.011	0.004	----	
REQ'D	1.2 σ event	2.3 σ event	2.7 σ event	5.4 σ event	
$P(y>y_3)$	0.01	0.01	0.01	0.01	What threshold produces 1% exceedance of threshold?
REQ'D	2.33 σ event	2.33 σ event	2.33 σ event	2.33 σ event	
y_3	0.42 in.	0.35 in.	0.33 in.	0.28 in.	
$P(y>y_4)$	0.1	0.1	0.1	0.1	What threshold produces 10% exceedance of threshold?
REQ'D	1.29 σ event	1.29 σ event	1.29 σ event	1.29 σ event	
y_4	0.36 in.	0.32 in.	0.28 in.	0.25 in.	

Table 3-8. Distributional Properties of RMS Crosslevel for Bolted Track

Length Feet	Mean Removed Crosslevel (Inch)		100-Foot RMS (Inch)		400-Foot RMS (Inch)	
	Mean	Standard Deviation	Mean	Standard Deviation	Mean	Standard Deviation
30772	0.000	0.244	0.231	0.078	0.236	0.060
40372	0.000	0.268	0.257	0.076	0.261	0.056
36372	0.000	0.326	0.317	0.075	0.322	0.050
41572	0.000	0.352	0.343	0.076	0.348	0.050
36672	0.000	0.210	0.210	0.058	0.205	0.042
52072	0.000	0.274	0.261	0.080	0.267	0.057
25872	0.000	0.315	0.301	0.091	0.308	0.062

Empirical results were obtained by processing two sections of track which exhibited the type of periodic behavior to which this technique should be sensitive. On the class 2 section of track, it was found that $\bar{y} = 0.21$ inch and $\sigma = 0.066$ inch for a 100-foot rms over 3,800 feet of track. These values are in fair agreement with the predicted values of $\bar{y} = 0.28$ inch and $\sigma = 0.06$ inch for class 2 track. On the class 3 section of track, the 100-foot rms yielded $\bar{y} = 0.17$ inch and $\sigma = 0.04$ inch over 9,700 feet of track, also in fair agreement with the predicted values of $\bar{y} = 0.22$ inch and $\sigma = 0.05$ inch. In both cases, the empirical expectation value is one σ lower than the predicted value.

Seven other zones of class 2 and class 3 bolted track were processed to study the consistency of the results which are tabulated in Table 3-8. Notice that the mean and standard deviation for the 100-foot rms are consistent with the analytic results presented in Table 3-7 for class 2 track. The 400-foot rms standard deviations are significantly larger than the theoretically expected values. The analytic results were based on the assumption that the joint amplitudes are independent of each other. However, the examination of field data reveals that a low joint on one rail produces a correlated depression on the opposite rail. Furthermore, the consecutive joints on one rail and adjacent joints on opposite rails correlate with one another. This is believed to be the main reason for the higher value of standard deviation for the 400-foot rms crosslevel.

Twenty miles of track geometry data were selected at random for each of the FRA track classes. Means and standard deviations for mean-removed crosslevel, 100-foot rms crosslevel and 400-foot rms crosslevel are tabulated in Table 3.9.

As expected, the mean values decrease as the track class increases. The mean values of both the 100-foot and 400-foot rms crosslevel are lower than the analytical values for class 2 and class 3 track. This is attributed to the random selection of the data without regard to whether the rail was bolted or continuously welded. Furthermore, the presence of a significant amount of tangent track will tend to lower the mean values of rms crosslevel. The standard deviations of rms crosslevel are significantly larger than the expected values. This again may be attributed to the correlation among joints. Notice that the standard deviation of rms crosslevel for class 3 track is larger than the values for class 2 track. A study of these data showed that the class 3 data had the largest percentage of curved track.

Table 3-9. Distributional Properties of RMS Crosslevel for Randomly Selected 20-Mile Sections of Track

Track Class	Standard Deviation of Mean-Removed Crosslevel (Inch)	100-Foot RMS Crosslevel (Inch)		400-Foot RMS Crosslevel (Inch)	
		Mean	Standard Deviation	Mean	Standard Deviation
1	0.40	0.38	0.115	0.39	0.079
2	0.19	0.18	0.055	0.18	0.039
3	0.15	0.12	0.079	0.13	0.068
4	0.10	0.09	0.048	0.10	0.039

As noted before, rms crosslevel descriptors are approximately
normally distributed, random variables. The cummulative
distribution properties of these descriptors are shown
in Figures 3-22 and 3-23. These figures reveal that both the
100-foot and 400-foot rms crosslevel lie below 0.4 inch for
class 3 track. For class 2 track, the 100-foot rms crosslevel
lies below 0.5 inch and the 400-foot rms crosslevel lies below
0.4 inch. The 0.3-inch limit (specified in the candidate perfor-
mance statement) for the 100-foot rms crosslevel would affect
less than five percent of class 3 track and approximately 37
percent of class 2 track. The same limit on 400-foot rms will
affect negligible amounts of class 3 track and approximately
25 percent of class 2 track. These distributions are based on
a least-squares regression line that includes four zones of
class 2 track, five zones of class 3 track and interpolations
from seven zones of class 4 track and one zone of class 1
track. Each zone averaged four miles in length with the short-
est being one mile long.

Twenty-mile sections of track for each FRA track class were
processed regardless of whether the track was bolted or welded.
Table 3-10 lists the percentage of track which does not meet a
0.3-inch specification limit for rms crosslevel. Notice that if
the track was selected without any prior knowledge of its type
or condition, most of class 1 track will not conform to a
0.3-inch specification limit, only a small percentage of class 2
and class 3 track will need upgrading, and track of class 4 or
better will not be affected. The percentage of lower-class track
affected as a function of different specification limits is shown
in Figures 3-24 and 3-25. Notice that a specification limit
above 0.8 inch will not affect any track while a limit of 0.1
inch will affect most of class 1, 2 and 3 track.
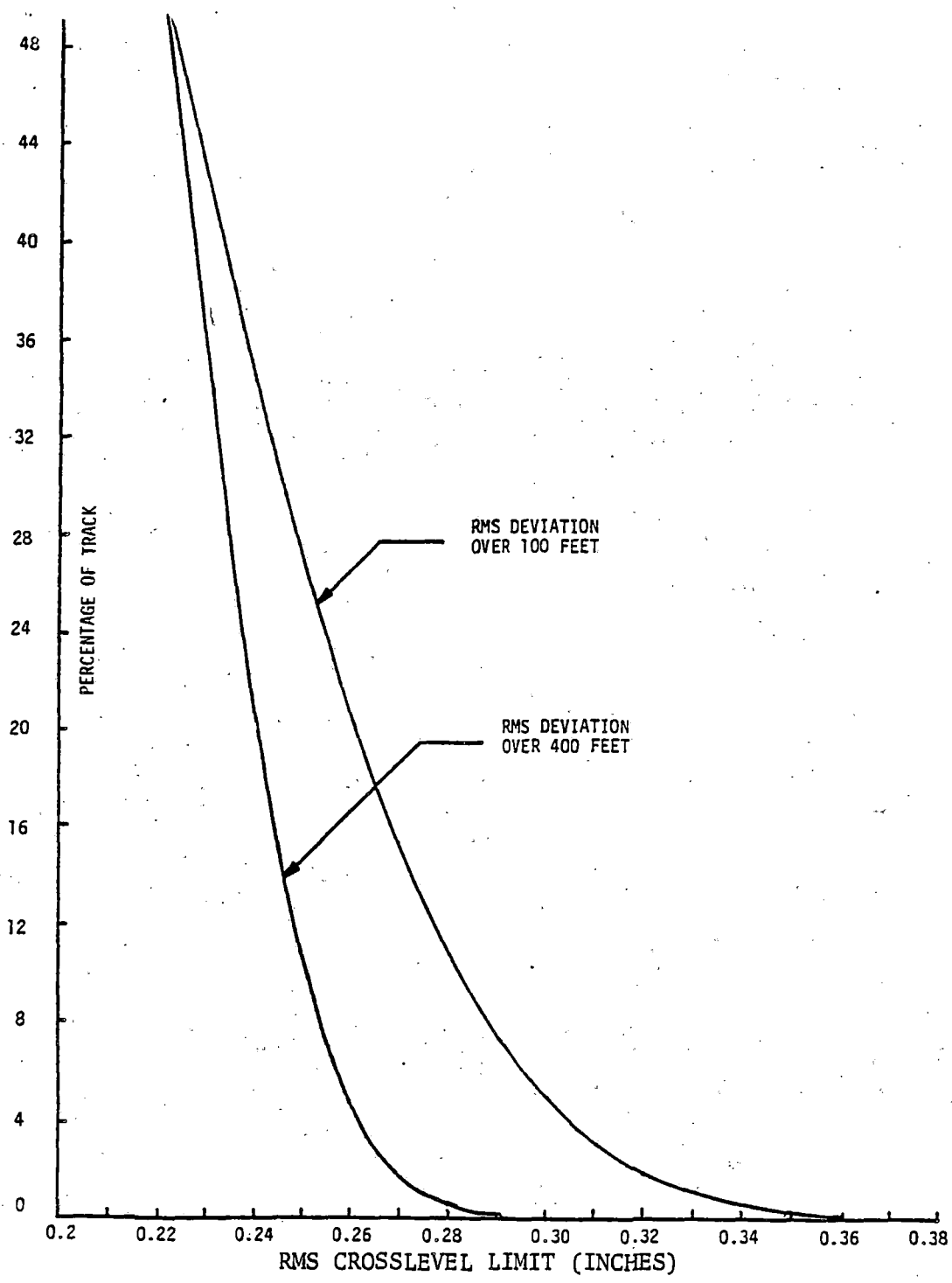
Figure 3-22.   Percent of Class 3, Bolted Track
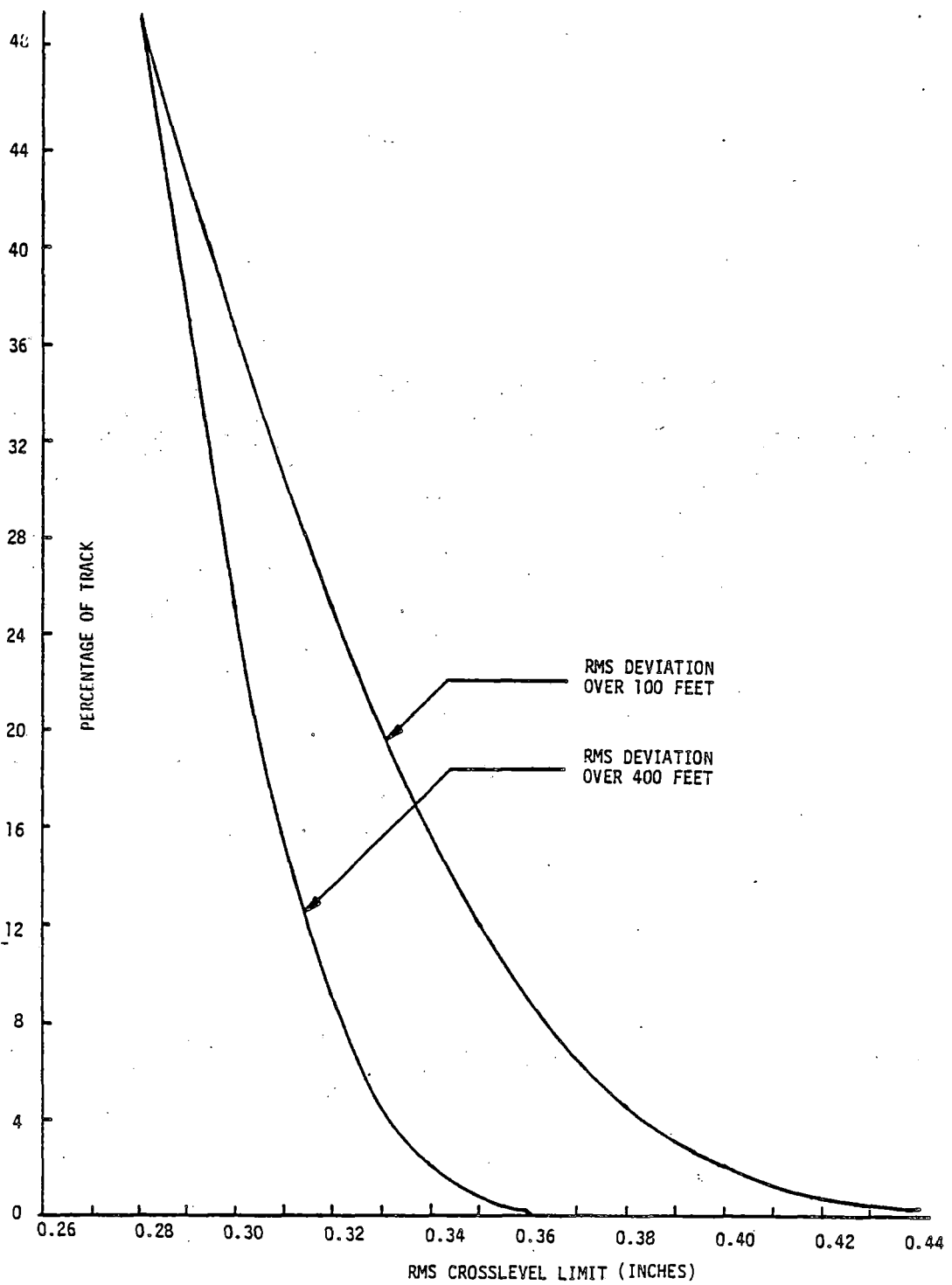   Requiring Upgrading vs. RMS Crosslevel

Figure 3-23. Percent of Class 2, Bolted Track
Requiring Upgrading vs. RMS Cross-
level Limit
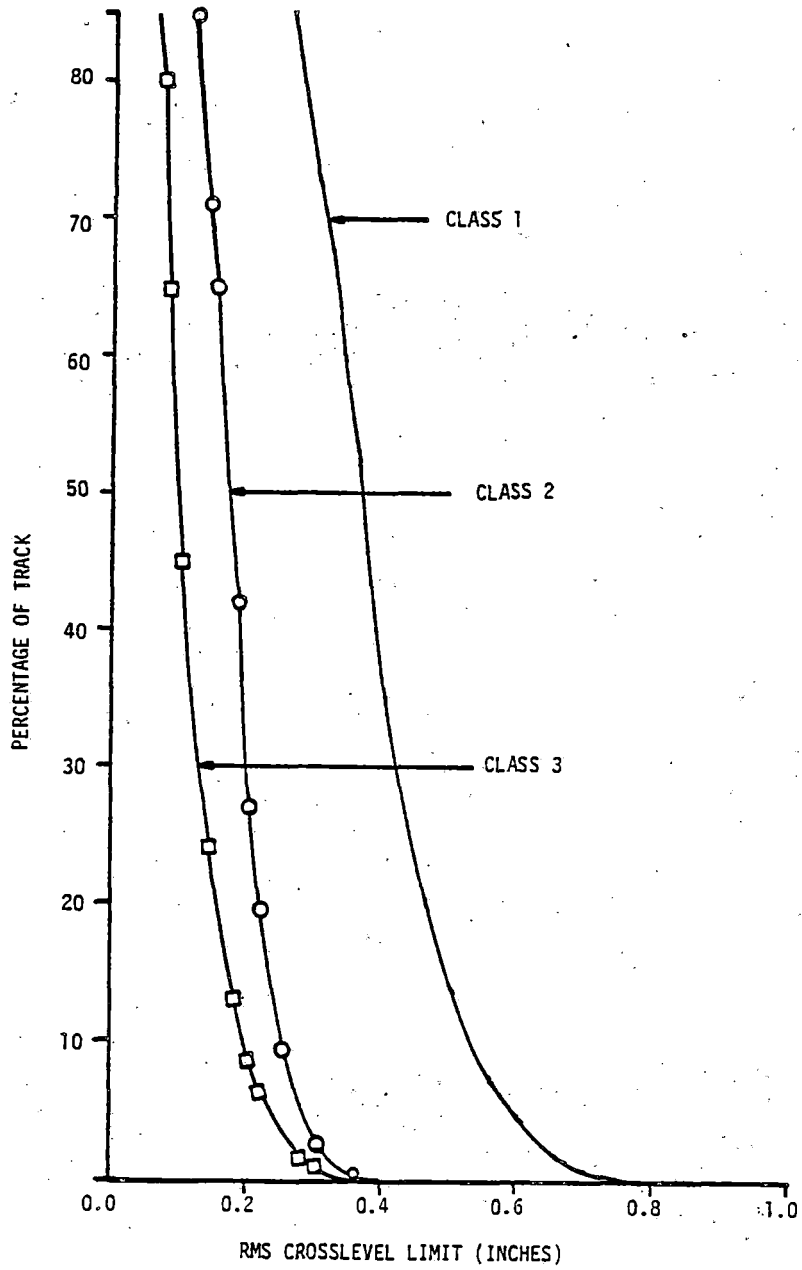
Figure 3-24. Percentage of Track Which Needs Upgrading
Versus 100-Foot RMS Crosslevel Limit
as Calculated from Actual Data Samples
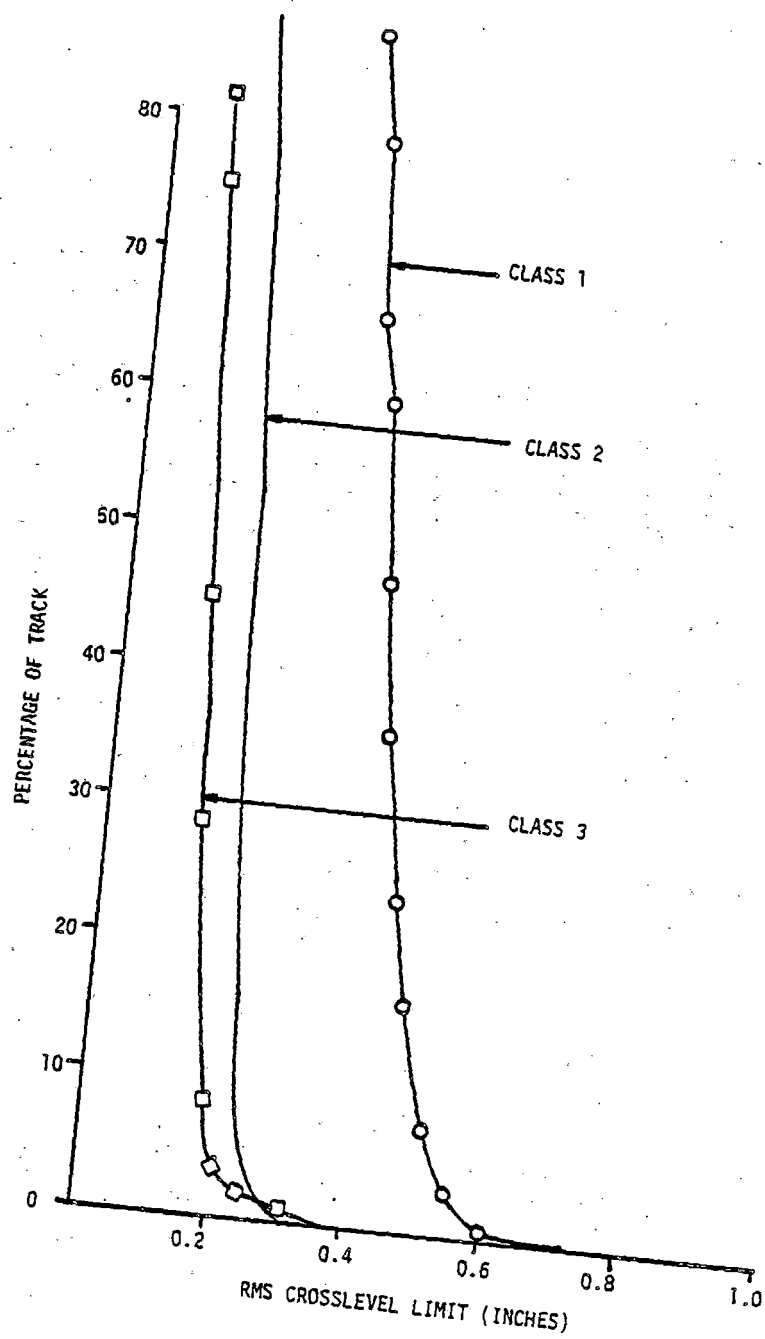
Figure 3-25. Percentage of Track Which Needs Upgrading Versus 400-Foot RMS Crosslevel Limit as Calculated from Actual Data Samples

Table 3-10.   Estimated Percentage of Track which Exceeds the
0.3-Inch Specification Limit of RMS Crosslevel

Class	100-foot RMS	400-foot RMS
1	74.0	88.0
2	2.9	1.75
3	1.27	1.65
4	0.53	0.19
5	0.58	0.03
6	0.47	0.0

3.4.2 SPACE CURVE

Table 3-11 lists the standard deviation of alignment and
profile space curves for typical track geometry variations
found in different track classes. These results are based
on 20-mile sections of track in each class selected randomly
from different geographical locations. The standard devia-
tions show a general decreasing trend as the track class
increases. However, track classes 2 and 3 do not show consistent
results. Furthermore, no distinction is indicated between class
5 and 6 track. These are preliminary results based on a small
statistical sample of track. Further qualification is re-
quired with regard to bolted/welded and curved/tangent track.

Table 3-11. Standard Deviation of the Alignment and Profile
Space Curve (Inches)

Track Class	Mean Alignment	Mean Profile
1	1.11	0.50
2	0.37	0.22
3	0.39	0.27
4	0.30	0.11
5	0.08	0.08
6	0.14	0.09

The cumulative distribution functions of mean profile and
mean alignment for the test data are shown in Figure 3-26.
Ninety-five and ninety-nine percentile levels of the dis-
tributions are shown in Table 3-12. Notice that the per-
centile levels of the space curve are good indicators of
track class.

MEAN PROFILE

MEAN ALIGNMENT

Class 1 Track

MEAN PROFILE

MEAN ALIGNMENT

Class 2 Track

MEAN PROFILE

MEAN ALIGNMENT

Class 3 Track
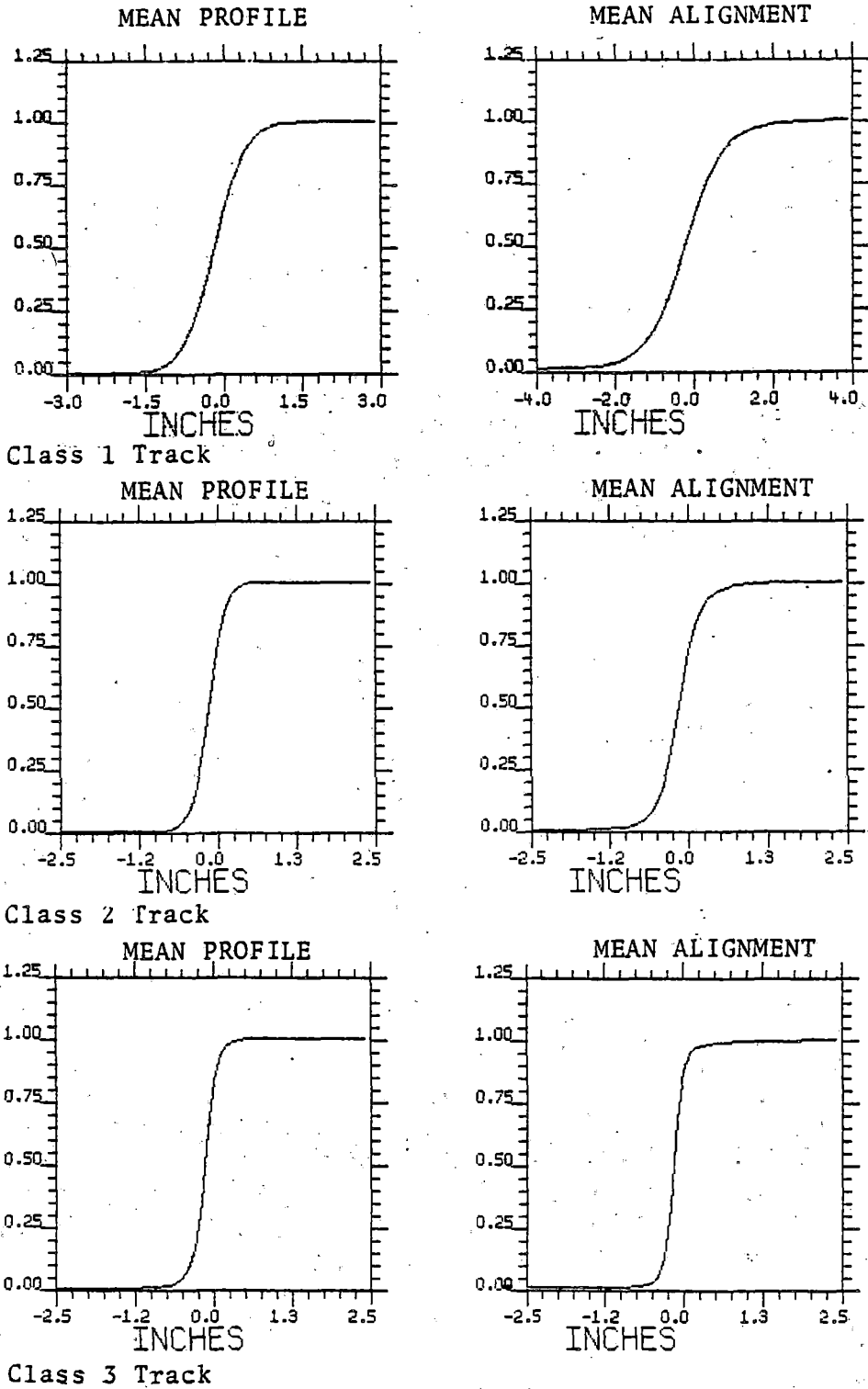
Figure 3-26.   Cumulative Distribution Functions of Mean
Profile and Mean Alignment

3-59

Table 3-12. Ninety-five and Ninety-nine Percentile Levels
of the Alignment and Profile Space Curve

Track Class	Mean Profile		Mean Alignment	
	95	99	95	99
1	0.78	1.19	1.44	2.6
2	0.31	0.49	0.49	0.94
3	0.24	0.43	0.23	0.80
4	0.13	0.25	0.12	0.36
5	0.09	0.17	0.08	0.16
6	0.08	0.11	*	*

*Reliable data not available.

3.5 CONSTRAINED TRACK

For the purpose of this study, the constrained track is
defined as the track for which the moving point crosslevel
does not exceed 0.3 inch at any point. For the analysis of
constrained track, a data base was established consisting
of track geometry data for each FRA track class. Each track
class contained approximately 20 miles of data which were
processed to generate mean-removed crosslevel, 100-foot
rms crosslevel, mean profile, mean alignment and crosslevel.
The processed data were separated into three categories:
Normal track, 100-foot constrained track and 400-foot con-
strained track. Data for the 100-foot constrained track

were extracted by limiting* the 100-foot rms crosslevel
to 0.3 inch. Similarly, the data for the 400-foot constrained
track were extracted by limiting the 400-foot rms crosslevel
to 0.3 inch. Due to limitations on spatial resolution, the
data were reformated to include only every fifth sample.
Statistical processing was performed on the reformated data
to generate the probability density functions, cumulative
distribution functions, means and standard deviations.

The probability density function, $f(y)$, provides a mathematical
model for the population-relative frequency histogram. The
total area under the curve, $f(y)$, is equal to one and the area
lying above a given interval will equal the probability that
y will fall in that interval.

For the purpose of this study, probability density estimates
were obtained by generating the sequence

$$P_j = \frac{N_j}{NW},$$
(3.14)

where, N_j is number of occurences of a sample value in the
j^{th} interval, N is the total number of occurrences, and W is
the interval width.

P_j can be interpreted as the derivative of the distribution
function at the midpoint of the jth interval. Thus, the dis-
tribution function can be obtained simply by summing the
probability density estimates. A maximum value of the prob-
ability density estimate will occur at the sample value with
the maximum number of occurrences.

---

*by eliminating data samples

Presented in Figures 3-27 through 3-38 are the probability
density functions for track classes 1 to 4. Probability
density functions for normal track are included along with
100-foot and 400-foot constrained track for comparison
purposes. As noted in the previous section, class 5 and
class 6 track are not affected by a constraint of 0.3 inch
on the rms crosslevel; therefore, these track classes are not
considered here.

Class 1 track shows a notable difference between the normal
and the constrained track. Differences in other track classes
are not as pronounced. However, certain general observations
are noteworthy. The mean-removed crosslevel, mean profile
and mean alignment have the highest probability density at
zero since these quantities have a zero mean. Among different
track classes, the probability density at zero increases with
the track class. The constrained track in general shows
higher densities than the normal track with the 100-foot
constrained track having the highest value. Traces for
crosslevel have peaks corresponding to non-zero crosslevel.
These peaks correspond to curved track.

From digital printouts of the probability density estimates,
the 100-foot rms crosslevel for class 1 track has its maximum
at 0.37 inch for normal track, 0.28 inch for 100-foot con-
strained track, and 0.24 inch for 400-foot constrained track.
For three track categories, i.e., normal, 100-foot
and 400-foot constrained track, the maximum densities appeared
at 0.17 inch for class 2 track, 0.07 inch for class 3 track
and 0.07 inch for class 4 track.

Figure 3-27. Probability Density Functions for Normal Class 1 Track

Figure 3-28. Probability Density Functions for 100-Foot Constrained Class 1 Track

Figure 3-29. Probability Density Functions for 400-Foot Constrained Class 1 Track

MEAN-REMOVED
CROSSLEVEL

100-FOOT RMS
CROSSLEVEL

400-FOOT RMS
CROSSLEVEL

MEAN PROFILE

MEAN ALIGNMENT

CROSSLEVEL
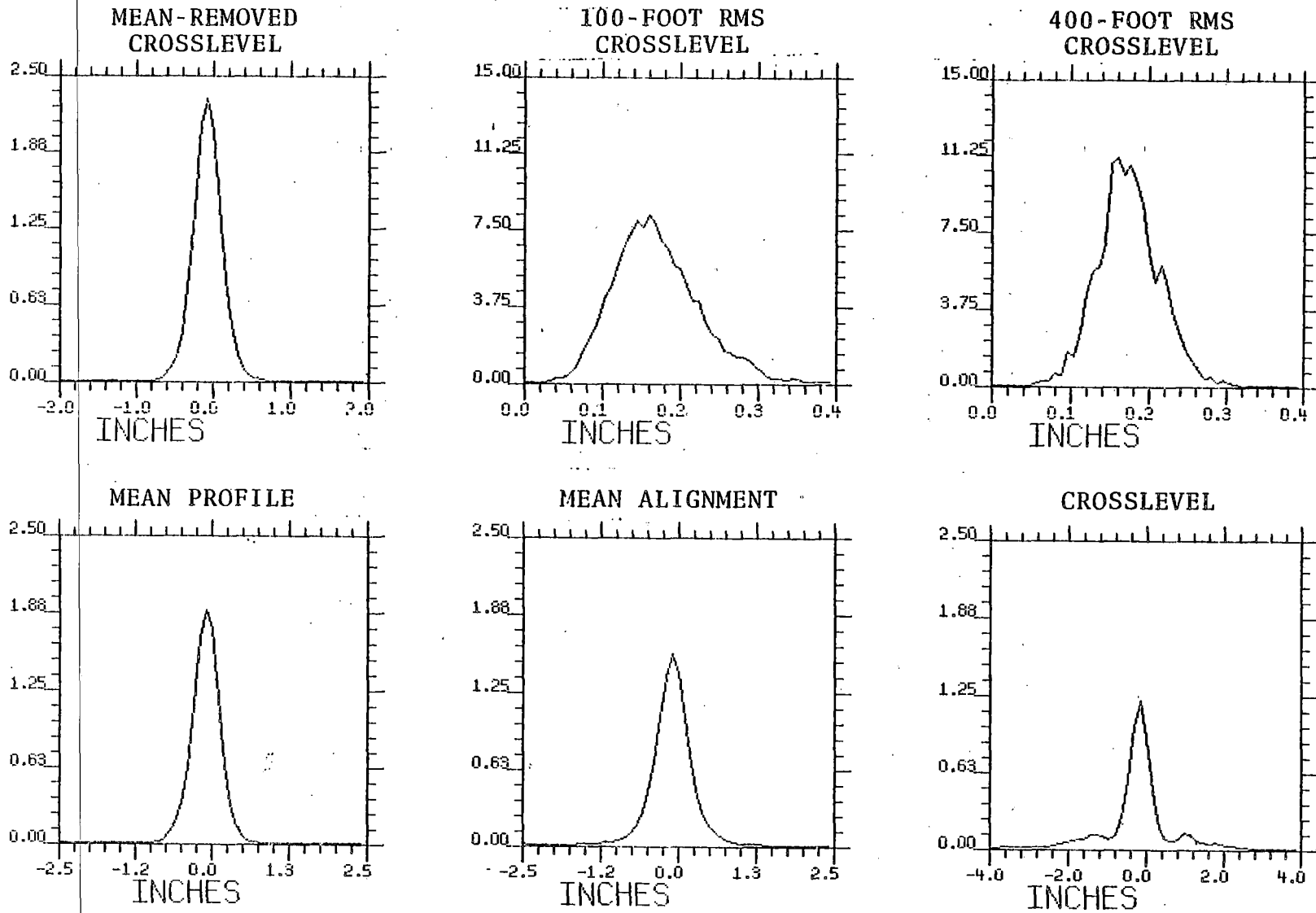
Figure 3-30. Probability Density Functions for Normal Class 2 Track

MEAN-REMOVED
CROSSLEVEL

100-FOOT RMS
CROSSLEVEL

400-FOOT RMS
CROSSLEVEL

MEAN PROFILE

MEAN ALIGNMENT

CROSSLEVEL
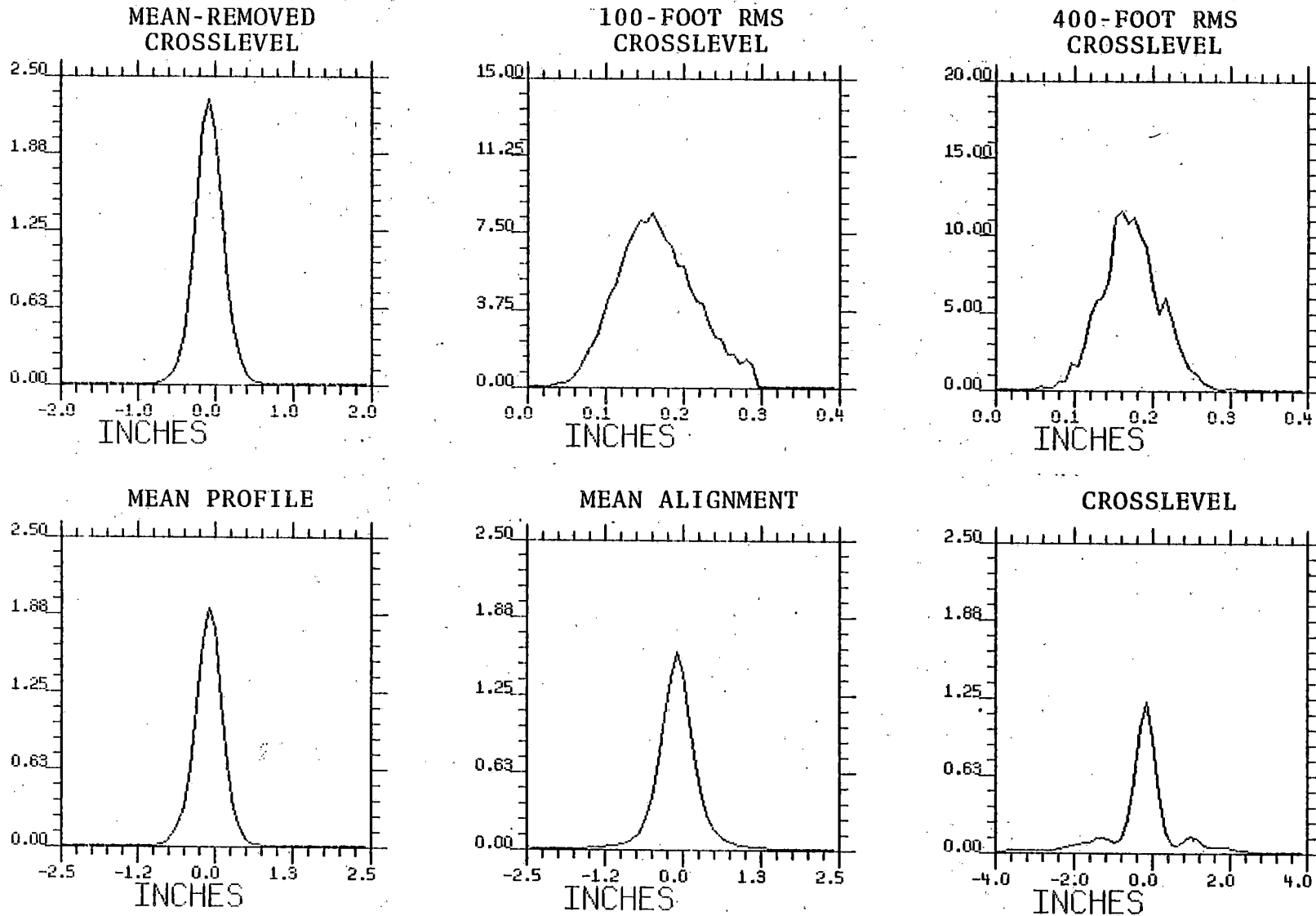
Figure 3-31. Probability Density Functions for 100-Foot Constrained Class 2 Track

MEAN-REMOVED
CROSSLEVEL

100-FOOT RMS
CROSSLEVEL

400-FOOT RMS
CROSSLEVEL

INCHES

INCHES

INCHES

MEAN PROFILE

MEAN ALIGNMENT

CROSSLEVEL

INCHES

INCHES

INCHES
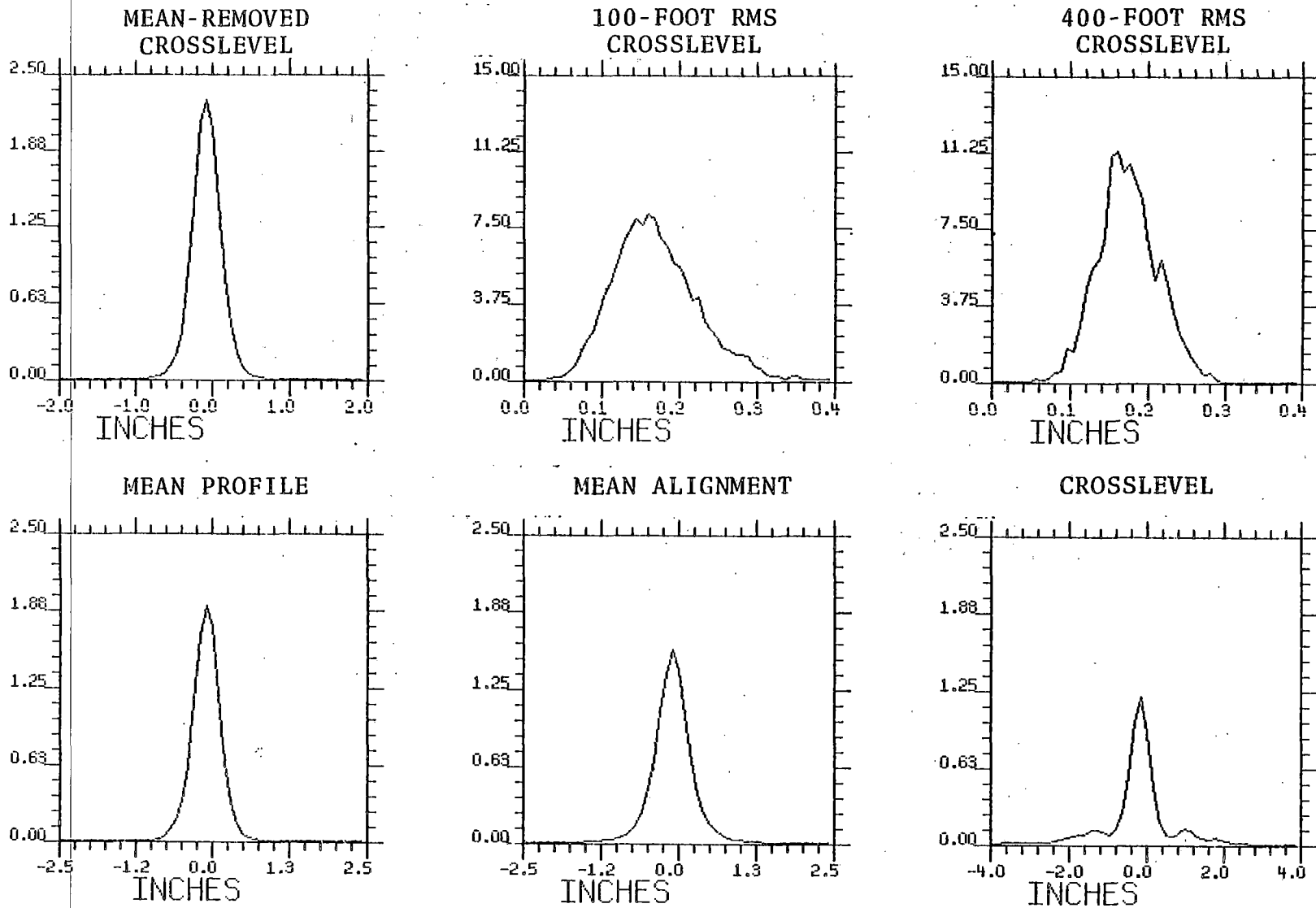
Figure 3-32.   Probability Density Functions for 400-Foot Constrained Class 2 Track
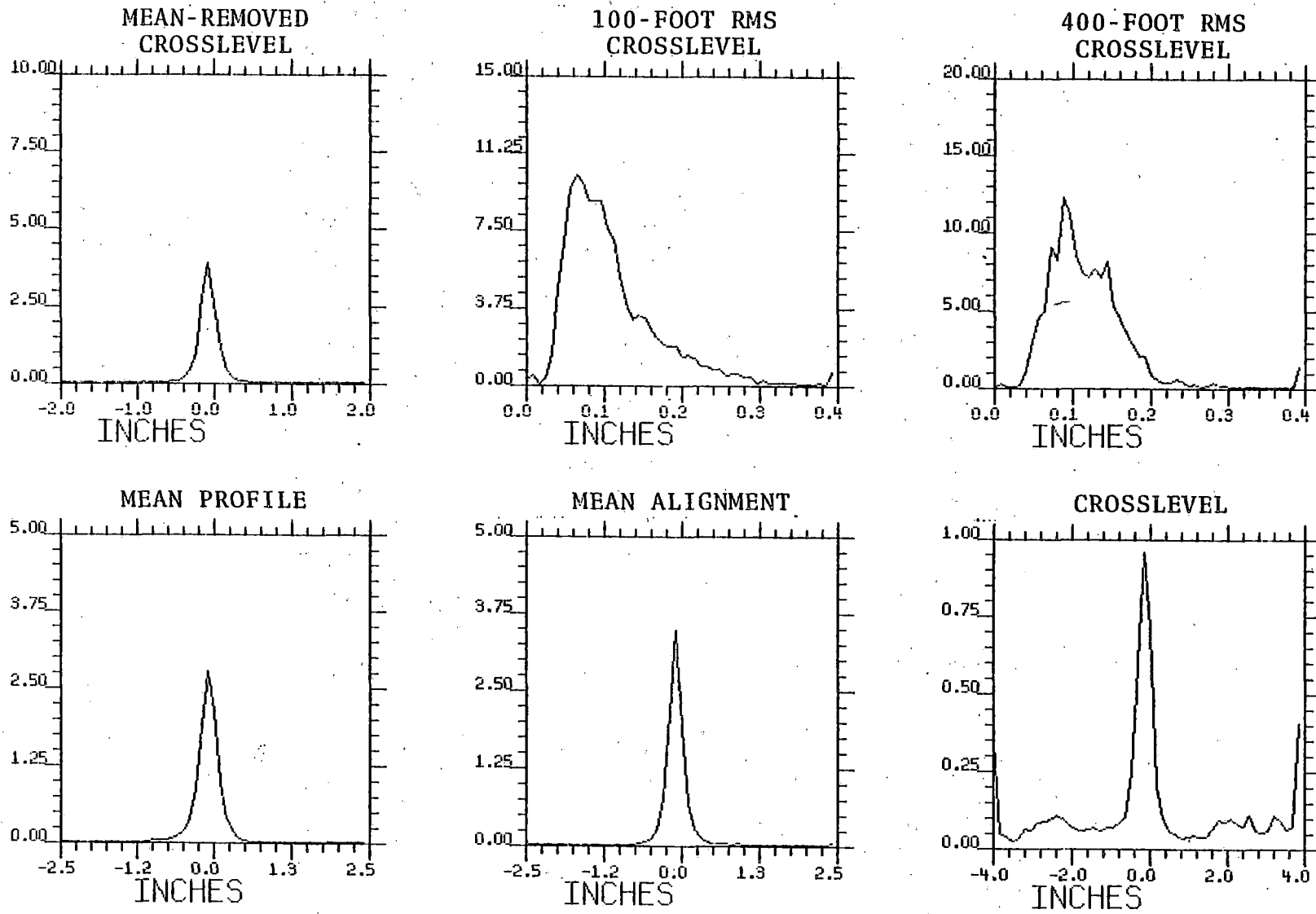
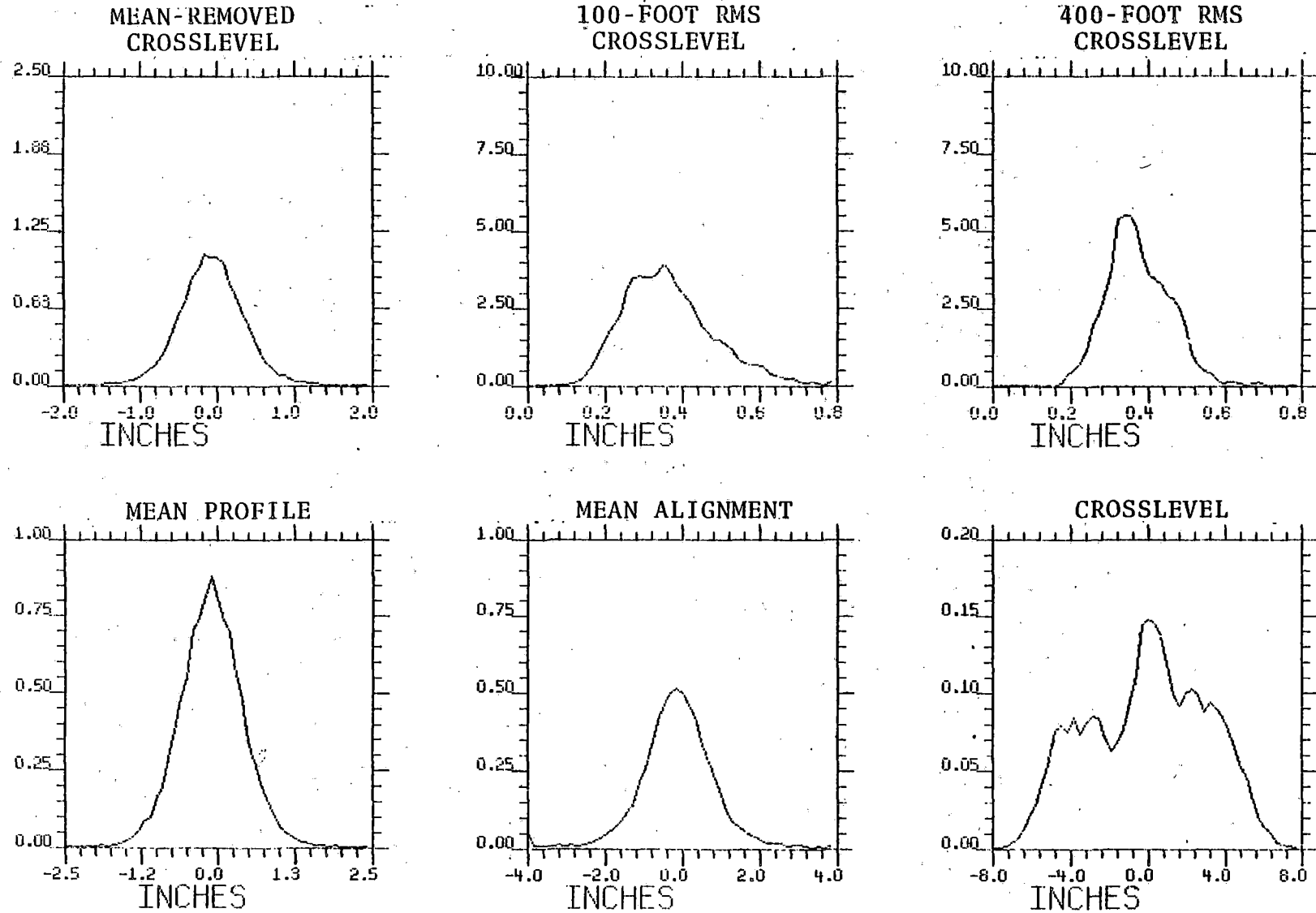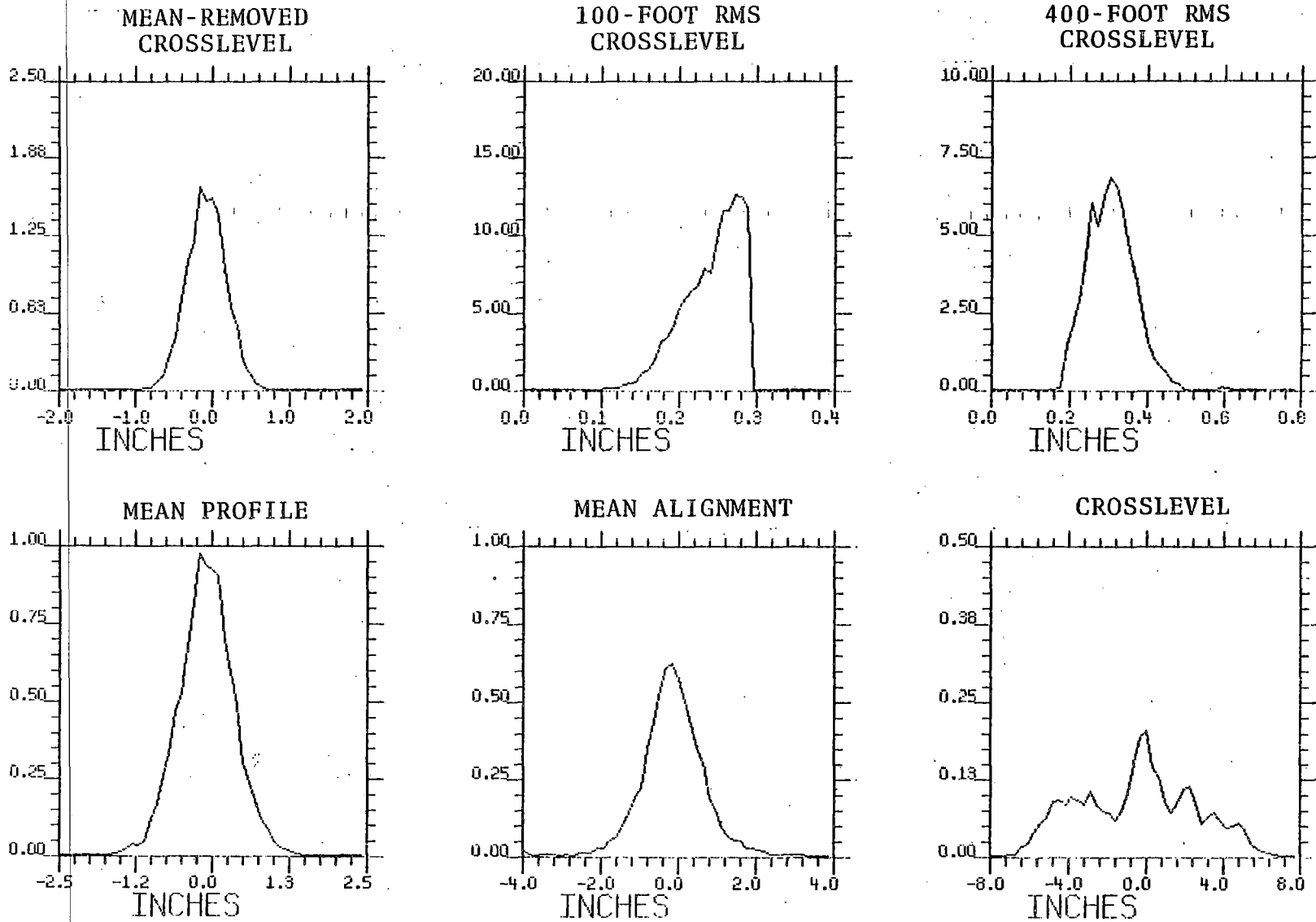Figure 3-33. Probability Density Functions for Normal Class 3 Track
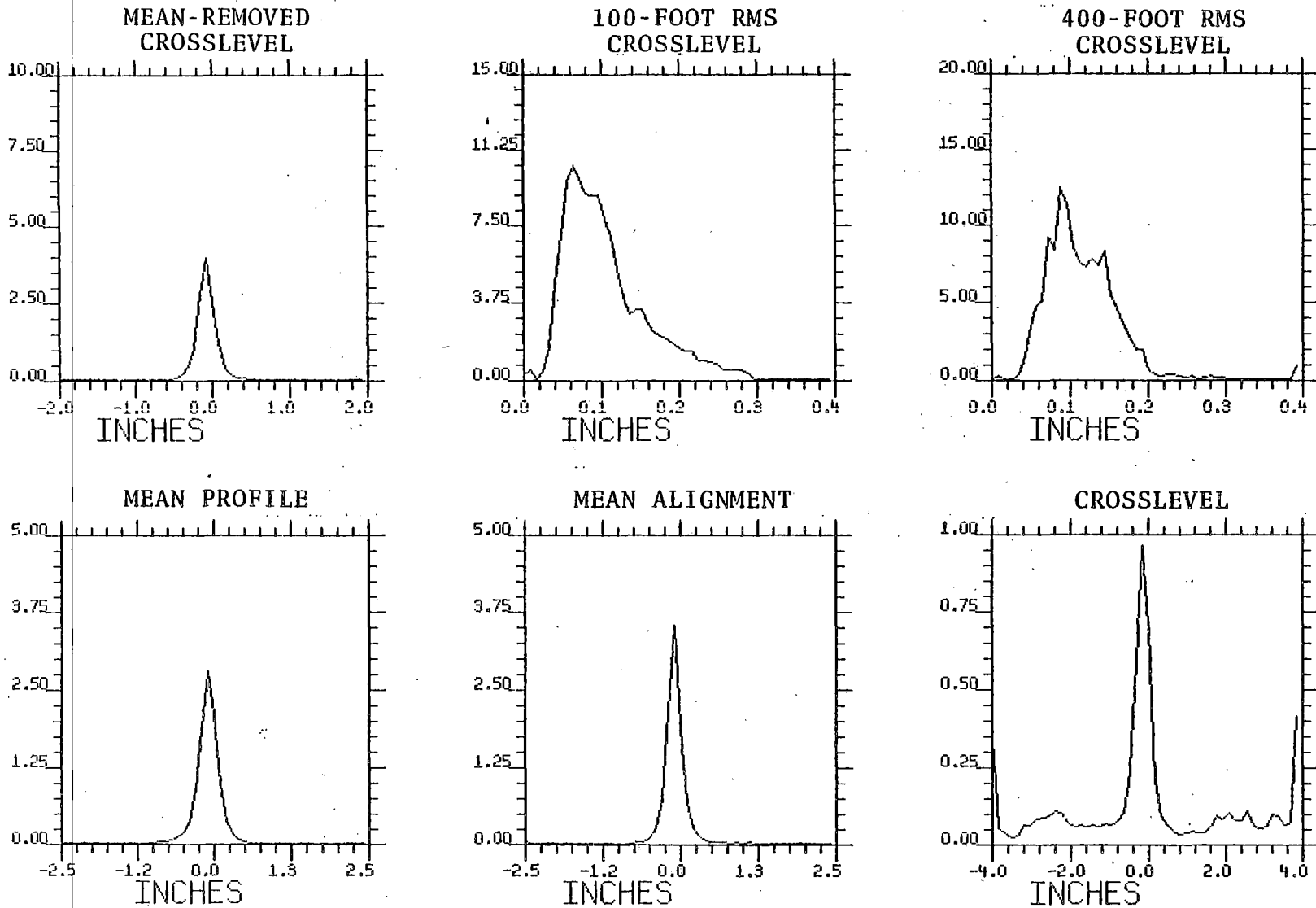
Figure 3-34.Probability Density Functions for
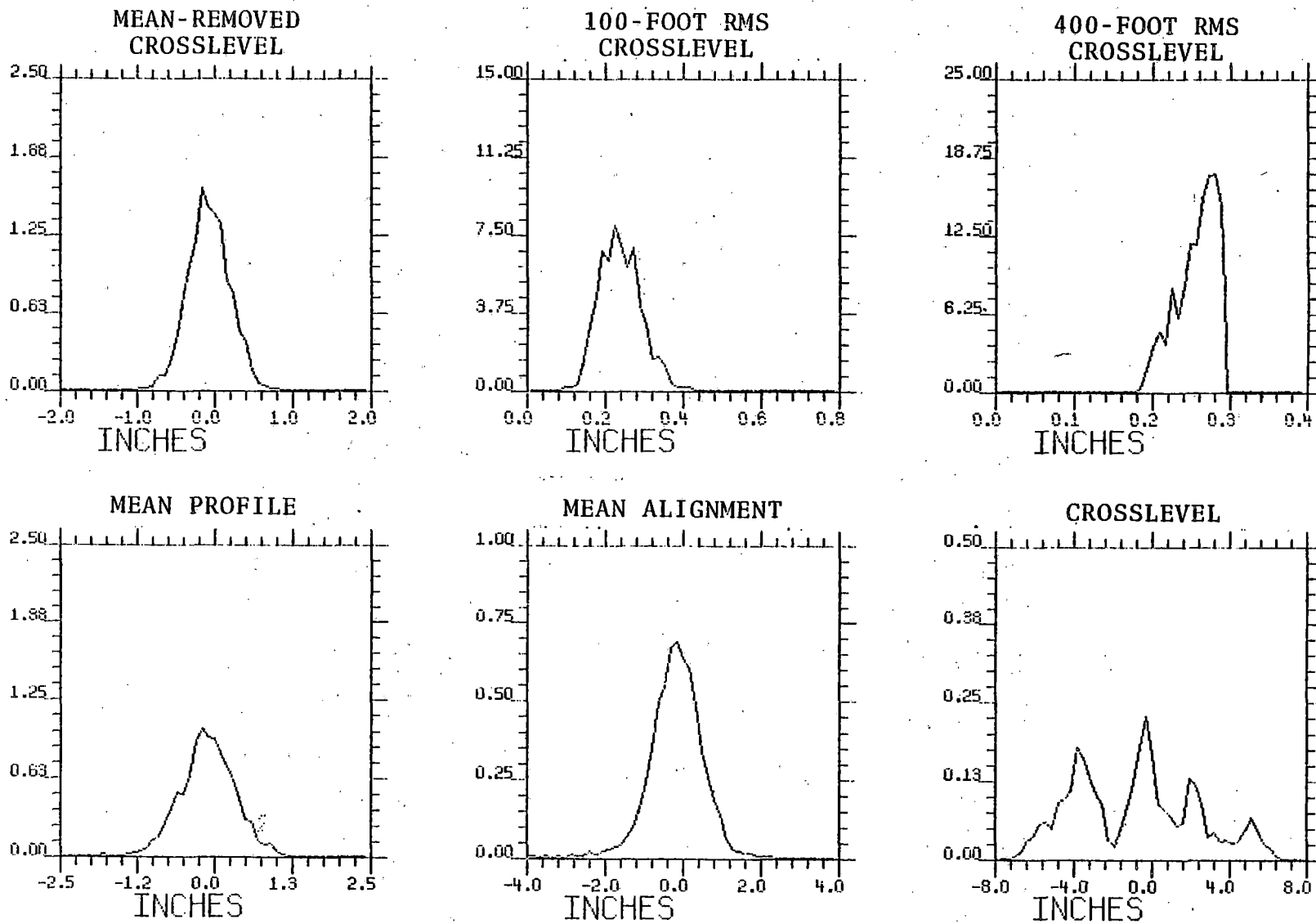100-Foot Constrained Class 3 Track
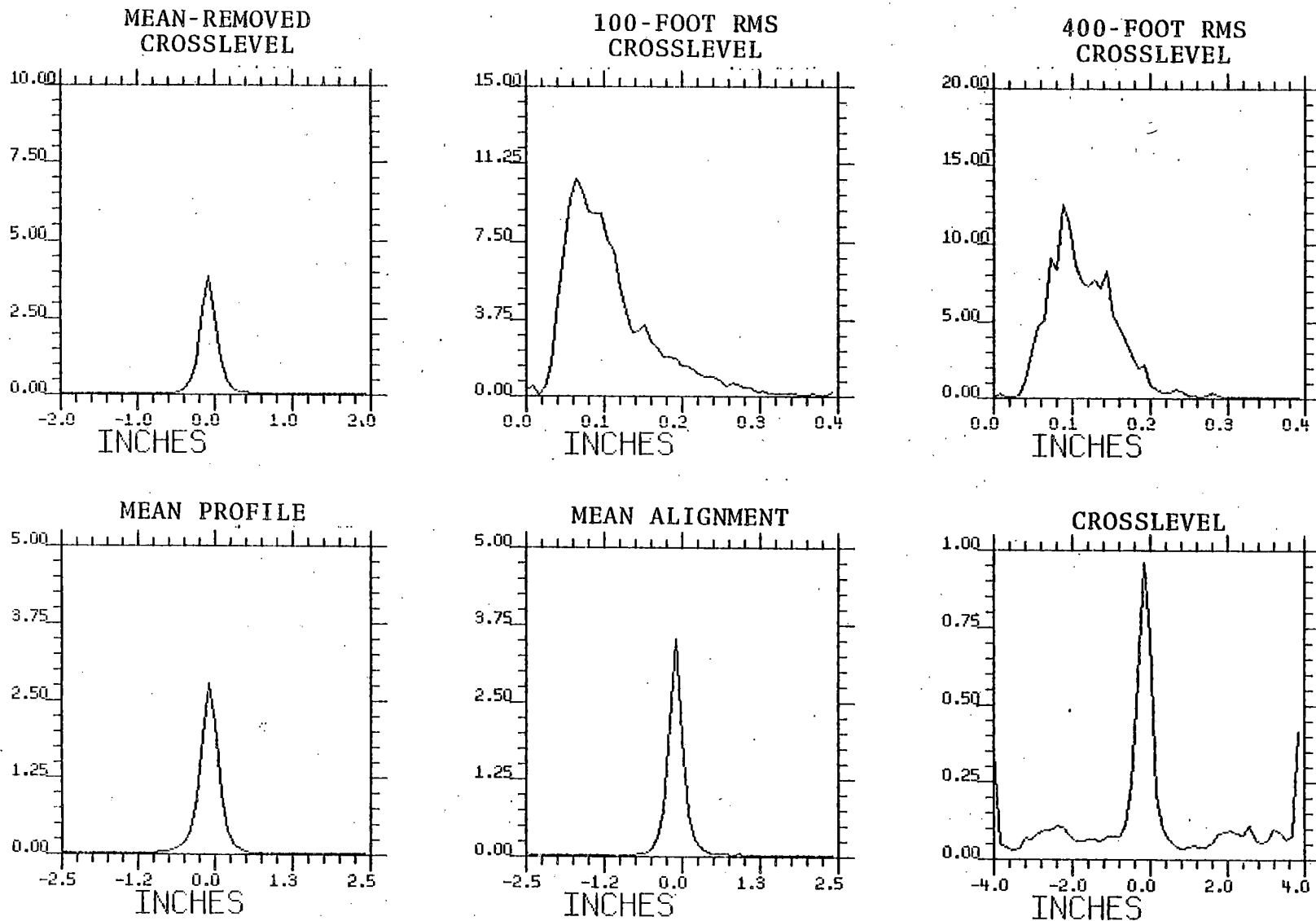
Figure 3-35. Probability Density Functions for 400-Foot Constrained Class 3 Track
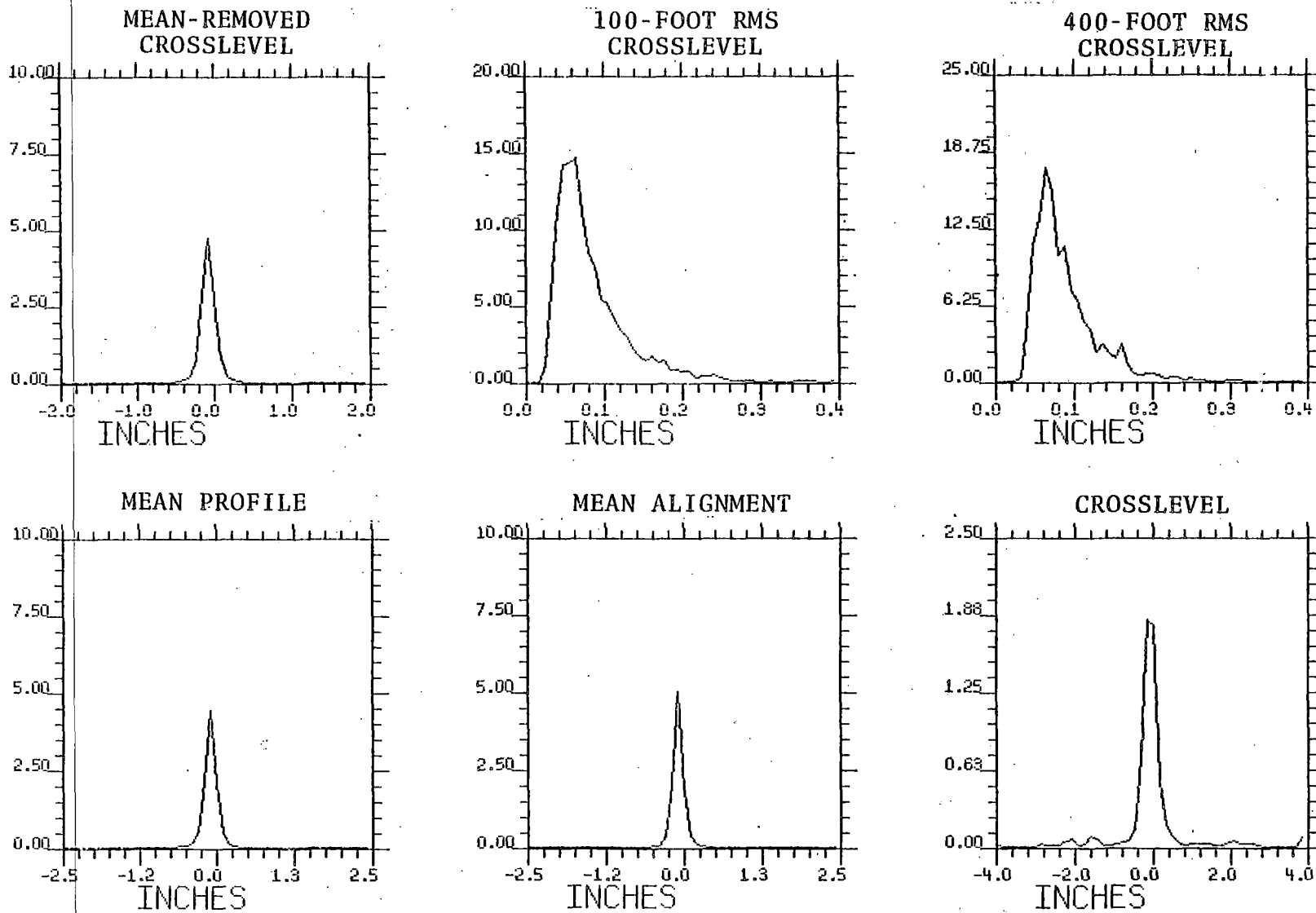
Figure 3-36. Probability Density Functions for Normal Class 4 Track

MEAN-REMOVED
CROSSLEVEL

100-FOOT RMS
CROSSLEVEL

400-FOOT RMS
CROSSLEVEL

MEAN PROFILE

MEAN ALIGNMENT

CROSSLEVEL

INCHES
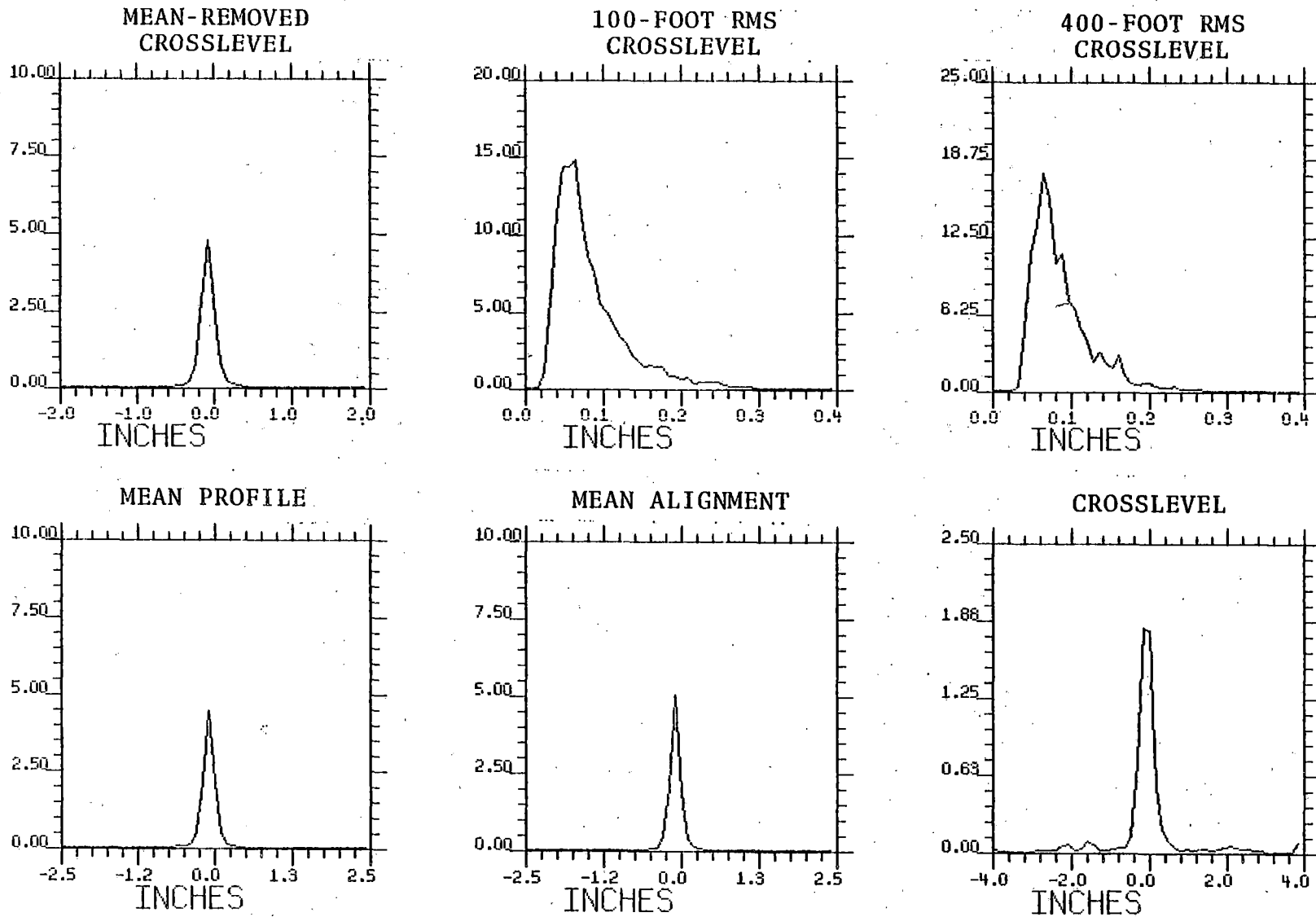
Figure 3-37, Probability Density Functions for
100-Foot Constrained Class 4 Track

MEAN-REMOVED
CROSSLEVEL

100-FOOT RMS
CROSSLEVEL

400-FOOT RMS
CROSSLEVEL

MEAN PROFILE

MEAN ALIGNMENT

CROSSLEVEL

INCHES

INCHES

INCHES
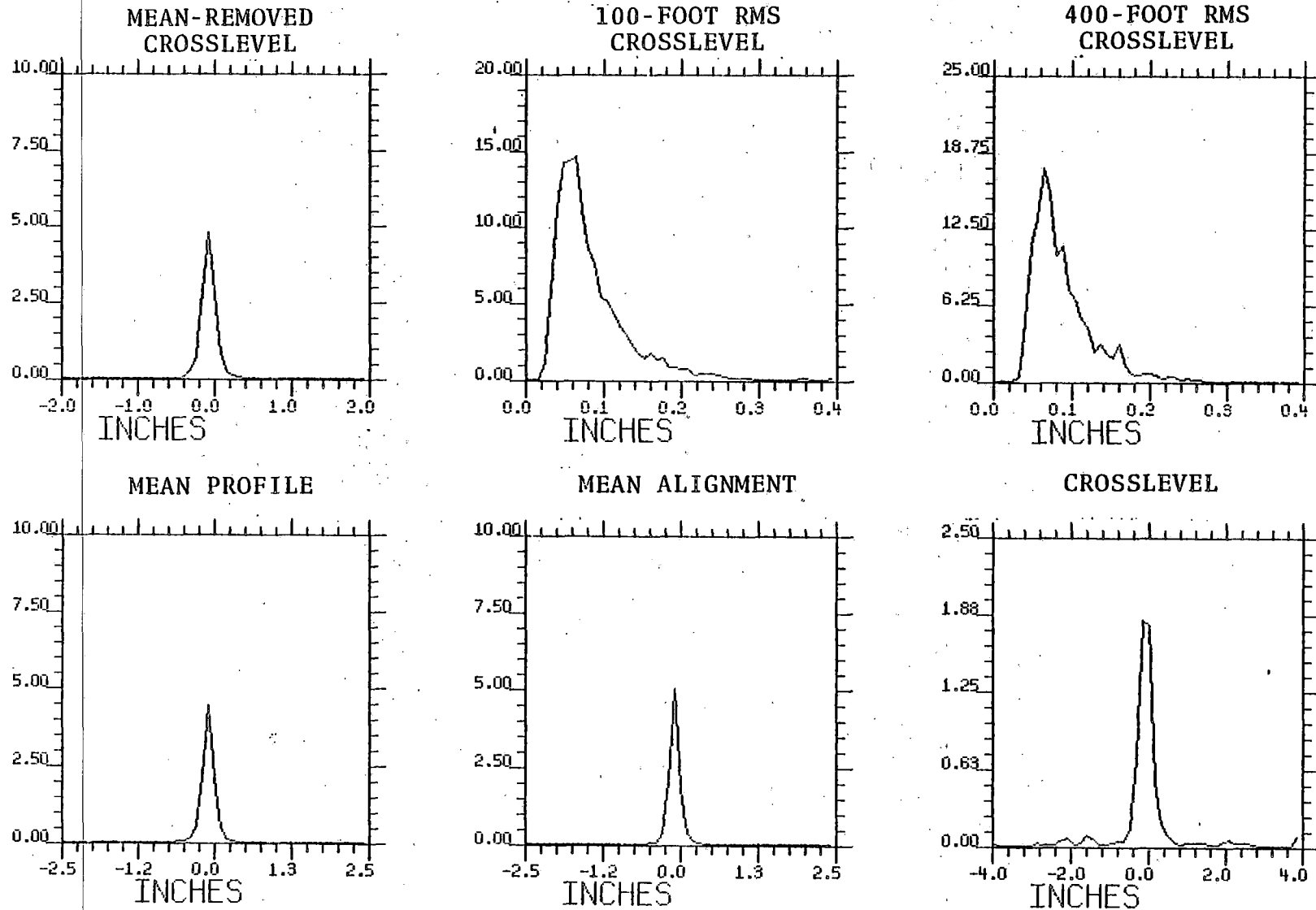
Figure 3-38. Probability Density Functions for
400-Foot Constrained Class 4 Track

The 400-foot rms crosslevel peaks for class 1 track appeared
at 0.35 inch for normal track, 0.32 inch for 100-foot con-
strained track and 0.29 inch for 400-foot constrained track.
All three track categories had their maximum densities at
0.17 inch for class 2 track, 0.1 inch for class 3 track,
and 0.07 inch for class 4 track.

Table 3-13 lists the ninety-five percentile levels for
normal and constrained track. The percentile level decreases
with the track class as expected. The most notable difference
is found between the normal and the constrained track in
class 1. Class 4 track does not show any difference between
the normal and constrained track in any track geometry
parameters.

Table 3-14 summarizes the means and standard deviations for
various parameters. Mean-removed crosslevel, mean profile
and mean alignment have a zero mean and are not listed in
the table. Constrained track, in general, has a lower mean
and standard deviation than normal track. Again class 4
track is found to have no difference between normal and con-
strained track.

From the description of the possible track geometry variations
for constrained track, constrained class 4 track based on a
0.3-inch rms crosslevel limit appears to be similar to normal
class 4 track. Mathematical representations of track geometry
variations for class 4 track as given in Reference 1 can also
be applied to constrained track. However, it should be noted
that these results are based on a statistically small sample
of track and should be verified by using a larger data base.

Table 3-13. Ninety-five Percentile Levels for Normal and Constrained Track (Inches)

	CLASS 1			CLASS 2			CLASS 3			CLASS 4		
	Normal	100-Foot Con-strained	400-Foot Con-strained	Normal	100-Foot Con-strained	400-Foot Con-strained	Normal	100-Foot Con-strained	400-Foot Con-strained	Normal	100-Foot Con-strained	400-Foot Con-strained
Mean Removed Crosslevel	0.61	0.37	0.38	0.28	0.26	0.27	0.17	0.15	0.16	0.13	0.13	0.13
100-Foot rms Crosslevel	0.59	0.29	0.34	0.28	0.25	0.27	0.23	0.22	0.23	0.18	0.18	0.18
400-Foot rms Crosslevel	0.51	0.41	0.29	0.25	0.23	0.24	0.20	0.19	0.19	0.17	0.17	0.17
Mean Profile	0.78	0.69	0.66	0.31	0.30	0.31	0.24	0.23	0.24	0.13	0.13	0.13
Mean Alignment	1.44	1.20	0.94	0.49	0.47	0.48	0.23	0.22	0.23	0.12	0.12	0.12

Table 3-14. Comparison Between Normal and Constrained Track

Class	Type	Mean Removed Crosslevel σ**	100-Foot RMS Mean	100-Foot RMS σ	400-Foot RMS Mean	400-Foot RMS σ	Mean Profile σ	Mean Alignment σ	Crosslevel Mean	Crosslevel σ
1	Normal	0.40	0.38	0.115	0.39	0.079	0.50	1.11	0.30	3.04
	100-Foot Constrained	0.24	0.25	0.036	0.32	0.059	0.43	0.82	-0.13	2.94
	400-Foot Constrained	0.26	0.25	0.052	0.26	0.025	0.43	0.67	-0.51	3.09
2	Normal	0.19	0.18	0.055	0.18	0.039	0.22	0.37	-0.06	0.82
	100-Foot Constrained	0.18	0.17	0.049	0.18	0.037	0.22	0.35	-0.71	0.81
	400-Foot Constrained	0.19	0.17	0.054	0.18	0.038	0.22	0.36	-0.07	0.81
3	Normal	0.15	0.12	0.079	0.13	0.068	0.27	0.39	0.16	2.18
	100-Foot Constrained	0.12	0.11	0.053	0.12	0.057	0.20	0.32	0.17	2.18
	400-Foot Constrained	0.13	0.11	0.057	0.12	0.040	0.19	0.32	0.15	2.18
4	Normal	0.10	0.09	0.048	0.09	0.039	0.11	0.29	0.09	0.92
	100-Foot Constrained	0.10	0.09	0.044	0.09	0.037	0.11	0.22	0.09	0.92
	400-Foot Constrained	0.10	0.09	0.047	0.09	0.038	0.11	0.22	0.09	0.92

* All quantities are in inches
** Standard deviation

3-77

3.6 TRACK DEGRADATION

Five zones of class 2 and class 3 bolted track were selected
at random to evaluate track degradation rates. Each zone
was approximately two miles in length. Track geometry data
were collected on these zones approximately one year apart
in 1978 and 1979. No maintenance was reported for these
zones between the two track geometry surveys. The rail
weight for these zones was 131 to 136 pounds per yard and the
annual gross tonnage was approximately 10 million tons.

The data were processed to compute the 100-foot rms and
400-foot rms crosslevel for the two time periods. The mean
and standard deviation for the rms descriptors for each time
period are shown in Table 3-15. The mean rms values for
1978 agree with the average for class 2 and class 3 track,
as given in Table 3-9. For 1979, these values correspond
to the value for class 2 track. The standard deviation of
the rms descriptor did not change significantly between 1978
and 1979.

The test data were divided into 1/8 mile segments. Mean values
of rms descriptors were computed for each segment. The rms
descriptors for 1979 were plotted against 1978 values.
Least squares regression lines were drawn between data points
to estimate the degradation rates. The results are shown
in Figures 3-39 and 3-40 for the 100-foot rms and 400-foot
rms crosslevel. For the purpose of this discussion, the
least squares regression lines are represented by an equa-
tion of the type:

$$y = a + bx, \qquad\qquad (3.15)$$

where y is the rms crosslevel for 1979, x is the rms cross-
level for 1978, a is the intercept, and b is the slope which
corresponds to the degradation rate per year per inch.

Table 3-15. RMS Crosslevel Descriptors for 1978 and 1979
           (Inches)

| PARAMETER | 1978 | | 1979 | |
	MEAN	STANDARD DEVIATION	MEAN	STANDARD DEVIATION
Mean Removed Crosslevel	0.000	0.160	0.000	0.190
100-Foot rms Crosslevel	0.143	0.051	0.179	0.057
400-Foot rms Crosslevel	0.146	0.041	0.183	0.044

For the 100-foot rms crosslevel, the intercept was 0.06 inch and the slope was 0.85.   For the 400-foot rms crosslevel, the corresponding values were 0.06 inch and 0.86.

Assuming an annual degradation rate of 0.85 inch/inch (average for the 100-foot and 400-foot rms crosslevel), a class 3 track will degrade to class 2 track in approximately one and one half years (refer to Table 3-9). On the otherhand, a class 4 track will degrade to class 3 track in approximately one year.

It should be pointed out that these results are based on a limited data base, and data show large variation about a regression line. This study does not take into account variations in other parameters which affect track degradation such as physical, traffic and environmental conditions. A further study is required to evaluate the degradation rates in relation to these conditions.
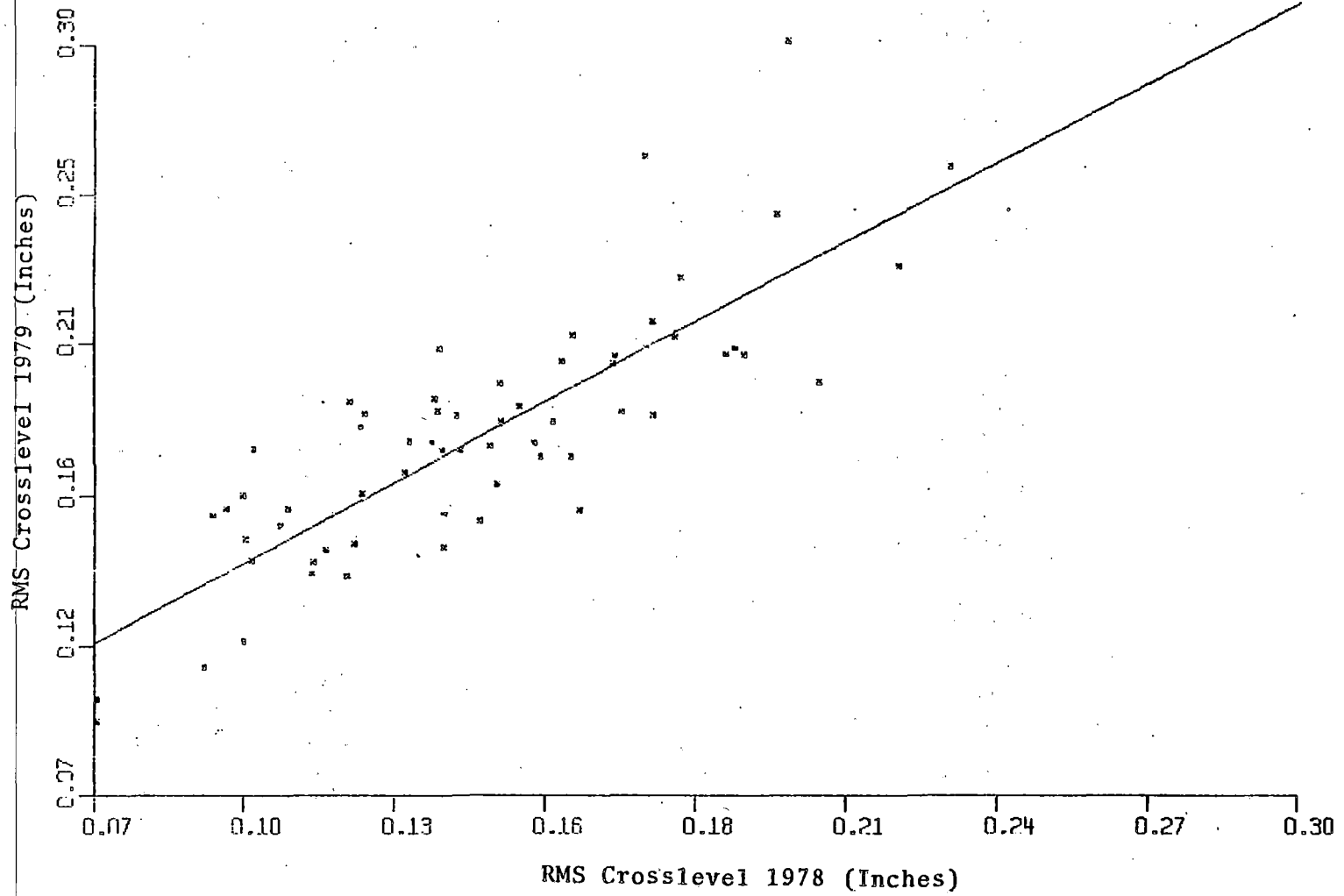
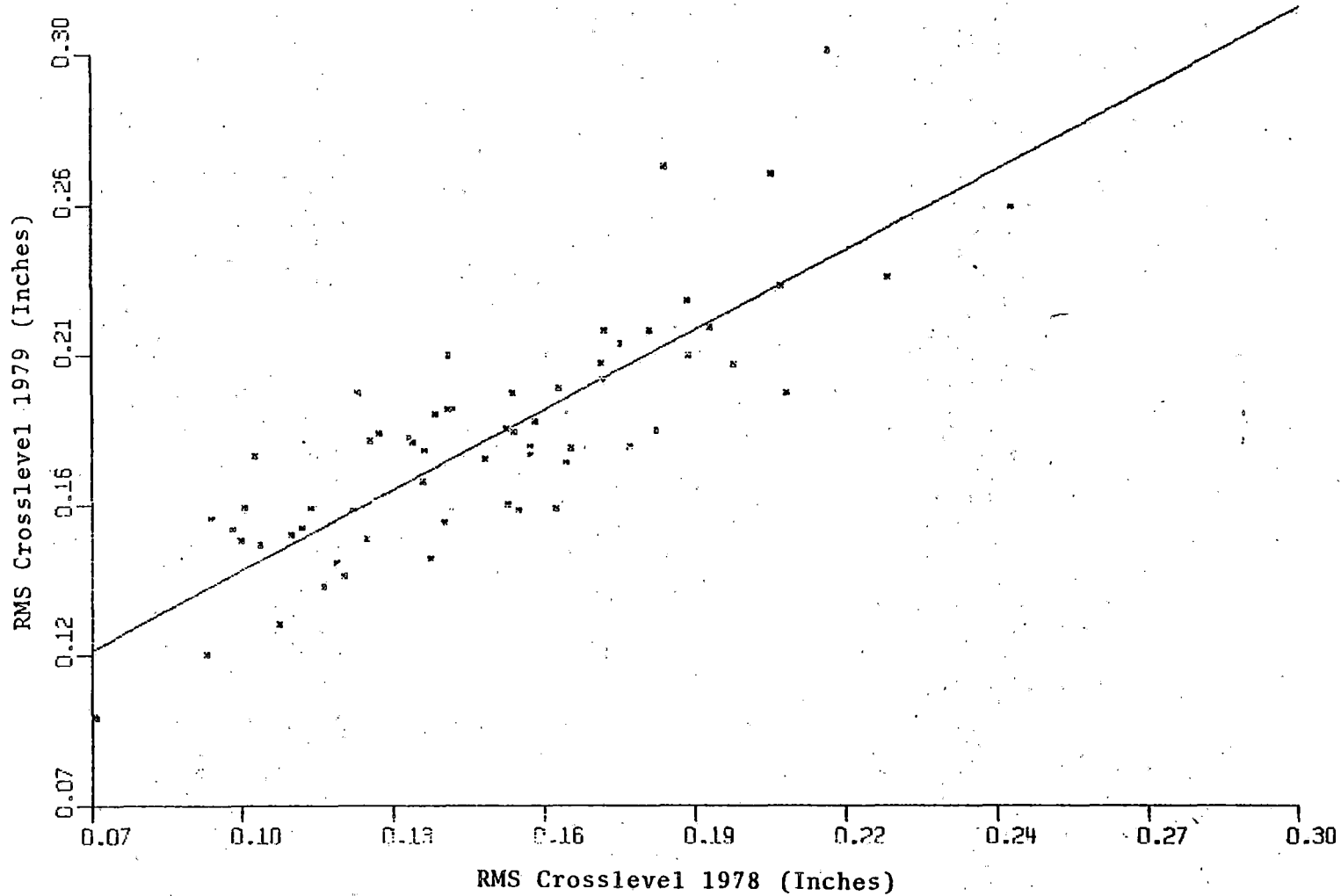Figure 3-39. Track Degradation Based on 100-Foot RMS Crosslevel

Figure 3-40. Track Degradation Based on 400-Foot RMS Crosslevel

4. CONCLUSIONS AND RECOMMENDATIONS

4.1 CONCLUSIONS

The principal conclusions from this study can be summarized as follows:

- Severe track geometry variations are composed of three key signatures: the cusp, bump and jog which occur either as single events, in periodic succession or in combination with each other.

- Track inputs in the wavelength range of 3 to 300 feet are important to vehicle dynamics. Therefore, a track geometry descriptor must address this wavelength range.

- The MCO measurements do not give enough weight to certain wavelengths and have blind spots at other wavelengths of interest.

- Severe track geometry variations can be monitored by such track geometry descriptors as peak-to-peak value, extreme value, and/or the rms value of the band-limited space curve of various track geometry parameters over a prescribed length of track.

- Track geometry descriptors can be implemented by modifying the data processing schemes used by current automated track geometry cars. For non-automated field measurements, an asymmetrical chord or a combination of two or more MCO's can remove the deficiencies of single MCO type measurements. The periodic crosslevel behavior can be estimated either by 20-Foot warp or by average crosslevel on consecutive joints.

- A 0.3-inch specification limit for rms crosslevel will affect most of class 1 track, a significant portion of class 2 and a small amount of class 3 track. Track classes 4, 5 and 6 will not be affected by this specification limit. For track class 4, constrained track does not show any variation from normal track.

4.2 RECOMMENDATIONS

Existing automated track geometry vehicles do not measure
the state-of-wear of the railhead. The contact point at
the wheel/rail interface plays an important role in vehicle
dynamic behavior. Therefore, a study should be conducted
to characterize railhead profiles. Measurement techniques
should be developed for automated measurements of railhead
profiles.

Track degradation rates are expected to be a function of the
physical and operating conditions of track. Short term
degradation is slow and data from successive runs may be
contaminated with instrumentation noise and sampling errors.
A long term data base should be established and analyzed
with respect to the physical and operating conditions and
the maintenance history of track to determine degradation
rates so that the frequency of inspections can be ascertained.

5. REFERENCES

1. Corbin, J.C., "Statistical Representations of Track Geometries," Vols. I and II, FRA/ORD-80/22,I,II -- DOT-TSC-FRA-80-4,I,II, March 1980.

2. Safety Recommendation Bulletins of the National Transportation Safety Board, Washington DC, 1975-1979.

3. "Track Train Dynamics, Accident Investigation," Association of American Railroads, Chicago IL, 1974.

4. A. E. Shulman and C. E. Taylor, "Analysis of Nine Years of Railroad Accident Data," Association of American Railroads, Washington DC, April 1976, p. 18, 21, 24-37.

5. "Track Safety Standards," Federal Railroad Administration, Reprinted from Railroad Track Structures, as published in the Federal Register, February 1973.

6. W. Flugge, "Handbook of Engineering Mechanics," McGraw Hill, New York, 1962, p. 56-11, 59-9.

7. "LIMRV Track Construction, High Speed Ground Test Center, Pueblo, Colorado," Federal Railroad Administration, Washington DC, 1974.

APPENDIX A

REPORT OF NEW TECHNOLOGY

The work performed under this contract significantly contributes to the state of the art in the area of analytical description of track geometry variations. Analytical descriptions were developed for dynamically severe track geometry variations. Track descriptors were developed to monitor these variations.

Critical signatures for severe track geometry variations consist of a cusp, bump and jog. These signatures can occur as single events, in systematic combination with one another, or in a periodic succession. Track geometry descriptors were developed to monitor the severe track geometry variations. These descriptors are based on either the extreme value or the rms value of a track geometry parameter over a prescribed length of track.

APPENDIX B
VEHICLE RESPONSE

It is important for the derivations which follow to consider three types of response functions: motion response of the carbody-to-track inputs, the relative displacement between the truck and carbody, and the forces acting across the wheel/rail interface.

These response functions are derived from the simple vehicle model shown in Figure B-1. As indicated in Section 2.2, this model is quite adequate to illustrate the important points about vehicle response to track inputs.

B.1 CARBODY RESPONSE TO TRACK INPUTS

The equation of motion for the simple model in Figure B-1 is given by:

$$m\ddot{y} + b(\dot{y} - \dot{x}) + k(y - x) = 0 , \qquad (B.1)$$

where m is the body mass, b is the damping coefficient, k is the spring constant, x is the track geometry input and y is the displacement induced in the carbody. The dots indicate time derivatives.

Equation B.1 can be written as:

$$m\ddot{y} + b\dot{y} + ky = b\dot{x} + kx , \qquad (B.2)$$

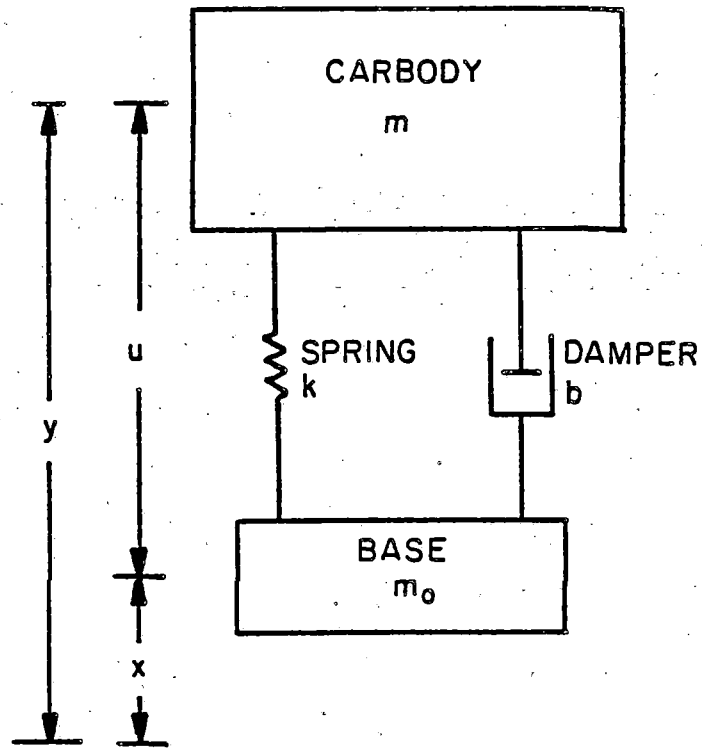whose solution is given in reference 6.

Figure B-1.   Simple Vehicle Model

The response function, $F_1(\omega)$ which describes the motion of m due to motion at m_0 is defined as

$$F_1(\omega) = \frac{Y(\omega)}{X(\omega)},$$ (B.3)

where ω is the radian frequency.

From reference 9

$$F_1(\omega) = \frac{2\beta i(\omega/\omega_0) + 1}{1 - (\omega/\omega_0)^2 + 2\beta i(\omega/\omega_0)}.$$ (B.4)

The magnitude of $F_1(\omega)$ is given by:

$$|F_1(\omega)| = \sqrt{\frac{1 + 4\beta^2 \frac{\omega^2}{\omega_0^2}}{\left(1 - \frac{\omega^2}{\omega_0^2}\right)^2 + 4\beta^2 \frac{\omega^2}{\omega_0^2}}},$$ (B.5)

where

$$\beta = \text{damping ratio} = \frac{b}{2\sqrt{mk}}$$ (B.6)

$$\omega_0 = \text{natural frequency} = \sqrt{\frac{k}{m}}.$$ (B.7)

B.2 RELATIVE DISPLACEMENT BETWEEN WHEELSET AND CARBODY

The response function for the relative displacement between m and m_0 can be derived as follows.

Substituting $u = y - x$ and $y = u + x$ in Equation B.1 it can be written as:

$$m(\ddot{u} + \ddot{x}) + b\dot{u} + ku = 0,$$ (B.8)

B-3

which can be rewritten as:

$$m\ddot{u} + b\dot{u} + ku = m\ddot{x},$$ (B.9)

whose solution is given in reference 6. Some of the inter-
mediate derivations which will be used in Section B-3 are given
below.

Let $U(s)$ be the Laplace Transform of $u(t)$ and $X(s)$ be the
Laplace Transform of $x(t)$. Upon substitution, the Laplace
Transform of Equation B.9 is given by

$$(ms^2 + bs + k)U(s) = -ms^2X(s).$$ (B.10)

The response function, $F_2(s)$ for the relative displacement
between m and m_0 is given by

$$F_2(s) = \frac{U(s)}{X(s)},$$ (B.11)

From Equations B.10 and B.11 the response function can be
written as

$$F_2(s) = \frac{-ms^2}{ms^2 + bs + k}.$$ (B.12)

Substituting $s = i\omega$, $\omega_0 = \sqrt{k/m}$ and $\beta = b/2\sqrt{mk}$

$$F_2(\omega) = \frac{\left(\frac{\omega}{\omega_0}\right)^2}{1 - \left(\frac{\omega}{\omega_0}\right)^2 + 2\beta i\left(\frac{\omega}{\omega_0}\right)}.$$ (B.13)

B.3 FORCE AT WHEEL/RAIL INTERFACE

Forces acting at the wheelset/sideframe of the model are shown
in Figure B-2. For equilibrium conditions, the force at the
wheel/rail interface can be written as

$$f(t) = m_0\ddot{x} - ku - b\dot{u}.$$ (B.14)

B-4

$$ku + b\mathring{u}$$

$$\uparrow$$

$$\boxed{\quad m_0 \quad} \quad \downarrow \; -m_0\ddot{x}$$
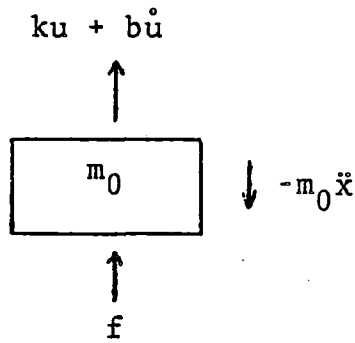
$$\uparrow$$

$$f$$

Figure B-2. Forces Acting at the Wheelset/Sideframe
for the Simple Vehicle Model

Taking the Laplace Transform of both sides of Equation B.14

$$F(s) = m_0 s^2 X(s) - (k + bs)U(s). \tag{B.15}$$

$F_3(s)$, the response function for the forces induced at the wheel/rail interface due to the track geometry input can be written as

$$F_3(s) = \frac{F(s)}{X(s)}. \tag{B.16}$$

From Equations B.15 and B.16

$$F_3(s) = m_0 s^2 - (k + bs) \frac{U(s)}{X(s)}. \tag{B.17}$$

Substituting $\dfrac{U(s)}{X(s)}$ from Equation B.12

$$F_3(s) = m_0 s^2 + \frac{(k + bs)ms^2}{ms^2 + bs + k}, \tag{B.18}$$

which can be written as

$$F_3(s) = m_0 s^2 \left(\frac{ms^2 + \left(1 + \frac{m}{m_0}\right)(bs + k)}{ms^2 + bs + k} \right). \tag{B.19}$$

B-5

Substituting $i\omega$ for s,

$$F_3(\omega) = -m_0\omega^2 \left(\frac{-m\omega^2 + \left(1 + \frac{m}{m_0}\right)(bi\omega + k)}{-m\omega^2 + bi\omega + k} \right).$$

(B.20)

B.4 ACCELERATION DUE TO LONG WAVELENGTH TRACK INPUTS

It was shown in the statistical characterization of track geometry (1) that in the long wavelength limits the alignment or profile power spectral density (PSD) is given by:

$$S(\phi) = \frac{A\phi_c^2}{\phi^4},$$

(B.21)

where $S(\phi)$ is the power spectral density in in^2/cy/ft, A is the roughness coefficient in in^2 cy/ft, ϕ_c is the break frequency in cy/ft, and ϕ is the spatial frequency in cy/ft.

The distance domain PSD, $S(\phi)$, can be converted to the time domain PSD, $S(f)$, by the transformation of variables. Since $\phi = f/v$

$$S(\phi)d\phi = S(f)df = A\phi_c^2 \frac{v^3}{f^4} df,$$

(B.22)

where v is the speed in ft/sec, and f is the temporal frequency in Hz.

The acceleration induced in the carbody for all the frequencies up to a certain frequency, f' is given by

$$\sigma_a^2 = \int_0^{f'} (2\pi f)^4 S(f) |F_1(f)|^2 df.$$

(B.23)

The function in the integral is multiplied by $(2\pi f)^4$ to convert the displacement type motions to acceleration since

$$\text{Acceleration} = \frac{d^2x}{dt^2} \xrightarrow{\text{F.T.}} (2\pi f)^2 \xrightarrow{\text{Power}} (2\pi f)^4.$$

The vehicle response as given by Equation B.5 is unity for very long wavelengths. Substituting the values of $S(f)\,df$ and $|F_1(f)|$ in Equation B.23

$$\sigma_a^2 = \int_0^{f'} (2\pi f)^4 \, A\phi_c^2 \, \frac{v^3}{f^4} \, df, \tag{B.24}$$

Thus, the standard deviation of acceleration is given by

$$\sigma_a = 4\pi^2 \phi_c \sqrt{v^3 A f'}. \tag{B.25}$$

B.5 RELATIVE DISPLACEMENT DUE TO LONG WAVELENGTH TRACK INPUTS

The power of the relative displacement for low frequency inputs is given by

$$\sigma_d^2 = \int_0^{f'} S(f) |F_2(f)|^2 df, \tag{B.26}$$

where f' is the frequency limit in Hz.

The response function for the relative displacement is given by Equation B.13. For low frequencies, the response function varies as

$$\frac{\omega^2 m}{k} = \frac{\omega^2}{\omega_0^2} = \left(\frac{f}{f_0}\right)^2. \tag{B.27}$$

B-7

Substituting the values of $\left|F_2(f)\right|$ and $S(f)$ in Equation B.26

$$\sigma_d{}^2 = \int_0^{f'} A\phi_c{}^2 \frac{v^3}{f^4} \left(\frac{f}{f_0}\right)^4 df, \qquad (B.28)$$

which gives

$$\sigma_d{}^2 = A\phi_c{}^2 v^3 \left(\frac{f'}{f_0{}^4}\right). \qquad (B.29)$$

Thus, the relative displacement due to long wavelength profile or alignment perturbations is

$$\sigma_d = \sqrt{A\phi_c{}^2 v^3 \left(\frac{f'}{f_0{}^4}\right)}. \qquad (B.30)$$

B.6 TWO-DEGREE-OF-FREEDOM MODEL

The vehicle dynamic behavior was analyzed using the two-degree-of-freedom model shown in Figure B-3. The analysis provides an understanding of vehicle sensitivity to track inputs for translation and yaw rotation of the carbody. For this analysis, it is assumed that the carbody is rigid, the center of mass is at the geometric center of the car, the damping is viscous and the angle-of-rotation is small, i.e., $\sin \theta \simeq \theta$.

Summing the forces yields

$$M\ddot{x} = -K_1 \left\{ x(t) - \frac{L}{2} \theta(t) \right\} + K_1 y \left(t + \frac{\tau}{2} \right)$$

$$-K_2 \left\{ x(t) + \frac{L}{2} \theta(t) \right\} + K_2 y \left(t - \frac{\tau}{2} \right)$$
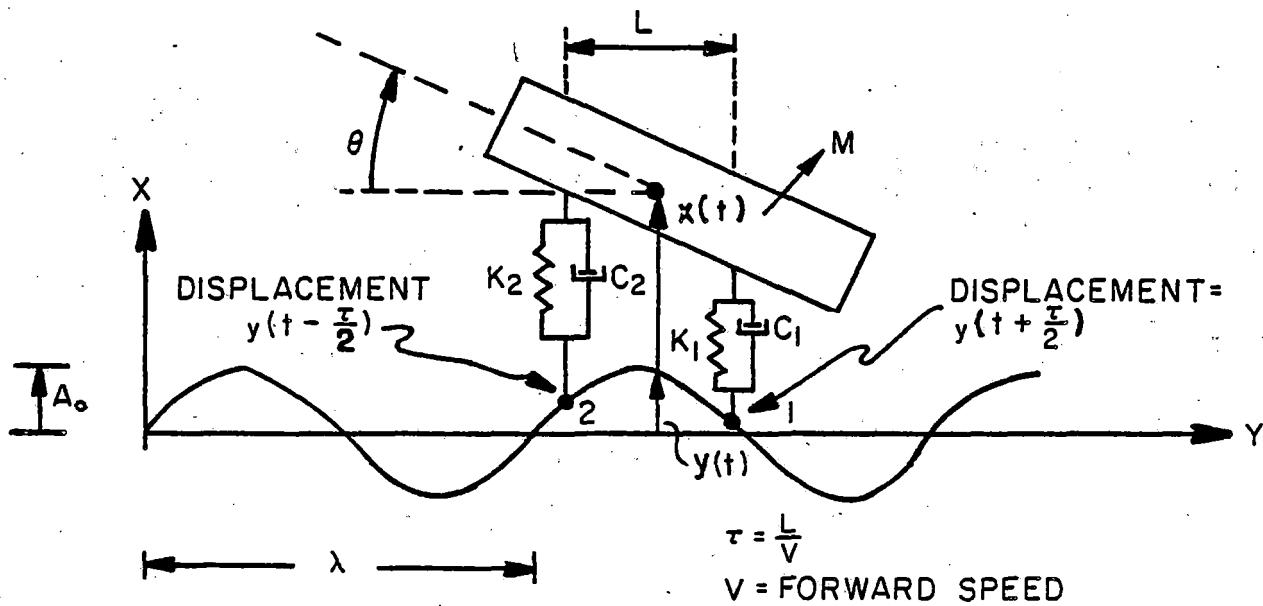
Figure B-3. A Two-Degree-of-Freedom Model

$$-C_1 \left\{ \dot{x}(t) - \frac{L}{2} \dot{\theta}(t) \right\} + C_1 \dot{y} \left(t + \frac{\tau}{2} \right)$$

$$-C_2 \left\{ \dot{x}(t) + \frac{L}{2} \dot{\theta}(t) \right\} + C_2 \dot{y} \left(t - \frac{\tau}{2} \right), \tag{B.31}$$

which after collecting like terms yields

$$M\ddot{x} + \left(K_1 + K_2 \right) x + \left(C_1 + C_2 \right) \dot{x}$$

$$+ \frac{L}{2} \left(K_2 - K_1 \right) \theta(t) + \frac{L}{2} \left(C_2 - C_1 \right) \dot{\theta}(t)$$

$$= K_1 y \left(t + \frac{\tau}{2} \right) + K_2 y \left(t - \frac{\tau}{2} \right)$$

$$+ C_1 \dot{y} \left(t + \frac{\tau}{2} \right) + C_2 \dot{y} \left(t - \frac{\tau}{2} \right). \tag{B.32}$$

Summing the moments, about the center-of-mass yields

$$MR^2\ddot{\theta} = + \frac{L}{2} K_1 \left\{ x(t) - \frac{L}{2} \theta(t) \right\} - \frac{L}{2} K_1 y \left(t + \frac{\tau}{2} \right)$$

$$- \frac{L}{2} K_2 \left\{ x(t) + \frac{L}{2} \theta(t) \right\} + \frac{L}{2} K_2 y \left(t - \frac{\tau}{2} \right)$$

$$+ \frac{L}{2} C_1 \left\{ \dot{x}(t) - \frac{L}{2} \dot{\theta}(t) \right\} - \frac{L}{2} C_1 \dot{y} \left(t + \frac{\tau}{2} \right)$$

$$- \frac{L}{2} C_2 \left\{ \dot{x}(t) + \frac{L}{2} \dot{\theta}(t) \right\} + \frac{L}{2} C_2 \dot{y} \left(t - \frac{\tau}{2} \right). \tag{B.33}$$

where R is the radius of gyration.

Euqation B.33 can be written as

$$MR^2\ddot{\theta} + \left(\frac{L}{2}\right)^2 K_1\theta + \left(\frac{L}{2}\right)^2 K_2\theta + \left(\frac{L}{2}\right)^2 C_1\dot{\theta} + \left(\frac{L}{2}\right)^2 C_2\dot{\theta}$$

$$+ \frac{L}{2}\left(K_2 - K_1\right)x + \frac{L}{2}\left(C_2 - C_1\right)\dot{x}$$

$$= -\frac{L}{2} K_1 y\left(t + \frac{\tau}{2}\right) + \frac{L}{2} K_2 y\left(t - \frac{\tau}{2}\right)$$

$$-\frac{L}{2} C_1\dot{y}\left(t + \frac{\tau}{2}\right) + \frac{L}{2} C_2\dot{y}\left(t - \frac{\tau}{2}\right). \tag{B.34}$$

If $\left(K_1 = K_2\right)$ and $\left(C_1 = C_2\right)$ then the equations of motion for translation and rotation can be decoupled and treated independently.

For translation:

$$M\ddot{x} + 2Kx + 2C\dot{x} = K\left\{y\left(t + \frac{\tau}{2}\right) + y\left(t - \frac{\tau}{2}\right)\right\}$$

$$+ C\left\{\dot{y}\left(t + \frac{\tau}{2}\right) + \dot{y}\left(t - \frac{\tau}{2}\right)\right\}. \tag{B.35}$$

For yaw rotation:

$$MR^2\ddot{\theta} + \frac{L^2}{2} K\theta + \frac{L^2}{2} C\dot{\theta} = K\frac{L}{2}\left\{y\left(t - \frac{\tau}{2}\right) - y\left(t + \frac{\tau}{2}\right)\right\}$$

$$+ C\frac{L}{2}\left\{\dot{y}\left(t - \frac{\tau}{2}\right) - \dot{y}\left(t + \frac{\tau}{2}\right)\right\}. \tag{B.36}$$

A track input can be assumed to be an alignment deviation of the form

$$y(t) = A_o\cos\frac{2\pi V t}{\lambda}, \tag{B.37}$$

where: A_o = peak amplitude in feet

$\quad\quad$ V = velocity of vehicle in feet per second

$\quad\quad$ λ = track wavelength in feet

$\quad\quad$ t = time in seconds.

After performing the trignometric transformation and substituting $\tau = L/V$, the equation of motion for body translation becomes

$$M\ddot{x} + 2C\dot{x} + 2Kx = 2KA_o\cos\left(\pi\frac{L}{\lambda}\right)\cos\left(2\pi\,\frac{Vt}{\lambda}\right).$$

$$- 4\pi CA_o\,\frac{V}{\lambda}\,\cos\left(\pi\frac{L}{\lambda}\right)\sin\left(2\pi\,\frac{Vt}{\lambda}\right) \quad\quad\text{(B.38)}$$

Similarly, the equation for yaw rotation can be written as:

$$MR^2\ddot{\theta} + \frac{L^2}{2}\,C\dot{\theta} + \frac{L^2}{2}\,K\theta = KLA_o\sin\left(\frac{\pi L}{\lambda}\right)\cos\left(\frac{2\pi Vt}{\lambda} - \frac{\pi}{2}\right)$$

$$\text{(B.39)}$$

$$+ 2\pi CA_o\,\frac{V}{\lambda}\,\sin\left(\frac{\pi L}{\lambda}\right)\sin\left(2\pi\,\frac{Vt}{\lambda} - \frac{\pi}{2}\right).$$

The solutions to Equations B.38 and B.39 can be written in complex algebra notations as:

$$X = A_o\cos\left(\frac{\pi L}{\lambda}\right)\sqrt{\frac{1 + \left(2\zeta_t\,\frac{\omega}{\omega_t}\right)^2}{\left[1 - \left(\frac{\omega}{\omega_t}\right)^2\right]^2 + \left(2\zeta_t\,\frac{\omega}{\omega_t}\right)^2}}\;e^{i\phi_t}\,e^{i\left(\frac{2\pi Vt}{\lambda}\right)} \quad\text{(B.40)}$$

$$\theta = A_o\sin\left(\frac{\pi L}{\lambda}\right)\sqrt{\frac{1 + \left(2\zeta_r\,\frac{\omega}{\omega_r}\right)^2}{\left[1 - \left(\frac{\omega}{\omega_r}\right)^2\right]^2 + \left(2\zeta_r\,\frac{\omega}{\omega_r}\right)^2}}\;e^{i\phi_r}\,e^{i\left(\frac{2\pi Vt}{\lambda} - \frac{\pi}{2}\right)}, \quad\text{(B.41)}$$

B-12

where

ω_t = natural frequency (translation)

ω_r = natural frequency (rotation)

ζ_t = damping ratio (translation)

ζ_r = damping ratio (translation)

ϕ_t = phase angle (translation)

ϕ_r = phase angle (rotation)

Thus, the carbody is most sensitive to alignment perturbations of wavelength equal to the truck spacing in the translation mode. The most detrimental wavelength in the yaw mode is equal to twice the truck spacing.

APPENDIX C
MID-CHORD OFFSET

C.1 WAVELENGTH RESPONSE OF MID-CHORD OFFSET

The mid-chord offset, $\delta(x)$, at point x is given by

$$\delta(x) = y(x) - \frac{1}{2}[y(x - L) + y(x + L)], \qquad (C.1)$$

where $y(x)$ is the track input and L is one-half the MCO length.

If the sample interval is one foot, the z-transform of Equation C.1 can be written as:

$$F(z) = -\frac{1}{2} + z^{-L} - \frac{1}{2}z^{-2L}. \qquad (C.2)$$

Substituting $z = e^{+i\omega}$ in Equation (C.2)

$$F(\omega) = -\frac{1}{2} + e^{-i\omega L} - \frac{1}{2}e^{-2i\omega L}, \qquad (C.3)$$

which can be written as

$$F(\omega) = e^{-i\omega L}[1 - \frac{1}{2}(e^{i\omega L} + e^{-i\omega L})], \qquad (C.4)$$

which can be simplified to

$$F(\omega) = e^{-i\omega L}[1 - \cos \omega L]. \qquad (C.5)$$

The magnitude of $F(\omega)$ is

$$|F(\omega)| = 1 - \cos \omega L = 2 \sin^2 \frac{\omega L}{2}. \qquad (C.6)$$

Substituting $\omega = 2\pi\phi$, the magnitude of the frequency response is

$$F(\phi) = 2 \sin^2 \pi\phi L. \tag{C.7}$$

The wavelength response of the MCO is then given by

$$F(\lambda) = 2 \sin^2 \frac{\pi L}{\lambda}. \tag{C.8}$$

C.2 RESPONSE OF KEY SIGNATURES TO MCO

C.2.1 CUSP

A cusp can be described by:

$$z = Ae^{-k|x|}, \tag{C.9}$$

where A is the maximum amplitude at $x = 0$ and k is the decay rate.

A mid-chord offset (MCO) of length 2L at $x = 0$ is given by:

$$T = \sum_{i=-1}^{1} C_i Ae^{-k|x_i|}, \tag{C.10}$$

where $C_{-1} = -\frac{1}{2}$, $C_0 = 1$, $C_1 = -\frac{1}{2}$, $x_{-1} = -L$, $x_0 = 0$, and $x_1 = L$. Thus Equation C.10 becomes:

$$\frac{T}{A} = -\frac{1}{2} e^{-kL} + 1 - \frac{1}{2} e^{-kL}, \tag{C.11}$$

which can be simplified to:

$$\frac{T}{A} = 1 - e^{-kL}. \tag{C.12}$$

For a 62-foot MCO, $\frac{T}{A}$ is given by:

$$\frac{T}{A} = 1 - e^{-31k}. \tag{C.13}$$

C.2.1   BUMP

A bump signature can be described by:

$$y = D e^{-1/2(kx)^2}, \tag{C.14}$$

where D is the amplitude at $x = 0$.

An MCO of length 2L at $x = 0$ is given by:

$$T = \sum_{i=-1}^{1} C_i D e^{-1/2(kx_i)^2}, \tag{C.15}$$

where C_i and x_i are the same as for Equation C.10. Thus,

$$\frac{T}{D} = 1 - e^{-1/2(kL)^2}. \tag{C.16}$$

For a 62-foot MCO, Equation C.16 becomes

$$\frac{T}{D} = 1 - e^{-1/2(31k)^2}. \tag{C.17}$$

C.2.3   JOG

A jog signature can be described by:

$$y = \frac{D}{\pi} \tan^{-1}(\pi k x), \tag{C.18}$$

where D is the maximum amplitude.

An MCO of length 2L at x_i is given by:

$$T = \frac{D}{\pi} \left\{ \tan^{-1}(\pi k x_i) - \frac{1}{2} \left\{ \tan^{-1} \pi k (x_i + L) \right. \right.$$

$$\left. \left. + \tan^{-1} \pi k (x_i - L) \right\} \right\}. \qquad \text{(C.19)}$$

The first derivative of the right hand side of Equation C.19 is 0 at $x_i^2 = \frac{1}{3} \left\{ \frac{1}{(\pi k)^2} + L^2 \right\}$. Thus, T will be a maximum at:

$$x_i = \pm \sqrt{\frac{1}{3} \left\{ \frac{1}{(\pi k)^2} + L^2 \right\}}.$$

For a 62-foot MCO with $k = \frac{1}{20}$ ft^{-1}, x_i will be ± 18.3 feet.

The ratio $\frac{T}{D}$ for $k = \frac{1}{20}$ ft^{-1} is approximately 0.43. For $k = \frac{1}{10}$, x_i will be ± 17.99 and the ratio $\frac{T}{D}$ will be approximately 0.47.

APPENDIX D

STATISTICAL REPRESENTATION OF
RMS CROSSLEVEL

Crosslevel data are high-pass filtered to eliminate long
wavelength trends. Then it is squared, averaged over a
predefined length, and the square root of the result is
taken. In this appendix, the distributional properties
and expectations of this statistical representation are
derived using the crosslevel models given in Reference 6.

D.1 ASSUMPTIONS

The assumptions are given as follows: crosslevel geometry
consists of a stationary random component completely character-
ized by a bivariate normal distribution; the key statistic
of this distribution is its correlation function, or equiva-
lently, its power spectral density; joints of bolted rail
are represented by a random amplitude operating on a joint
shape function and joint related crosslevel, or half-stagger
track is given (1):

$$y_4(x) = \sum_{n=-\infty}^{\infty} c_n (-1)^n e^{-k|x-\frac{1}{2}nL|} ; \qquad (D.1)$$

where:

    x = distance along track

    $y_4(x)$ = crosslevel as a function of distance
                 along track

    n = counting index

    c_n = amplitude of nth joint

    k = joint decay rate

    L = rail length.

The c_n are independent of one another and have a probability distribution given by

$$p(c) = \frac{128c^3}{3\bar{c}^4} e^{-4c/\bar{c}} \; ; \qquad (D.2)$$

randomness in the joints is independent of variations associated with the stationary process, both in the raw geometry, filtered geometry, and filtered geometry squared.

D.2 METHODOLOGY

The cumulant generating function, $T(\xi)$ is related to the moment generating function, $\Xi(\xi)$, by

$$T(\xi) = \ln[\Xi(\xi)], \qquad (D.3)$$

where ξ is a dummy variable generated in the Fourier transform of a probability density, $p(c)$:

$$\Xi(\xi) = \Xi\left[e^{i\xi c}\right] = \int p(c)e^{i\xi c}dc. \qquad (D.4)$$

The nth moment about the origin is given by

$$\mu_n' = \frac{d^n}{d\xi^n} \Xi(\xi)\bigg|_{\xi=0} ; \quad \mu_0' = 1, \qquad (D.5)$$

and the nth cumulant is given by

$$\kappa_n = \frac{d^n}{d\xi^n} \gamma(\xi)\bigg|_{\xi=0} ; \quad \kappa_0 = 0. \qquad (D.6)$$

The κ_n and the μ'_n are related by

$$\mu'_n = \sum_{m=0}^{n-1} \binom{n-1}{m} \mu'_m \kappa_{n-m}, \tag{D.7}$$

which gives the nth moment as the combination of previously computed moments and cumulants. The relationship is easily inverted to give the nth cumulant as a combination of previously computed cumulants and moments:

$$\kappa_n = \mu'_n - \sum_{m=1}^{n-1} \binom{n-1}{m} \mu'_m \kappa_{n-m}. \tag{D.8}$$

Cumulants are important to this analysis because of the following properties:

- the nth cumulant for the sum of two statistically independent process is the sum of the nth cumulants for each of the two processes.

- The nth cumulant for a random amplitude operating on a fixed shape function that occurs at periodic intervals is the nth moment of the shape function times the nth cumulant of the random amplitudes.

- In the case of a normal distribution, cumulants of higher order than the 2nd cumulant vanish.

D.3 ANALYTICAL TREATMENT

The time series associated with the joints, $y_4(x)$, has a zero mean since the sequence, $\left(c_n (-1)^n\right)$, has a zero mean.

and

$$\sigma_y = \left(\frac{\beta_1}{1 + e}\right)^{\frac{1}{2}} \simeq \sqrt{\beta_1 / e},$$

where the approximations apply when e is large.

95 copies

Characterization of Relatively Large Track Geometry Variations, 1982
US DOT, FRA, ENSCO, Inc, A Hamid, R Owings, M Kenworthy

U.S. Department
of Transportation

**Research and
Special Programs
Administration**

Kendall Square
Cambridge, Massachusetts 02142

Official Business
Penalty for Private Use $300